A Behavioral and Molecular Approach for Understanding Angelman Syndrome

A Behavioral and Molecular Approach For Understanding Angelman Syndrome

A dissertation presented

by

Caleigh Mandel-Brehm

to

The Division of Medical Sciences

in partial fulfillment of the requirements

for the degree of

Doctor of Philosophy

in the subject of

Neuroscience

Harvard University

Cambridge, Massachusetts

October, 2015

Dissertation Advisor: Michael E. Greenberg Caleigh Mandel-Brehm

A Behavioral and Molecular Approach for Understanding Angelman Syndrome

Abstract

Autism Spectrum Disorder (ASD) is a set of human developmental disorders that affects ~1 in 68 children. The clinical features of ASD include deficits in social behavior and frequent co-morbidity of motor, emotional and sensory impairment. Currently, there are no effective treatments for ASD. A major obstacle for treating ASD is the limited knowledge of the neuronal circuits that drive these complex behaviors.

Several monogenic, or single-gene, disorders that possess similar features to ASD have been identified, implicating a role for molecular pathways in the development of these behavioral circuits. This dissertation focuses on Angelman Syndrome (AS), a neurodevelopmental disorder characterized by social communication deficits, movement disorder and hyper-excitable behavioral traits. The phenotype of AS arises from mutation of the E3 ubiquitin ligase, *UBE3A*. The overarching goal of this study is to understand how deregulation of UBE3A-dependent pathways contribute to the behavioral phenotype of AS.

Neuronal substrates of UBE3A have been identified and their expression has been shown to be up-regulated in AS neurons. I now test the hypothesis that this deregulation contributes to specific pathology of AS. First, I described clinically relevant behavioral phenotypes in an AS mouse model. Next, I genetically reduced the expression level of two UBE3A substrates, ARC (Activity-Regulated Cytoskeleton-Associated Protein) and

EPHEXIN5 (Rho Guanine Nucleotide Exchange Factor 15) in the AS mouse and assayed for reversal of behavioral abnormalities.

I find that the AS mouse model has impaired communication and motor behavior during early postnatal development, enhanced seizure-like activity and an abnormal cortical electroencephalogram (EEG). Reducing the levels of ARC reversed the enhanced seizure-like activity and EEG, but not the communication or motor deficits. The specific rescue of seizure-like activity by reducing ARC, but not EPHEXIN5, reveals a role for molecular diversity in the development of behavioral circuits. Further, these findings suggest that therapeutic interventions that reduce the level of ARC expression have the potential to reverse the seizures associated with AS. Lastly, the identification of aberrant behaviors in AS mice provides clues regarding the neural circuit defects that occur in AS and ultimately allow new approaches for treating this disorder, and broader ASDs.

Table of Contents

List of Figures

Acknowledgements

I would like to acknowledge my thesis advisor, Dr. Michael Greenberg, for his continual mentorship and support throughout my graduate student experience. I feel very fortunate to have been trained in the rigorous and enthusiastic environment that Mike has created, in the company of many other fantastic scientists who I greatly admire. I had an absolute blast during my time here, and I especially want to thank Mike for making sure I never felt alone or without guidance. I am forever grateful for Mike's commitment to my success and I hope him to make him proud as I move forward in the next steps of my career.

I would like to acknowledge John Salogiannis for being there as a friend, colleague and mentor throughout my entire course as a graduate student. With regard to the work in this thesis, John helped perform and analyze experiments and provided valuable input when it came to writing the paper in Chapter 2. I am forever grateful for having had the opportunity to work with John throughout this process. Long live #8.

I would like to acknowledge my dad (Dr. Paul Brehm), mom (Dr. Gail Mandel), brother (Josh Mandel-Brehm) and sister-in-law (Nicole Hodgman) for their patience and understanding during the ups and downs of my graduate career. We are a small bunch but thick as thieves and I could not have gotten through this process unscathed without their love and support.

I dedicate this thesis to my girlfriends,

Danielle Ciofani, Elizabeth Itkowsky, Diane Ivy and Roberta Sciascia,

Who have not the slightest clue how much their love, support and wild antics have helped me through. I am forever grateful to have these strong, amazing women in my life.

#Kinglife

Attributions

Chapter 1:

Figure 1.1 is from Williams CA et al., 2010; **Figure 1.2** is from Bowen and Jeavons, 1967; **Figure 1.3** is from Williams CA et al., 2010; **Figure 1.4** is from Mabb AM et al., 2011; **Figure 1.5** is from http://www.hucc.hokudai.ac.jp/~d20505/en/research/; **Figure 1.6** is from Sadikovic et al., 2014; **Figure 1.7** is from Zhou X et al.,2015; **Figure 1.8** is from Peter Scheiffile and Asim A. Beg, 2010; **Figure 1.9** is from Huang H et al., 2013 and Jiang H et al., 1999 ; **Figure 1.10** was generated by myself.

Chapter 2:

Chapter 2 is re-formatted from "**Mandel-Brehm C,** Salogiannis J, Dhamne S, Rotenberg A, Greenberg ME. (2015) Seizure-like activity in a juvenile Angelman Syndrome mouse model is attenuated by reducing *Arc* expression. PNAS 112(16):5129-34"

Ephexin5 knockout mice were generated by Mustafa Sahin and Tam Thompson in the Children's Hospital Boston core facility. Arc knockout mice were provided as a gift from Dr. Marc Bear's laboratory at Massachusetts Institute of Technology. Ephexin5 antibodies were generated previously by Seth Margolis, John Salogiannis and Linda Hu. I performed all other behavioral and molecular assays under the supervision of Michael Greenberg

Chapter 3:

Figure 3.1 + 3.3 was generated by myself

Figure 3.2 is data generated by myself and is from the previously published work "**Mandel-Brehm C,** Salogiannis J, Dhamne S, Rotenberg A, Greenberg ME. (2015) Seizure-like activity in a juvenile Angelman Syndrome mouse model is attenuated by reducing *Arc* expression. PNAS 112(16):5129-34"

"The history of medicine is full of interesting stories about the discovery of illnesses. The saga of Angelman's syndrome is one such story. It was purely by chance that nearly thirty years ago (e.g., circa 1964) three handicapped children were admitted at various times to my children's ward in England. They had a variety of disabilities and although at first sight they seemed to be suffering from different conditions I felt that there was a common cause for their illness. The diagnosis was purely a clinical one because in spite of technical investigations which today are more refined I was unable to establish scientific proof that the three children all had the same handicap. In view of this I hesitated to write about them in the medical journals. However, when on holiday in Italy I happened to see an oil painting in the Castelvecchio museum in Verona called . . . a Boy with a Puppet. The boy's laughing face and the fact that my patients exhibited jerky movements gave me the idea of writing an article about the three children with a title of Puppet Children. It was not a name that pleased all parents but it served as a means of combining the three little patients into a single group. Later the name was changed to Angelman syndrome. This article was published in 1965 and after some initial interest lay almost forgotten until the early eighties."

- Dr. Harry Angelman[1]

[1] Angelman, H., Personal "Communication" (letter)" to Dr. Charles Williams. 1991.

CHAPTER 1

Introduction

All writings and figures in this chapter were created by Caleigh Mandel-Brehm/CMB

Autism Spectrum Disorders (ASDs) embody a set of developmental disabilities that are highly prevalent among humans, affecting ~ one in every 68 children[1]. The core features of an ASD are persistent deficits in social communication and social behavior, as well as restrictive and repetitive behaviors, also known as stereotypies. The biological underpinnings of ASD pathology are largely unknown and there are currently no effective treatments[1,2].

The word "spectrum" refers to the heterogeneous mix of symptoms, skills and level of impairment observed among children who are affected[1]. For example, ~30% children with ASD are unable to speak or remain minimally verbal, while others may display a rich vocabulary[3,4]. Reading comprehension skills, the ability to use gestures to communicate and the level of purposeful social interaction can vary in onset and severity. Further, the deficits in social behaviors are frequently co-morbid with motor, sensory and emotional deficits, as well as seizures[5-8]. Initially, the variability in symptoms observed among individuals motivated diagnosis as separate disorders. The concept of an ASD was introduced through scientific consensus that these previously separated behavioral disorders are actually a single spectrum disorder with varying levels of severity[6].

Studies of monozygotic twins with ASD suggest a strong genetic component, with ~60% concordance, but identifiable ASD-causing mutations account for only 10% of known cases[2,9]. Simulations based on the observed number of reoccurring genetic mutations predict that there are ~ 600-1200 ASD risk causing genes[10-12]. Examples of ASD-risk causing genes include *OXTR*, *SHANK3*, *BCL2*, *RORA*, *EN2*, *RELN*, *MECP2, AUTS2, NLGN3,*

NRXN1, SLC6A4, UBE3A, GABA, AFF2, CHD8, ADNP, TBR1 and *ANK2*[13,14]. Interestingly, the biological function for several genes, such as *CHD8, ADNP* and *TBR1*, is not restricted to the nervous system and knockdown of these genes in various animal models results in peripheral dysfunctions, such as cardiac arrhythmias and renal defects[13]. The diverse biological function of ASD-risk causing genes adds an additional layer of complexity for studies that aim to identify the primary biological dysfunctions that gives rise the behavioral abnormalities in ASD.

The genetic basis of the individuals with idiopathic ASD remains a subject of debate. Two common hypotheses include chance combinations of commonly occurring genetic mutations that otherwise would be harmless or ultra-rare mutations that occur *do novo* during development[9,13]. Thus far, the genetic findings do not readily inform about the biological mechanism that leads to the specific impairment of social behaviors observed in ASD. In addition, the absence of identifiable genetic mutations precludes the possibility of molecular markers that can be used for follow-up analyses. The variability of the behavioral phenotype, in conjunction with a lack of robust genetic markers, impedes hypothesis driven questioning of the biological dysfunction that is occurring in the developing brain in ASD.

Modern advancements in imaging technology over the last decade have allowed for preliminary characterization of the physiological deficits present in the ASD brain [15]. Magnetic Resonance Imaging (MRI) and Diffusion Tensor Imaging (DTI) from children with ASD reveal abnormal morphology of axon white matter tracts and disorganization of cortical micro-architecture[2,16]. Several structural MRI studies have shown that toddlers with ASD (aged two to four years) have on average, a larger brain volume than age-

matched unaffected children. This significant increase in brain volume is transient and disappears around 6-8 years of age[15]. The development of the human brain is thought to be a dynamic and protracted process; the architecture of neuronal networks is established during the embryonic period and refined in its organization and function during postnatal development[17,18]. These physiological data suggest that ASD could arise from dysfunction during the period of refinement; however, the extent to which genetic and/or experience-dependent mechanisms influence this process is largely unclear, adding additional difficulty for generating hypotheses regarding the neurological basis of ASD.

The study of monogenic, or single-gene, neurodevelopmental disorders offers a candidate approach for elucidating the pathology that is occurring in ASD[19]. Monogenic neurodevelopmental disorders often manifest a complex behavioral phenotype early in development (<5 years of age), similar to what is observed in ASD, albeit more severe and more highly stereotyped. Some monogenic disorders, such as Tuberous Sclerosis Complex-1 and Fragile-X Syndrome, express an ASD (such as Autism) as a secondary symptom. Alternatively, a monogenic disorder may only contain some features of an ASD, such as nonverbal behavior, motor stereotypies or seizures[19-21]. The complex phenotype of ASD can be broken down into its parts among these single gene disorders and individual traits can be studied in a more simplified and tractable experimental context.

The co-morbidities of behavioral traits within a single-gene neurodevelopmental disorder are complex, but reproducible. For example, behavioral traits that are consistently observed among girls with Rett Syndrome include hand-wringing stereotypies, breathing abnormalities and regression of communication and motor skills[22]. These co-morbidities reveal potential links between behavioral circuits that might have otherwise

gone unappreciated. In the example of Rett Syndrome, loss of MECP2 leads to a specific dysfunction in both motor and communicative contexts, suggesting these behaviors are linked through some common, unknown biology that occurs in normal development. With a genetic and molecular marker in hand, one can elucidate the biological pathways that are common to these discrete behavioral traits.

Lastly, the fact that single-gene mutations express unique behavioral phenotypes implicates a role for diversity among molecular pathways in the development of behavioral circuits. The mechanism through which molecular pathways influence the development and function of specific behavioral circuits is a central question for this dissertation.

The following study examines a monogenic neurodevelopmental disorder that expresses a complex behavioral phenotype, with overlapping features to an ASD. Angelman Syndrome (AS) is caused by mutation of a single gene, *UBE3A*, and is characterized by a specific combination of communication impairment, movement disorder, seizures and behavioral stereotypies[23,24]. Notably, copy number variations in the UBE3A gene are a significant finding (1-3%) among individuals with ASD[25]. Thus, the study of UBE3A-dependent pathways in the context of AS is useful for addressing the question of how molecules influence the development of complex behavioral circuits, and for generating hypotheses about how these circuits go awry in complex disorders, such as ASDs.

1.1 Angelman Syndrome: Clinical Phenotype

The Behavioral Phenotype of Angelman Syndrome

Angelman Syndrome (AS, MIM 105830) is a neurological disorder that expresses a unique behavioral phenotype in early development. The clinical phenotype of AS was first described as 'Happy Puppet Syndrome' in 1965, when Dr. Harry Angelman noticed three children expressing a similar a set of unusual traits [26]. The primary deficits are purely behavioral and include severe cognitive delay, absence of speech, movement disorder and hyper-excitable traits such as excessive laughter and hand flapping[27-29]. The movement disorder is characterized by ataxia, or rigidity in movements, infantile spams, jerky limbs, tremors and a wide gait[29,30] (Figure 1.1). The deficits in communication and motor behaviors confound accurate description of cognitive abilities, however, psychometric testing suggests the upper developmental potential is in the two to three year range[31]. The primary behavioral disorder is robust, highly stereotyped and invariant with respect to gender or genetic background.

In addition to these primary deficits, the presence of three or more secondary abnormalities are frequently observed (>80%) in AS[30]. These secondary features can be behavioral or physiological in nature and include epilepsy, sleep disturbances, hyperactivity, fascination with water, drooling and postnatal deceleration in head growth[27,32]. Deficits in sensory and emotional processing are also observed; for example, a child with AS will laugh in response to a tuning fork, whereas an unaffected child would exhibit an aversive behavior [33]. The incidence of seizures varies across longitudinal studies, ranging from 40%-95%, and can manifest as exaggerated tremors, spastic limbs

and complete loss of balance[34,35]. Although epilepsy is not present among all individuals it is one of the most debilitating symptoms of this disorder.

The pathogenesis of AS, including both the primary and secondary features, is highly restricted to the nervous system. Some dysmorphic features have been described, such as mid-face hypoplasia, widely spaced teeth, deep-set eyes, prognathism and changes in skin and hair color[36]. However, these features are not considered to be clinical markers for AS, as they are observed in fewer than 30% of children across large-scale longitudinal studies and only become prominent as an individual ages[30,31] (Figure 1.1). The specific and isolated dysfunction of the developing nervous system in is a defining feature of AS[29]. The progression of the neurobehavioral phenotype is highly stereotyped in early development[27,28,32,33]. Speech and motor impairment occurs at six months of age and is realized when primary developmental milestones, such as babbling and crawling, are not achieved. Conversational speech never develops in even the most highly functional individuals, showing none-to-minimal use of words. Sensory and emotional deficits are present after one year; for example, the tuning fork response can be observed by 17 months of age. Co-morbidity of seizures, if present, is frequently observed between one to three years of age (<25% observed before 12 months) and often precedes clinical diagnosis[32]. Thus, the behavioral traits observed in AS manifest entirely between 6 months and three years of age.

Figure 1.1 Behavioral traits of Angelman Syndrome. Frequent smiling, abnormal gait and hand-flapping behaviors are depicted. At times the facial appearance can suggest syndromic diagnosis but usually there is no significant facial dimorphism (Image taken from Williams CA et al., 2010).

Interestingly, sparing of learning and memory functions can be observed indirectly in the outcomes of aggressive behavioral therapy[37]. Although individuals remain nonverbal, receptive communication skills are more developed and older children can learn to communicate through gestures and communication boards[38]. And despite persistent ataxia, the ability to learn new motor movements is robust. Sitting can be achieved around one year of age and 45-90% of individuals can walk by five years of age. In addition, there is no evidence of regression, i.e. there is no loss in any previously acquired or learned skill[31]. Thus, the learning and memory functions in AS appear to be somewhat intact.

The clinical phenotype of AS in older individuals remains poorly defined[39]. There is limited data on life expectancy by epidemiologic measurements, but there does not seem to be an obvious shortening of lifespan[31]. The oldest individual is 75 years old, suggesting AS is not a degenerative disorder[36]. The emergence of new behavioral abnormalities beyond childhood is rare, although the onset of aggression during preadolescence has been noted[31]. Pubertal onset and development are generally normal in AS for both men and women, and procreation appears possible[36].

Some of the core behavioral features of AS may vary in frequency and severity over time. Seizure activity may go through periods of remission during juvenile years and reappear in adulthood. The excessive bouts of laughter become less frequent and more spontaneous after childhood. Thus, the behavioral phenotype of AS is highly robust and stereotyped during infancy and early childhood (one to three years old) and becomes more variable as individuals age[27,29,35].

Physiological correlates of Angelman Syndrome

An abnormal electroencephalogram (EEG) is a robust physiological marker of AS, observed in 100% of the individuals who have been clinically diagnosed with AS through behavioral assessment[27]. The abnormalities in cortical activity include rhythmic 4-6 Hz bursts of activity that persists with eye closure and high-voltage, slow (2-3 Hz) delta activity with spokes and sharp waves[24,27,34] (Figure 1.2). Due to a delay in symptom presentation and limitations in clinical diagnosis, a precise onset for the EEG phenotype has not been determined, but has been observed as early as 8 months of age[34]. There is little understanding of how the abnormal EEG relates to the specific abnormalities of AS.

Due to the unaltered lifespan there is limited postmortem tissue to investigate the physiological basis of AS. The hyperactive traits and movement disorder in children create an obstacle for imaging technologies, such as MRIs[15]. A limited number of studies have successfully utilized Diffuse Tensor Imaging and MRI technology to measure the anatomical pathways related to language in the AS brain[16,40]. Individuals with AS have unidentifiable white matter tracts within the arcuate fasciculus on the left side of the brain. The arcuate fasciculus is a bundle of axons that houses the reciprocal connections between two major language centers in the brain, namely Broca's area and Weirneke's area. Mild cortical atrophy and demyelination within the cortex have also been observed[30]. The contribution of these physiological deficits to the behavioral abnormalities not yet understood.

In sum, the behavioral phenotype of AS is complex and is characterized by severe impairment of social communication and motor behaviors. Some of these features, such as nonverbal behaviors, seizures, abnormal gait and hand-flapping stereotypies are

overlapping features with broader ASDs, such as Autism[7]. The specific dysfunction of the nervous system and the progression of symptoms, including the onset in early development and persistence through adulthood, are also highly reminiscent of what is observed in ASDs. Thus, the study of AS offers a compelling context to begin dissection of the complex phenotype in ASD.

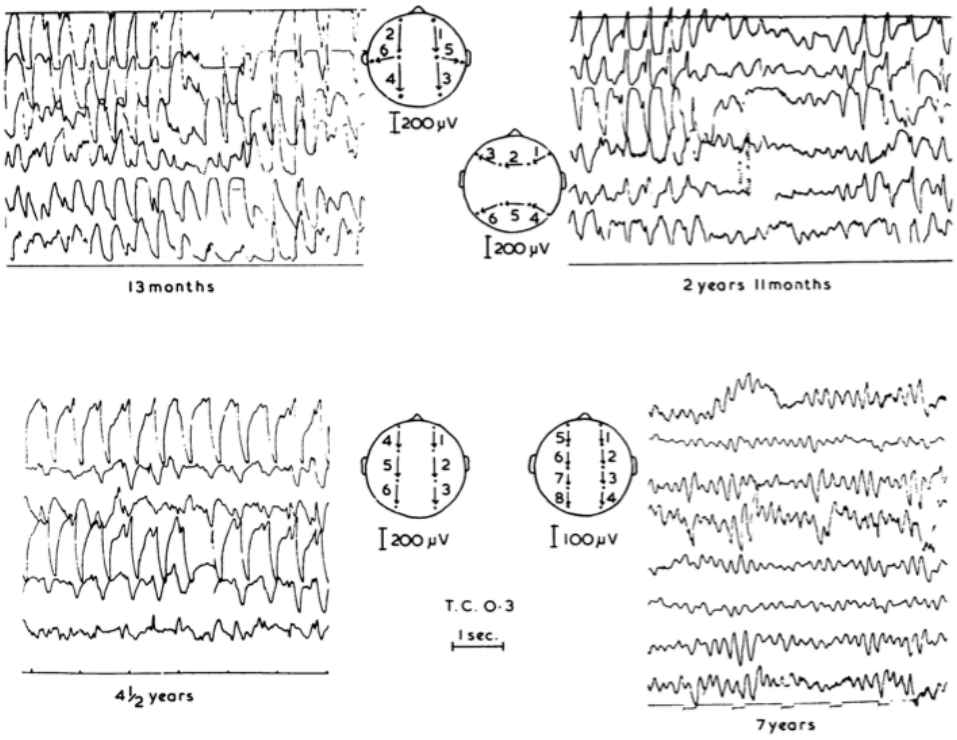

Figure 1.2 Representative Electroencephalogram from an individual with AS. Characteristic high amplitude, 2-3 Hz spiking events are observed in a child with AS, at different ages during development (Image taken from Bowen and Jeavons, 1967).

1.2 Angelman Syndrome: Genotype-Phenotype Correlation

Single gene mutation, complex behavioral phenotype

The clinical phenotype of AS arises from mutation of the maternally inherited, chromosomal locus 15q11.2-13[28,30,23]. Approximately 75-85% of individuals have a large (~6 Mb) chromosomal microdeletion spanning several commonly identified breakpoints (Figure 1.2). In ~ 10-15% of the cases, a mutation occurs in a single gene, UBE3A[23]. Rare mutations include inheritance of two copies of the paternal 15q11-13 locus (uniparental disomy or UPD), or mutations in a DNA sequence upstream of the UBE3A gene, known as the imprinting center (IC). The only feature that is shared among all molecular subtypes is the disruption of the maternal UBE3A gene (Figure 1.2)[30,36].

All molecular subtypes result in a somewhat uniform clinical picture of developmental delay, absence of speech, movement disorder, hyper-excitable traits and an abnormal EEG[41]. Notably, the nonverbal behavior and abnormal EEG are present among the 15q11.2-13 deletion and UBE3A genotypes. These data suggest that mutation of UBE3A alone is sufficient to give rise to the neurobehavioral phenotype of AS, thus motivating the classification of Angelman Syndrome as a monogenic, or single-gene, neurodevelopmental disorder.

The individuals with 15q11.2-13 microdeletions and paternal UPD have more severe of symptoms compared to UBE3A mutations, while the IC mutations are the least severe of all subtypes[34,41]. Deletion and UPD mutations result in a more robust movement disorder (ataxia, feeding difficulties), increased frequency and earlier onset of seizures,

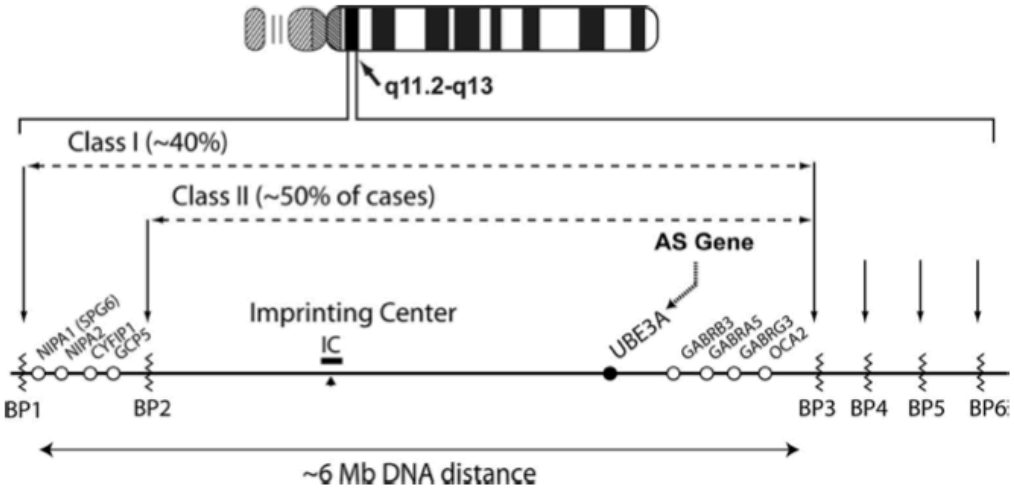

Figure 1.3 Schematic organization of the 15q11.2-12 genomic locus. Location of the AS gene, *UBE3A*, is indicated by the arrow. Common Break Points (BPs) are indicated by the vertical arrows and jagged lines; the most common Class I and Class II deletions are noted by the dashed lines. The IC is depicted, located approximately 500 Kb centromeric to *UBE3A*. (Figure from Williams CA et al., 2010).

more pronounced microcephaly, and there is a higher likelihood of expressing hypopigmentation of the skin and hair[32,41]. Loss of additional genes within the 15q11.2-13 deletion region are thought to contribute to these differences; Loss of an inhibitory GABA receptor cluster and the OCA-2 gene likely increase the severity in seizures and hypopigmentation, respectively. A genotype-phenotype analysis cannot be performed for the physiological deficits that have been discovered, as the MRI and DTI studies have been restricted to individuals with a 15q11.2-13 deletion[16,40].

The mutations that occur in the maternal UBE3A gene include single nucleotide polymorphisms (SNP), and small insertions and duplications of short DNA sequences[23,42]. Novel splice sites and translational error variants are a result from these mutations and are predicted to disrupt the normal processing of UBE3A mRNA. In addition, some pathogenic variants are predicted to disrupt the translation of UBE3A protein through mutation in stop codons or introduction of novel, premature stop codons within the transcript. Several mutations do not impair transcription or translation of the UBE3A gene, but instead, disrupt the specific function of UBE3A protein [discussed in section 1.3][42]. Thus, the majority of UBE3A mutations are predicted to cause loss of protein or specific disruption to UBE3A function.

Among individuals with UBE3A mutations there is variability in the level of speech impairment, seizures, hyper-excitable traits and movement disorder. Although many individuals with UBE3A mutations are non-verbal, some may have instead, a severe developmental delay of speech. In one case of AS, an individual could display a minimal use of words and harbored a SNP in the second nucleotide of the UBE3A gene. It is likely that

this mutation, as well as others, cause a reduction in UBE3A expression instead of total loss of expression. If the level of speech impairment varies with the level of UBE3A expression it would further support the idea that UBE3A is a critical player in the development of language circuits. Analysis of UBE3A expression in cell lines from patients with UBE3A mutations is an active field of research within the AS field.

UBE3A duplication and disease

The connection of UBE3A to the impairment of social and motor behaviors is replicated in clinical findings from individuals that possess duplications of the 15q11.2-13 locus[25,43,44]. This genomic locus is highly unstable and duplications or triplications have been identified as one of the most common copy-number variants (CNV) in patients with ASD (up to 3%). Interstitial duplication of this maternal locus shows incomplete penetrance and results a variable phenotype that includes developmental delay and disability of language and social communication skills. The duplication often contains multiple genes such that the direct role of UBE3A dysfunction has been difficult to tease apart. However, a recent report describes the first female patient with a maternal 15q11.2-13 duplication that contains only the UBE3A gene [45]. This patient has global developmental delay in motor behavior (crawling at 16 months, walking at 18 months) and was non-verbal until the age of three. With intense behavioral therapy, this individual was able to learn new motor and social communication skills such as sign language, although they remained highly non-verbal. The specific delay of motor development, nonverbal behavior and sparing of learning and memory that results from duplication of the UBE3A gene are reminiscent of features that occur in AS.

Imprinting of UBE3A in the nervous system

Several genes within the AS-causing locus 15q11.2-13 are imprinted, or expressed in a parent-of-origin dependent manner. The imprinting mechanism involves preferential CpG methylation at several locations within maternal chromosome 15q11.2-13 (Figure 1.3)[46]. The maternal specific methylation pattern leads to the silencing of several maternally inherited genes (MKRN3, MAGEL2, NDN, SNURF-SNRPN) resulting in exclusive expression from the paternal allele. The remaining genes are expressed bi-allelically, from both the paternal and maternal copy. This differential methylation pattern is established in oocytes, escapes erasure and is stable throughout postnatal development. For most of the genes in locus 15q11.2-13, the imprinting status is stable and not cell-type specific.

However, in differentiated neurons, the UBE3A gene switches from bi-allelic expression to being expressed exclusively from the maternal chromosome[46]. The preferential expression of UBE3A from the maternal allele is an indirect result from the imprinting, or silencing, of the paternal UBE3A copy. The imprinting mechanism involves the transcription of a 2 Kb antisense RNA transcript (UBE3A-ATS) that is initiated on the paternal chromosome, at a site where the maternal allele is preferentially methylated[47]. The antisense transcript acts in a *cis* regulatory manner to impede expression of the paternal UBE3A gene. Knockdown or truncation of the UBE3A-ATS has been shown to alleviate repression of the paternal UBE3A gene *in vivo*[46,48,49]. The antisense transcript is not found in other cell-types and the biological mechanism that dictates neuronal specificity is not known[50-52].

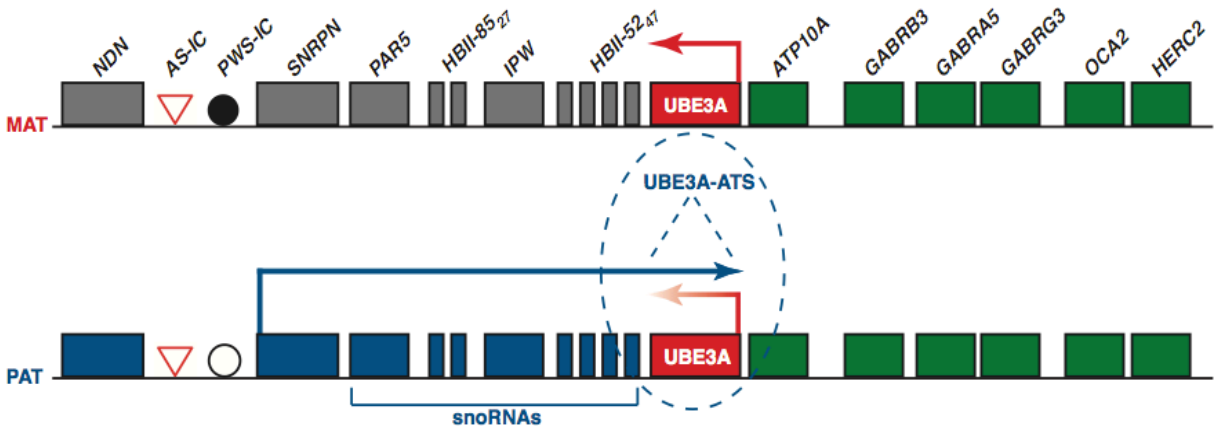

Figure 1.4 Schematic of UBE3A imprinting mechanism in neurons. Red indicates genes that are expressed exclusively from the maternal copy (paternally imprinted), Green represents genes that display bi-allelic expression and Blue represents genes are expressed exclusively from the paternal allele (maternally imprinted). The UBE3A-ATS is only found in the nervous system. (Image taken from Mabb AM et al., 2011).

Findings from these expression studies offer a molecular mechanism to explain the purely neurological phenotype of AS. In non-neurological tissues, mutations in maternal UBE3A result in only partial loss of function, as the paternal allele can compensate. However in neurons, a mutation in the maternal UBE3A gene results in complete loss of UBE3A expression. Thus, although UBE3A is ubiquitously expressed in all cell-types, the nervous system is uniquely vulnerable to AS causing mutations.

A favored approach for treating AS involves de-repressing the non-mutated paternal copy of UBE3A in the nervous system[52,53]. A class of topoisomerase inhibitors, which preferentially down-regulate long transcripts, have been shown to down-regulate the UBE3A-ATS involved in the silencing of paternal UBE3A[49]. This has also been achieved through pharmacological means via delivery of antisense oligonucleotides (ASO) that target the UBE3A-ATS in neurons[53]. The targeting by ASOs is highly specific and result in degradation of the UBE3A-ATS. Molecular and genetic therapies that reduce the UBE3A-ATS have been efficacious in recovering expression from the paternal UBE3A allele, and these approaches are currently being tested in mouse models of AS.

To summarize, mutation in a single-gene, UBE3A, is sufficient to produce all of the core behavior and physiological features in AS. The AS-causing mutations in UBE3A occur specifically on the maternal allele, which is the only source UBE3A expression in neurons due to the neuronal specific imprinting of the paternal copy. Thus, loss of UBE3A specifically in neurons is thought to produce the discrete set of behavioral abnormalities observed in AS.

1.3 UBE3A Structure and Function

UBE3A is an E3-ubiquitin ligase

UBE3A is an E3 ubiquitin ligase that functions within a biological cascade known as the ubiquitin-proteasome pathway (UPP)[54-56]. The UPP is a highly regulated and specific pathway that is important for controlling the degradation of proteins in a cell. The UPP is comprised of three enzymes (E1, E2, and E3) that function sequentially to shuttle freely available ubiquitin molecules onto a specific protein target, or substrate. Depending on the type of polyubiquitin chain that is attached, the substrates will endow different functions or fates. The majority of ubiquitination events form Lysine-48 polyubiquitin chains, which target the substrate to the proteasome for degradation[56,57]. Alternative ubiquitin chains have been shown to regulate endocytosis and recycling of membrane receptors, or target the endoplasmic-reticulum associated degradation pathways.

The steps involving the transfer of ubiquitin from the E1 enzyme to the E2 enzyme are highly stereotyped, but the transfer of the ubiquitin molecule from the E2 enzyme onto the substrate varies by type of E3 ubiquitin ligase (Figure 1.5). In mammals, there is one E1 ubiquitin ligase, several E2 (10-40) ubiquitin ligases and hundreds (>600) of E3 ubiquitin ligases[58]. Thus, the E3 ubiquitin ligases are predicted to be the key players within the UPP that mediate the specific recognition of protein substrates.

Figure 1.5 Three main types of E3 ubiquitin ligases. Schematic of UPP containing (from left to right): HECT (Homologous to E6AP-Carboxy terminus) domain ligases, RING (Really Interesting New Gene) type E3 ligases and U-box type E3 ligases (Figure 1.7). Note: HECT domain ligases are the only type of E3 ligase that actively participates in the transfer of the ubiquitin from the E2 enzyme onto the protein substrate (Image taken from http://www.hucc.hokudai.ac.jp/~d20505/en/research/).

UBE3A: The inaugural E3 HECT domain ligase

The E3 ligase activity of UBE3A (under the alias E6AP) was first demonstrated in cancer related studies using cells infected with the Human Papilloma Virus[54,59]. During infection, UBE3A was identified as the cellular factor that mediated the interaction between the virally expressed protein E6 and the endogenous tumor suppressor protein, p53. The binding of UBE3A to E6 protein, and subsequent binding and ubiquitination of p53 by UBE3A, revealed UBE3A's function as an E3 ubiquitin ligase. Subsequent degradation of p53 following ubiquitination provided further evidence that the UBE3A-E6 complex functions within the ubiquitin-proteasome pathway (UPP).

In later studies, it was discovered that UBE3A could ubiquitinate a different substrate, HHR23A, even in the absence of E6 protein[60]. UBE3A was also shown to possess strong auto-ubiquitinating properties, i.e. it could target itself for ubiquitination and degradation[61]. Findings from these later studies suggested UBE3A had endogenous E3 ligase activity that likely played an important biological role in cells. The catalytic domain of UBE3A that mediated ubiquitination of p53 subsequently characterized and termed a "HECT" domain for Homologous to E6AP-Carboxy's Terminus (E6AP).

UBE3A is a 100 kDa protein (865 aa residues) and the founding member of the family of E3 ligases known as HECT domain ligases. The HECT domain in UBE3A is located within a 350 aa residue in the Carboxy-terminal of the protein. The HECT domain is characterized by a highly conserved N-terminal E2-enzyme binding lobe, and a C-terminal catalytic domain that harbors an active cysteine (Cys) residue[58,59]. This Cys residue forms the strong thioester bond with ubiquitin during the transfer onto the protein substrate

(Figure 1.5). The majority of ubiquitinating events by UBE3A involve the addition of a Lys-48 ubiqutin chain, thus substrates of UBE3A are subsequently degraded by the proteasome.

Mutations in the catalytic site of the HECT domain have been identified among individuals with AS, and demonstrated to disrupt UBE3A 's ligase activity in experimental contexts. Protein modeling approaches can also be used to predict the likelihood of a given mutation in the HECT domain to disrupt UBE3A ligase activity. Two such mutations, Serine582 and M802 frame-shift deletions are modeled in Figure 1.6.

In addition to the HECT domain, UBE3A has several receptor interacting LXXLL motifs[42,60,62]. These motifs have been found to mediate binding of UBE3A to E6 protein, E6-dependent binding to p53, and binding of UBE3A to steroid receptors. The steroid receptor responsive element is contained within three consensus-receptor interacting LXXLL motifs, two of which are contained within the N terminus, and a third located in the carboxy terminus of the protein. Via these motifs UBE3A has been shown to interact with the progesterone receptor (PR), androgen receptor (AR) and estrogen receptor (ER). The fifth domain (amino acid residues 170-680) is an activation domain that is critical for Steroid-Hormone Receptor transcriptional co-activation. In addition to the ligase activity, UBE3A has been shown to act as a transcriptional co-activator of steroid hormone receptors[60]. The co-activator transcriptional activity of UBE3A is not coupled to the ligase activity within the HECT domain and can function in its absence. Thus, loss of the transcriptional function of UBE3A is not considered a contributing factor the pathology of AS.

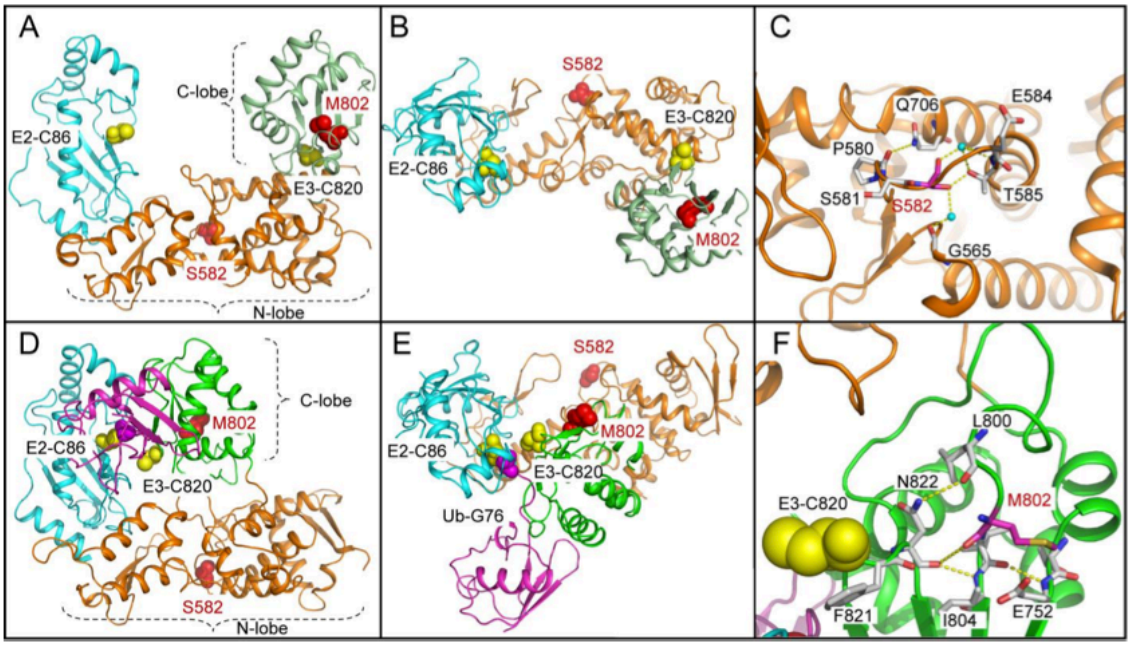

Figure 1.6 Predicted structure of UBE3A with AS-causing mutations. AS causing mutations S582 and M802 are incorporated into the protein structure of UBE3A. The blue structure represents the E2-enzyme, the orange and green structures are the N and C-terminal of UBE3A, respectively. The yellow circles mark catalytic sites on the E2 and E3 enzyme. Both mutations are present in a single model (Image from Sadikovic et al., 2014).

(A) Depicts the E2-E3 complex, the S582 and M802 mutations are highlighted in pink text. Note the proximity of M802 to the E3-820 site, which is the catalytic site required for the transfer of ubiquitin to a substrate. Also note that the S582 is located in the region where UBE3A kinks during the interaction with the E2 enzyme (see panel D).

(B) Sideview of (A).

(C) Chemical interactions surrounding the S582 mutation.

(D) Depicts the E2-E3-ubiquitin complex (Ubiquitin in purple).

Figure 1.6 Cont'd

(E) Sideview of (D)

(F) Zoomed in view of the M802 mutation in the context of the E2-E3-ubiquitin complex. Note that the M802 mutation influences the geometric shape of the C820 catalytic cleft, and this influences the binding of this pocket to the ubiquitin (lower left corner of this panel).

To summarize, UBE3A is an E3 Ligase that catalyzes the ubiquitination of a specific set of proteins in the cell. Mutations in UBE3A found in AS cause disruption of UBE3A ligase activity either directly through specific mutation, or indirectly through destabilization of UBE3A protein or transcript. There is a strong correlation between the occurrence of Angelman syndrome and the loss of UBE3A catalytic activity, suggesting that the dysregulation of UBE3A substrates is an important factor in AS.

1.4 The UBE3A Substrate Hypothesis

The UBE3A Substrate Hypothesis predicts that deregulation of a specific set of UBE3A substrates, in neurons, contributes to the specific pathophysiology that underlies AS.

The precedent for this hypothesis has been demonstrated in the study of UBE3A function outside the context of the nervous system, prior to its implication in AS. Deregulation of UBE3A substrates have been identified as contributing factors in other non-neurological diseases, such as cancer[55] (See Figure 1.7). Many of these UBE3A substrates that have been identified are not relevant in nervous system biology or not thought to interact with UBE3A outside the pathological context of HPV infection. However, these studies serve as a proof-of-principle that deregulation of UBE3A substrates have been shown to contribute to robust, biological phenotypes.

Identifying neuronal substrates of UBE3A

In order to identify neuronal substrates of UBE3A, studies have employed the use of mice. The UBE3A gene is located on the mouse orthologous chromosome 7C and the imprinting of this locus appears to be evolutionarily conserved. In addition, the human UBE3A protein sequence exhibits 99% similarity with that of the mouse, thus allowing for mouse models of AS. The most common AS mouse model contains a deletion in a ~3 Kb region in Exon2, resulting in a frameshift mutation that leads to nonsense mediated decay of UBE3A transcript and total loss of protein in the brain[63]. These mice have been extremely useful for identifying molecular targets of UBE3A, and for testing molecular hypotheses regarding the contribution of these substrates to the pathology of AS[64,65].

To identify substrates of UBE3A in neurons, a stepwise series of molecular approaches are generally employed. Candidate molecules can be identified through bioinformatics or proteomic based approaches, including mass-spectrometry and yeast-two hybrid screens[39,66-69]. Alternatively in some cases, the neuronal pathophysiology observed in AS neurons can inform about a potential substrate[70-72]. A potential candidate is considered a substrate of UBE3A if it is observed to have UBE3A-dependent ubiquitination and degradation in *in vitro* and cell culture assays. A candidate substrate that displays UBE3A-dependent ubiqutination and degradation *in vitro* is then quantified *in vivo* in the brain of AS mice. Substrates that are direct targets of UBE3A in neurons are predicted to have increased levels of expression in AS neurons compared to WT. This experimental pipeline has led to the identification of several neuronal targets of UBE3A, including PBL/ECT2[68], GAT1[39], SASCIN[67], EPHEXIN5[66], ARC[67], alpha-synuclein[70], SK2[71] and proteasome-associated proteins RPN10, UCH-L5 and CG8209[69].

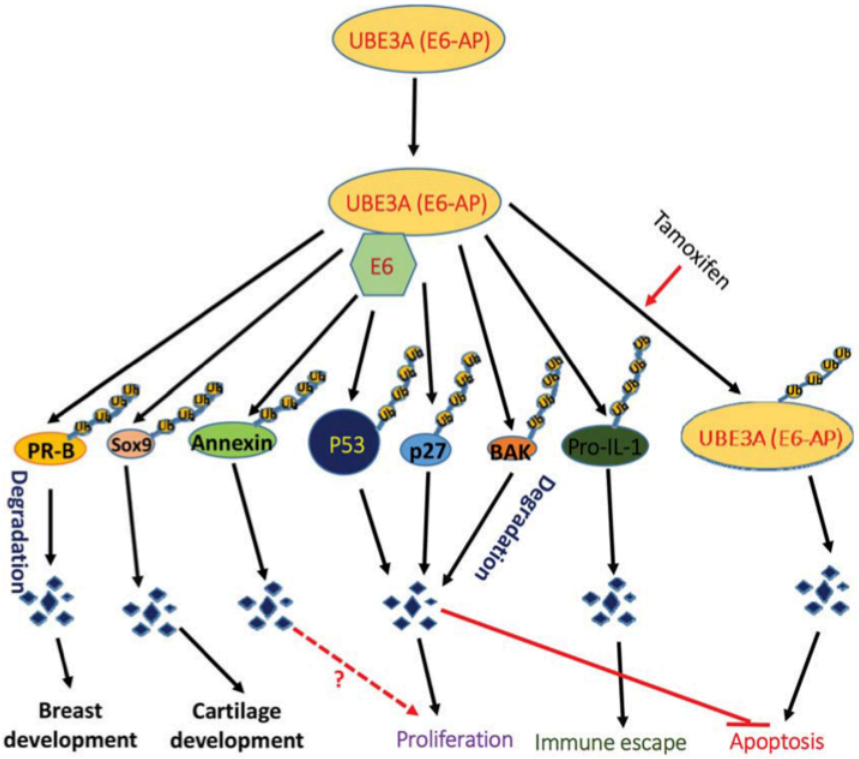

Figure 1.7 Biological processes of UBE3A substrates Deregulation of UBE3A (E6AP) substrates contribute to a diverse set of biological pathologies related to cancer (image taken from Zhou X et al.,2015).

The majority of these substrates have ascribed biological functions. The Rho-GEF PBL was identified in a screen using *Drosophila melangastor* and is known to regulate cytokinesis and migration of cells during embryonic development[68]. Alpha-synuclein is most commonly studied for its aggregation in amyloid plaques of Alzheimer's disease; the function is largely unknown but thought to be involved in neurotransmitter release in the nervous system. The GABA transporter (GAT1) is important for mediating the uptake of extracellular GABA into the intracellular compartments, and SK2 is a calcium-activated channel that is essential for regulating the excitability of a cell through conductance of potassium ions[39,71,73]. The function for SACSIN is not known, however, mutations in this gene result in the neurological disorder Charlevoix-Saguenay, characterized by cerebellar ataxia and peripheral neuropathy[73].

A target that has received a great deal of attention of late is the immediate early gene, ARC (Activity Regulated Cytoskeleton-Associated Protein)[74,75]. Transcripts encoding *Arc* are localized to dendrites and *Arc* mRNA is translated rapidly in response to an increase in synaptic activity. At the synapse, ARC plays a critical role in regulating the levels of excitatory glutamate receptors in the postsynaptic membrane, affecting plasticity mechanisms such as LTP[76]. More broadly, ARC is considered a "master of synaptic homeostasis" and can gait the excitability of a neuronal network through removal of AMPA receptors from the postsynaptic membrane[74]. In the context of AS, ARC levels have been reported to be increased and lead to a significant reduction of AMPA receptors in the postsynaptic membrane of neurons[67,77]. The reduction of ARC levels in AS neurons has been shown to reverse this phenotype. Taken together, these experiments suggest that deregulation of ARC in AS may abrogate the ability of neurons to respond properly to

changes in activity, in addition to global dampening of excitability within neuronal networks.

EPHEXIN (E5) is a RhoA-GEF (Guanine Nucleotide Exchange Factor) that regulates the timing of synapse formation and maturation in the hippocampus of mice[66]. During the period of early synapse formation, E5 activates a small GTPase, RhoA, which inhibits cytoskeleton arrangements within the postsynaptic density and spine. The maturation of a synapse requires active rearrangements at the postsynaptic spine, thus the presence of E5 inhibits this biological process. Similar to ARC, the levels of E5 expression are increased in the hippocampus of the AS mouse. Increased levels of E5 are predicted to result in fewer and less mature synapses in the hippocampus of the AS mouse[77].

In this dissertation I test the hypothesis that deregulation of UBE3A substrates ARC and EPHEXIN5 contribute to the behavioral abnormalities observed in AS. I have tested this hypothesis by genetically reducing the levels of these substrates individually, in the background of the AS mouse model. If reduction of ARC or EPHEXIN5 is able to modify any of the behavioral abnormalities this would provide supporting evidence that these specific substrates play a direct role in the symptoms of AS (Figure 1.8).

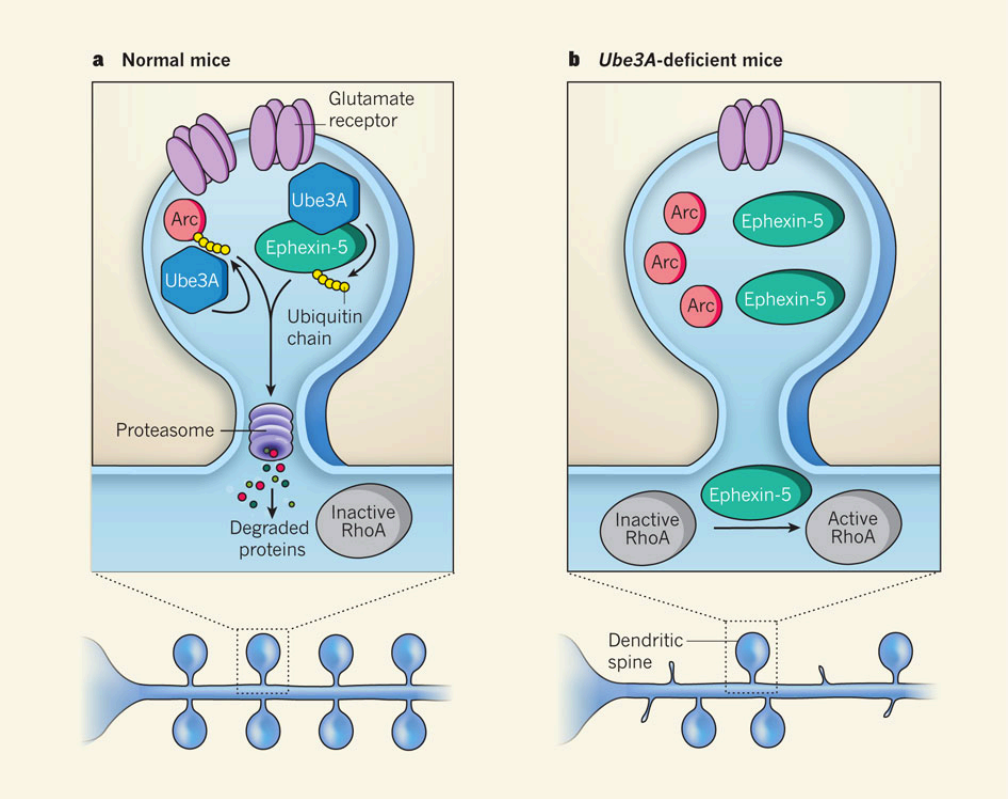

Figure 1.8 Model for the UBE3A substrate hypothesis. Deregulation of ARC and EPHEXIN5 in AS mice is predicted to result in a specific dysfunction in excitatory synapse development and function. In the WT condition, the postsynaptic proteins, EPHEXIN5 and ARC, regulate the number of synapses and excitatory glutamate receptors in the postsynaptic membrane. In AS, deregulation of ARC and EPHEXIN5 results in reduced synapse number and increased endocytosis of AMPA receptors from the postsynaptic membrane, thereby dampening excitability of the neuron. (Image taken from Peter Scheiffile and Asim A. Beg, 2010)

1.5 Limitations of a Mouse Model of Angelman Syndrome

To test the UBE3A substrate hypothesis there needs to be a set of robust and reproducible phenotypes that can be quantified from the AS mouse model. In addition to this study, the phenotypes in the AS mouse serve as critical endpoints to test the efficacy of candidate genetic and/or molecular therapies that are currently in development. Many physiological deficits have been elucidated, including (but not limited to) a reduced number of synapses in the hippocampus and cortex, altered neurotransmitter release from inhibitory neurons, reduced dendritic complexity and abnormal myelination of axonal tracts[63,78-81]. By contrast, there are few behavioral deficits that are robust and reproducible across studies. The lack in reliable clinically relevant phenotypes in the AS mouse has emerged to be a pressing issue for AS-related research.

Deficits in long-term potentiation, or LTP, is a highly reproducible physiological deficit observed in AS neurons of the hippocampus[63]. In this experimental paradigm, WT neurons have a sustained depolarization following high frequency stimulation, and this sustained response is absent in AS neurons. LTP is thought to be a cellular correlate of learning and memory and thus, behavioral studies have largely focused on measuring the learning and memory functions of AS mice. However, unlike the LTP deficits, the learning and memory phenotypes in AS mice are highly variable across independent studies [63-65,78,82,83] (Figure 1.9). The non-reproducibility of learning and memory phenotypes can be observed in the Conditioned Fear Assay, Morris Water Maze, and Novel Object paradigm.

A B

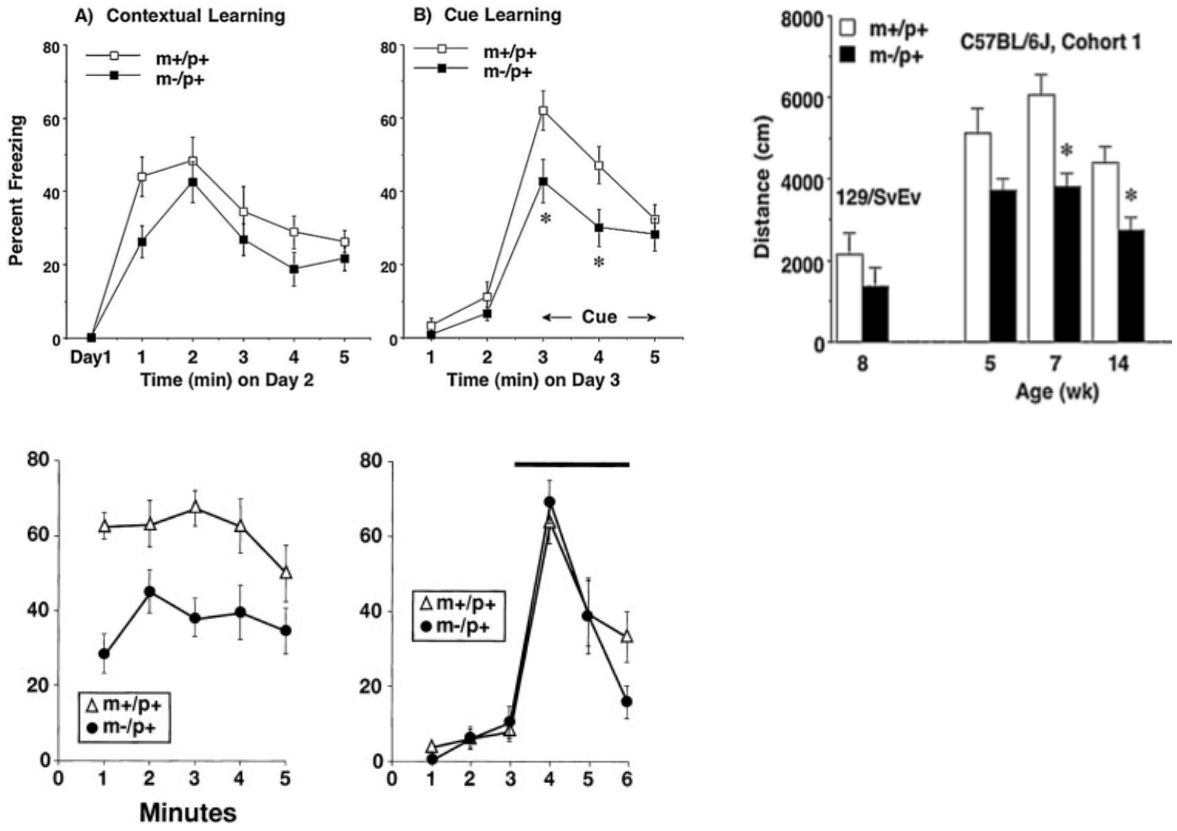

Figure 1.9 Variability in the behavioral phenotype of AS mice

(A) A representative example of non-reproducible learning and memory phenotypes. Findings from the conditioned fear assay are displayed. The difference in phenotypes between AS mice in these studies cannot be explained by age, gender, or genetic background (TOP; image taken from Huang H et al., 2013, BOTTOM: Image taken from Jiang H et al., 1999).

(B) The hypoactivity phenotype in AS mice depends on genetic strain and age. The 129SvE strain does not produce a phenotype when measured at an equivalent time point to the C57B6 counterpart (Image taken from Huang et al., 2013).

Motor coordination phenotypes are among the most reproducible behavioral phenotypes observed in AS mice. Findings from these studies include hypoactivity, poor motor coordination, pronounced hind-limb clasp and an abnormal gait[64]. Some of these phenotypes, such as hypoactivity and deficits in motor coordination, may vary depending on the background strain of the AS mouse and age at time of testing. Additional phenotypes that vary by strain, age or gender include sensory deficits, susceptibility to seizures and increased body weight[64]. The lack of robustness of these behavioral abnormalities in the AS mouse is difficult to reconcile with what is observed among humans with AS. These behavioral findings warrant the question:

Does the AS mouse model possess behavioral features of the human disorder?

Reflecting back to the human disorder, it is more difficult to diagnose a child with AS in their adult years, compared to when they were children[31]. This can be due to differences in the exposure to behavioral therapies, or secondary changes that naturally occur in behavioral circuits. Some features, such as the movement disorder and seizures, are found to improve over time[27,41]. In addition, there is sparing of learning and memory deficits observed among humans with AS, provided enough stimulation or training[29,38].

I hypothesize that the AS mouse will have robust, clinically relevant phenotypes during early development. With the experiments described in this dissertation I examined behaviors that have correlates to the clinical disorder, including communication, locomotor activity, seizure susceptibility and EEG (Figure 1.10). Behavioral deficits that vary according to gender, age and strain were concluded to be clinically non-useful phenotypes. With these guidelines, I have described in this thesis the consistent features of juvenile

mice with Angelman Syndrome that can be used to examine the mechanisms of cellular, neural circuit, and behavioral dysfunction that lead to AS.

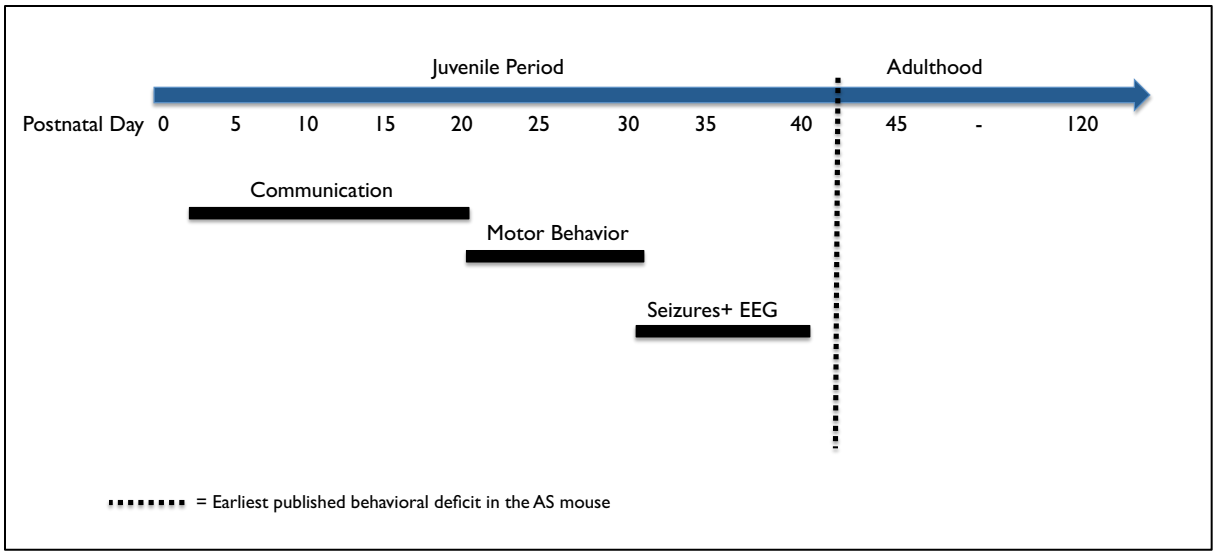

Figure 1.10 Schematic of behavioral battery The timecourse for behavioral testing of AS and WT mice is depicted. The juvenile developmental period is defined by postnatal day 0 through postnatal day 42, the adult developmental period is > postnatal day 42 (age of sexual maturity in mice). The dotted line signifies the earliest published behavioral deficit in the AS mouse.

References

1. Baio J: Prevalence of Autism Spectrum DisordeAmong Children Aged 8 Years — Autism and Developmental Disabilities Monitoring Network, 11 Sites, United States, 2010. MMWR 63:1-22, 2014

2. Parellada M, Penzol MJ, Pina L, et al: The neurobiology of autism spectrum disorders. Eur Psychiatry 29:11-9, 2014

3. Kasari C, Brady N, Lord C, et al: Assessing the minimally verbal school-aged child with autism spectrum disorder. Autism Res 6:479-93, 2013

4. Tager-Flusberg H, Kasari C: Minimally verbal school-aged children with autism spectrum disorder: the neglected end of the spectrum. Autism Res 6:468-78, 2013

5. Dawson G, Osterling J, Meltzoff AN, et al: Case Study of the Development of an Infant with Autism from Birth to Two Years of Age. Journal of Applied Developmental Psychology 21:299-313, 2000

6. Lee BH, Smith T, Paciorkowski AR: Autism spectrum disorder and epilepsy: Disorders with a shared biology. Epilepsy Behav 47:191-201, 2015

7. Kindregan D, Gallagher L, Gormley J: Gait deviations in children with autism spectrum disorders: a review. Autism Res Treat 2015:741480, 2015

8. Maski KP, Jeste SS, Spence SJ: Common neurological co-morbidities in autism spectrum disorders. Curr Opin Pediatr 23:609-15, 2011

9. Robinson EB, Neale BM, Hyman SE: Genetic research in autism spectrum disorders. Curr Opin Pediatr, 2015

10. Neale BM, Kou Y, Liu L, et al: Patterns and rates of exonic de novo mutations in autism spectrum disorders. Nature 485:242-5, 2012

11. Iossifov I, O'Roak BJ, Sanders SJ, et al: The contribution of de novo coding mutations to autism spectrum disorder. Nature 515:216-21, 2014

12. Iossifov I, Ronemus M, Levy D, et al: De novo gene disruptions in children on the autistic spectrum. Neuron 74:285-99, 2012

13. De Rubeis S, Buxbaum JD: Genetics and genomics of autism spectrum disorder: embracing complexity. Hum Mol Genet 24:R24-31, 2015

14. Behnia F, Parets SE, Kechichian T, et al: Fetal DNA methylation of autism spectrum disorders candidate genes: association with spontaneous preterm birth. Am J Obstet Gynecol 212:533 e1-9, 2015

15. Ecker C, Bookheimer SY, Murphy DGM: Neuroimaging in autism spectrum disorder: brain structure and function across the lifespan. The Lancet Neurology, 2015

16. Peters SU, Kaufmann WE, Bacino CA, et al: Alterations in white matter pathways in Angelman syndrome. Dev Med Child Neurol 53:361-7, 2011

17. Ziats MN, Edmonson C, Rennert OM: The autistic brain in the context of normal neurodevelopment. Front Neuroanat 9:115, 2015

18. Liu X, Takumi T: Genomic and genetic aspects of autism spectrum disorder. Biochem Biophys Res Commun 452:244-53, 2014

19. Oddi D, Crusio WE, D'Amato FR, et al: Monogenic mouse models of social dysfunction: implications for autism. Behav Brain Res 251:75-84, 2013

20. Dindot SV, Antalffy BA, Bhattacharjee MB, et al: The Angelman syndrome ubiquitin ligase localizes to the synapse and nucleus, and maternal deficiency results in abnormal dendritic spine morphology. Hum Mol Genet 17:111-8, 2008

21. Gogolla N, Takesian AE, Feng G, et al: Sensory integration in mouse insular cortex reflects GABA circuit maturation. Neuron 83:894-905, 2014

22. Cianfaglione R, Clarke A, Kerr M, et al: A national survey of Rett syndrome: age, clinical characteristics, current abilities, and health. Am J Med Genet A 167:1493-500, 2015

23. Tatsuya Kishino MLJW: UBE3A/E6-AP mutations cause Angelman Syndrome. Nature Genetics, 1997

24. Jeavons BDBaPM: The 'Happy Puppet' Syndrome. Arch. Dis. Childh 42:298, 1967

25. Glessner JT, Wang K, Cai G, et al: Autism genome-wide copy number variation reveals ubiquitin and neuronal genes. Nature 459:569-73, 2009

26. Angelman H: 'Puppet' children. A report on 3 cases. Develop. Med. Child Neurol. 7, 1965

27. Tan WH, Bacino CA, Skinner SA, et al: Angelman syndrome: Mutations influence features in early childhood. Am J Med Genet A 155A:81-90, 2011

28. j Cayton-Smith LL: Angelman Syndrome: a review of the clinical and genetic aspects. Journal of Medical Genetics 40:87-95, 2003

29. Williams CA: The behavioral phenotype of the Angelman syndrome. Am J Med Genet C Semin Med Genet 154C:432-7, 2010

30. Williams CA, Driscoll DJ, Dagli AI: Clinical and genetic aspects of Angelman syndrome. Genet Med 12:385-95, 2010

31. Larson AM, Shinnick JE, Shaaya EA, et al: Angelman syndrome in adulthood. Am J Med Genet A 167A:331-44, 2015

32. Thibert RL, Larson AM, Hsieh DT, et al: Neurologic manifestations of Angelman syndrome. Pediatr Neurol 48:271-9, 2013

33. Hall BD: Adjunct diagnostic test for Angelman syndrome: the tuning fork response. Am J Med Genet 109:238-40, 2002

34. Vendrame M, Loddenkemper T, Zarowski M, et al: Analysis of EEG patterns and genotypes in patients with Angelman syndrome. Epilepsy Behav 23:261-5, 2012

35. Pelc K, Boyd SG, Cheron G, et al: Epilepsy in Angelman syndrome. Seizure 17:211-7, 2008

36. Dagli A, Buiting K, Williams CA: Molecular and Clinical Aspects of Angelman Syndrome. Molecular Syndromology, 2011

37. agli AI MJ, Williams CA.: Angelman Syndrome, GeneReviews® 1998

38. Radstaake M, Didden R, Oliver C, et al: Functional analysis and functional communication training in individuals with Angelman syndrome. Dev Neurorehabil 15:91-104, 2012

39. Kiyoshi Egawa KK, Koichi Inoue, Masakazu Takayama, Chitoshi Takayama, Shinji Saitoh, Tatsuya Kishino,Masatoshi Kitagawa, Atsuo Fukuda: Decreased Tonic Inhibition in Cerebellar Granule Cells Causes Motor Dysfunction in a Mouse Model of Angelman Syndrome. Sci Transl Med 4:1-10

40. Wilson BJ, Sundaram SK, Huq AH, et al: Abnormal language pathway in children with Angelman syndrome. Pediatr Neurol 44:350-6, 2011

41. Mertz LG, Thaulov P, Trillingsgaard A, et al: Neurodevelopmental outcome in Angelman syndrome: genotype-phenotype correlations. Res Dev Disabil 35:1742-7, 2014

42. Bekim Sadikovic PF, Victor Wei Zhang, Patricia A. Ward, Irene Miloslavskaya, William Rhead, Richard Rosenbaum, RObert Gin, Benjamin Roa and Ping Fang: Mutation Update for UBE3A variants in Angelman Syndrome. Human genome variation society 35:1407-1417, 2014

43. Coppola A, Ruosi P, Santulli L, et al: Neurological features and long-term follow-up in 15q11.2-13.1 duplication. Eur J Med Genet 56:614-8, 2013

45. Noor A, Dupuis L, Mittal K, et al: 15q11.2 Duplication Encompassing Only the UBE3A Gene Is Associated with Developmental Delay and Neuropsychiatric Phenotypes. Hum Mutat 36:689-93, 2015

46. Mabb AM, Judson MC, Zylka MJ, et al: Angelman syndrome: insights into genomic imprinting and neurodevelopmental phenotypes. Trends Neurosci 34:293-303, 2011

47. Robert D. Nicholls JHMK, Merlin G. Butlet, Susan Karam & Marc Lalande: Genetic imprinting suggested by maternal heterodisomy in non-deletion Prader-Willi syndrome. Nature 342:281-284, 1989

48. Meng L, Person RE, Huang W, et al: Truncation of Ube3a-ATS unsilences paternal Ube3a and ameliorates behavioral defects in the Angelman syndrome mouse model. PLoS Genet 9:e1004039, 2013

49. Huang HS, Allen JA, Mabb AM, et al: Topoisomerase inhibitors unsilence the dormant allele of Ube3a in neurons. Nature 481:185-9, 2012

50. Yamasaki K: Neurons but not glial cells show reciprocal imprinting of sense and antisense transcripts of Ube3a. Human Molecular Genetics 12:837-847, 2003

51. Grier MD, Carson RP, Lagrange AH: Toward a Broader View of Ube3a in a Mouse Model of Angelman Syndrome: Expression in Brain, Spinal Cord, Sciatic Nerve and Glial Cells. PLoS One 10:e0124649, 2015

52. Malkki H: Neurodevelopmental disorders. Unmuting Ube3a in mice alleviates Angelman syndrome. Nat Rev Neurol 11:66, 2015

53. Meng L, Ward AJ, Chun S, et al: Towards a therapy for Angelman syndrome by targeting a long non-coding RNA. Nature 518:409-12, 2015

54. Jon M. Huibregtse MSaPMH: A cellular protein mediates association of p53 with the E6 oncoprotein of human papillomavirus types 16 or 18. The EMBO Journal 10:4129-4135, 1991

55. Xiaofang Zhou NJ, Shishan Deng, Cai Huang: The Function of Ubiquitin Protein Ligase E3A and its Roles in Human Diseases. Journal of Biochemistry and Molecular Biology 1:14-18, 2015

56. Chowdhury M, Enenkel C: Intracellular Dynamics of the Ubiquitin-Proteasome-System. F1000Res 4:367, 2015

57. Kravtsova-Ivantsiv Y, Sommer T, Ciechanover A: The lysine48-based polyubiquitin chain proteasomal signal: not a single child anymore. Angew Chem Int Ed Engl 52:192-8, 2013

58. Winn PJ, Religa TL, Battey JN, et al: Determinants of functionality in the ubiquitin conjugating enzyme family. Structure 12:1563-74, 2004

59. Huang L: Structure of an E6AP-UbcH7 Complex: Insights into Ubiquitination by the E2-E3 Enzyme Cascade. Science 286:1321-1326, 1999

60. El Hokayem J, Nawaz Z: E6AP in the brain: one protein, dual function, multiple diseases. Mol Neurobiol 49:827-39, 2014

61. WYNN H. KAO SLB, ANDREA L. TALIS, JON M. HUIBREGTSE, AND PETER M. HOWLEY Human Papillomavirus Type 16 E6 Induces Self-Ubiquitination of the E6AP Ubiquitin-Protein Ligase. JOURNAL OF VIROLOGY 74:408–6417, 2000

62. Cooper EM, Hudson AW, Amos J, et al: Biochemical analysis of Angelman syndrome-associated mutations in the E3 ubiquitin ligase E6-associated protein. J Biol Chem 279:41208-17, 2004

63. Yong-hui Jiang DA, Urs Albrecht, Coleen M. Atkins, Jeffrey L. Noebels, Gregor Eichele, J. David Sweatt and Arthur L. Beaudet: Mutation of the Angelman Ubiquitin Ligase in Mice Causes Increased Cytoplasmic p53 and Deficits of Contextual Learning and Long-Term Potentiation. Neuron 21:799-811, 1998

64. Huang HS, Burns AJ, Nonneman RJ, et al: Behavioral deficits in an Angelman syndrome model: effects of genetic background and age. Behav Brain Res 243:79-90, 2013

65. Jana NR: Understanding the pathogenesis of Angelman syndrome through animal models. Neural Plast 2012:710943, 2012

66. Margolis SS, Salogiannis J, Lipton DM, et al: EphB-mediated degradation of the RhoA GEF Ephexin5 relieves a developmental brake on excitatory synapse formation. Cell 143:442-55, 2010

67. Greer PL, Hanayama R, Bloodgood BL, et al: The Angelman Syndrome protein Ube3A regulates synapse development by ubiquitinating arc. Cell 140:704-16, 2010

68. Reiter LT, Seagroves TN, Bowers M, et al: Expression of the Rho-GEF Pbl/ECT2 is regulated by the UBE3A E3 ubiquitin ligase. Hum Mol Genet 15:2825-35, 2006

69. Lee SY, Ramirez J, Franco M, et al: Ube3a, the E3 ubiquitin ligase causing Angelman syndrome and linked to autism, regulates protein homeostasis through the proteasomal shuttle Rpn10. Cell Mol Life Sci 71:2747-58, 2014

70. Mulherkar SA, Sharma J, Jana NR: The ubiquitin ligase E6-AP promotes degradation of alpha-synuclein. J Neurochem 110:1955-64, 2009

71. Sun J, Zhu G, Liu Y, et al: UBE3A Regulates Synaptic Plasticity and Learning and Memory by Controlling SK2 Channel Endocytosis. Cell Rep 12:449-61, 2015

73. Blumkin L, Bradshaw T, Michelson M, et al: Molecular and functional studies of retinal degeneration as a clinical presentation of SACS-related disorder. Eur J Paediatr Neurol 19:472-6, 2015

74. Shepherd JD, Bear MF: New views of Arc, a master regulator of synaptic plasticity. Nat Neurosci 14:279-84, 2011

75. Bramham CR, Worley PF, Moore MJ, et al: The immediate early gene arc/arg3.1: regulation, mechanisms, and function. J Neurosci 28:11760-7, 2008

76. Plath N, Ohana O, Dammermann B, et al: Arc/Arg3.1 is essential for the consolidation of synaptic plasticity and memories. Neuron 52:437-44, 2006

77. BEG PSAA: Angelman syndrome connections. nature 468:907-908, 2010

78. Miura K, Kishino T, Li E, et al: Neurobehavioral and electroencephalographic abnormalities in Ube3a maternal-deficient mice. Neurobiol Dis 9:149-59, 2002

79. Mardirossian S, Rampon C, Salvert D, et al: Impaired hippocampal plasticity and altered neurogenesis in adult Ube3a maternal deficient mouse model for Angelman syndrome. Exp Neurol 220:341-8, 2009

80. Yashiro K, Riday TT, Condon KH, et al: Ube3a is required for experience-dependent maturation of the neocortex. Nat Neurosci 12:777-83, 2009

81. Riday TT, Dankoski EC, Krouse MC, et al: Pathway-specific dopaminergic deficits in a mouse model of Angelman syndrome. J Clin Invest 122:4544-54, 2012

82. van Woerden GM, Harris KD, Hojjati MR, et al: Rescue of neurological deficits in a mouse model for Angelman syndrome by reduction of alphaCaMKII inhibitory phosphorylation. Nat Neurosci 10:280-2, 2007

83. Godavarthi SK, Sharma A, Jana NR: Reversal of reduced parvalbumin neurons in hippocampus and amygdala of Angelman syndrome model mice by chronic treatment of fluoxetine. J Neurochem 130:444-54, 2014

CHAPTER 2

Seizure-like activity in a juvenile Angelman Syndrome mouse model is attenuated by reducing *ARC* expression

Author Contributions

C.M.-B. and M.E.G. designed research

C.M.-B. and J.S. performed research

S.C.D. and A.R. contributed new reagents/analytic tools

C.M.-B. and S.C.D. analyzed data

C.M.-B., J.S., and M.E.G. wrote the paper.

At the time of the submission of this dissertation, much of the work presented is this chapter has been compiled as a manuscript entitled:

Seizure-like activity in a juvenile Angelman Syndrome mouse model is attenuated by reducing ARC expression

Authors and author addresses

Caleigh Mandel-Brehm[a], John Salogiannis[a], Sameer C. Dhamne[b], Alexander Rotenberg[b], Michael Greenberg[a1]

[a]Neurobiology, Harvard Medical School, Boston MA 02115; Harvard Medical School, Boston MA 02115; [b]Department of Neurology, Boston Children's Hospital, Harvard Medical School, Boston, Massachusetts 02115

[1]Corresponding author

Michael E. Greenberg (meg@hms.harvard.edu)

2.1 Abstract

Angelman Syndrome (AS) is a neurodevelopmental disorder arising from loss-of-function mutations in the maternally inherited copy of the *UBE3A* gene, and is characterized by an absence of speech, excessive laughter, cognitive delay, motor deficits and seizures. Despite the fact that the symptoms of AS occur in early childhood, behavioral characterization of AS mouse models has focused primarily on adult phenotypes. In this report we describe juvenile behaviors in AS mice that are strain-independent and clinically relevant. We find that young AS mice, compared to their wild-type littermates, produce an increased number of ultrasonic vocalizations (USVs). In addition, young AS mice have defects in motor coordination, as well as abnormal brain activity that result in an enhanced seizure-like response to an audiogenic challenge. The enhanced seizure-like activity, but not the increased USVs or motor deficits, are rescued in juvenile AS mice by genetically reducing the expression level of the activity-regulated cytoskeleton-associated protein, ARC. These findings suggest that therapeutic interventions that reduce the level of ARC expression have the potential to reverse the seizures associated with AS. In addition, the identification of aberrant behaviors in young AS mice may provide clues regarding the neural circuit defects that occur in AS and ultimately allow new approaches for treating this disorder.

2.2 Background and Significance

Angelman syndrome (AS) is a human neurodevelopmental disorder that occurs in the first few years of life and is characterized by severe developmental delay, an absence of purposeful speech, motor dis-coordination, an abnormal electroencephalogram (EEG), and unusual behavioral traits such as easily provoked laughter and hand flapping [1,2]. Individuals with AS have mutations in the maternally inherited copy of the *UBE3A* gene, resulting in a loss of function of the UBE3A protein (also known as E6AP) [3]. This gene resides within the genomic locus 15q11.2-q13 that is paternally imprinted selectively in neurons such that the allele of *UBE3A* inherited from the father is silenced in neurons, while the maternally inherited copy is expressed [4,5]. How loss of *UBE3A* results in the distinct clinical phenotype of AS is for the most part unknown.

The imprinting of *UBE3A* is evolutionarily conserved and thus AS can be modeled in mice that lack a functional copy of maternally inherited *UBE3A* but have a wild-type copy of the paternally inherited *UBE3A* allele [AS mice] [6]. AS mice have been useful for defining the cellular and molecular function of UBE3A in neurons.

The *UBE3A* gene encodes an E3 ubiquitin ligase that catalyzes the addition of ubiquitin to specific proteins thereby modifying their function and/or targeting the protein for degradation by the proteasome [7]. Recent studies have identified several neuronal proteins that are mis-regulated in AS neurons, including CAMKII, EPHEXIN5, ARC, GAT1, α1-NAKA, NAV1.6 and ANKYRIN-G [8-12]. Some of these proteins are thought to be direct substrates of UBE3A whose expression is increased in the absence of UBE3A due to the failure of these substrates to be targeted for degradation. However, it is possible that some

of these proteins are not direct targets of the UBE3A ligase but rather, their mis-regulation could be an indirect consequence of the disruption of UBE3A function. It remains to be determined how proteins that are mis-regulated upon loss of UBE3A contribute to the etiology of AS.

The AS mouse model has been used extensively for testing potential drugs and gene therapies for treating AS [13,14]. One therapeutic approach has been to identify proteins that are up-regulated in the brains of AS mice and to then search for pharmacological agents that target the expression or activity of the up-regulated protein. An alternative approach has been to restore the expression of *UBE3A* in the brains of AS mice by de-repressing the paternal *UBE3A* allele [15,16]. With approaches for reversing the effects of *UBE3A* loss now in hand, a set of robust behavioral assays is needed to assess the efficacy with which various therapeutic agents reverse the phenotypes of AS.

AS mice have significant neural circuit defects suggesting that in the absence of *UBE3A* there is a disruption of excitatory/inhibitory balance in the brain [6,10,12,13,17-19]. In addition, AS mice display defects in learning and memory, motor coordination, locomotor activity [14,17,20,21] and an increased number of seizures when exposed to an audiogenic challenge [6,11]. However, there have been conflicting reports regarding the robustness of the AS phenotypes observed [22]. One possible explanation for the disparate findings is that these studies have been conducted using adult mice at a time when the aberrant AS behaviors may have begun to subside. Indeed, seizures are prominent in AS in early childhood (<3 years of age) but begin to vary considerably in frequency and severity as children with AS age [2,23,24]. In addition, some core features of human AS that are seen in early childhood such as abnormal communication, have not yet been characterized in the AS mouse. Finally, it

remains a possibility that the behavioral abnormalities observed in adult AS mice might be due to secondary rather than primary effects of mutating the UBE3A protein.

In this study we characterized behaviors in young AS mice to identify robust and reproducible abnormalities that are a direct consequence of the *UBE3A* mutation, and thus might provide useful assays for testing the efficacy of therapies for AS. Here, we report the identification of significant strain-independent behavioral phenotypes in juvenile AS mice. We find that previously described motor behaviors, including hypoactivity and the hindlimb clasp, have developed in AS mice by the time of weaning. Similarly, we observe an abnormal cortical EEG [25] in AS mice prior to adulthood. In addition, we report two new phenotypes in young AS mice, abnormal ultrasonic vocalizations and enhanced latency to recover from an audiogenic stimulus. Finally, we find that reducing the level of the activity-regulated cytoskeletal protein ARC in AS mice selectively attenuates the seizure-like and EEG deficits in these animals. We conclude that young AS mice recapitulate hallmark features of AS in children, and that the early onset behaviors we have characterized in these mice may provide new approaches for evaluating the efficacy of therapies for treating AS in humans.

2.3 Materials and Methods

Animals:

Mice harboring a null mutation in *Ube3a* were obtained from Jackson Laboratories and maintained on C57BL/6J [B6] or 129S2/SvPasCrl [129] background. For all behavioral experiments, B6 Ube3a$^{m+/p-}$ females were used for mating, with the exception of experiments performed on a pure 129 background. To generate mice that have maternal deficiency of *Ube3a* [referred to in this paper as AS mice], Ube3a$^{m+/p-}$ females were crossed with either a B6 or 129 wildtype male. F1 progeny [Hybrid] represent a 50:50 contribution of B6 and 129. For genetic interaction experiments, male mice heterozygous for *ARC* [referred to as ARC$^{+/-}$] or *Ephexin5* [referred to as E5$^{+/-}$] were crossed to Ube3a$^{m+/p-}$ females. ARC$^{+/-}$ mice were provided as a gift from the lab of Dr. Paul Worley and maintained on a B6 background for at least 10 generations. E5$^{+/-}$ mice were generated in-house and maintained on a 129 background for at least 10 generations. Animals were kept on a 12-h light/dark cycle and given food and water ad lib. All experiments were performed and analyzed blind to genotype. Genotyping was conducted by PCR from tail tissue samples at least twice for validation. All procedures were conducted in strict compliance with the Institutional Animal Care and Use Committee at Harvard Medical School.

Maternal-isolation induced Ultrasonic Vocalization Assay (PND 3 – 19):

Pregnancies were recorded by visual inspection and the day of birth was considered postnatal day 0 (PND 0). For the duration of the experiment (E18 - PND 19) the mating pair remained together in the cage and the bedding was changed minimally (PND 8, PND 16) to

keep odors unperturbed. USV testing occurred every other day from PND 3-19 during the hours 9AM – 1PM. Pups were moved from the home cage into the recording environment by holding their tail, and the presence or absence of hindlimb clasp activity was noted. Pups were kept in a warming cage until all littermates had been tested.

Individual pups were placed into a plastic bucket contained within a sound attenuated chamber (Med-Associates, Inc.) for four minutes. USVs were sampled at 250 kHz using a broadband microphone (Avisoft) suspended 10 inches above the pup. Following testing on PND 3, pups were given unique identifiers on their paws using tattoo ink (Ketchum Inc.).

Ultrasonic Vocalization Analysis*:*

For acoustical analysis, sound files were analyzed using Avisoft SASLab Pro (version 4.50). The total four minute recording time for each trial was used for analysis. Fast Fourier Transformation was conducted using Hamming window, 512 FFT Length, 100% Frame and 50% Overlap providing 488 Hz frequency resolution and 1.024 ms temporal resolution. USV detection was performed using a fixed amplitude threshold of -60 dB and minimum call duration of 1 ms. For structural analysis, we measured the frequency (Hz) at the point of maximum amplitude and the mean amplitude of each vocalization. For the temporal analysis, we analyzed intercall interval (the time in-between sequential calls that occur less than 100 ms from one another) and interburst interval (time in-between bursts of calls that occur more than 101 ms and less than 500ms from one another) for each recording (see Figure 2.1). Background/movement noise was eliminated using an entropy algorithm with a max entropy threshold of 0.4. USV data was visually inspected for

false positives and analysis settings were validated with trials of adult mice moving freely about the testing chamber. Zero vocalizations identified in our automated analysis were removed from the dataset or modified.

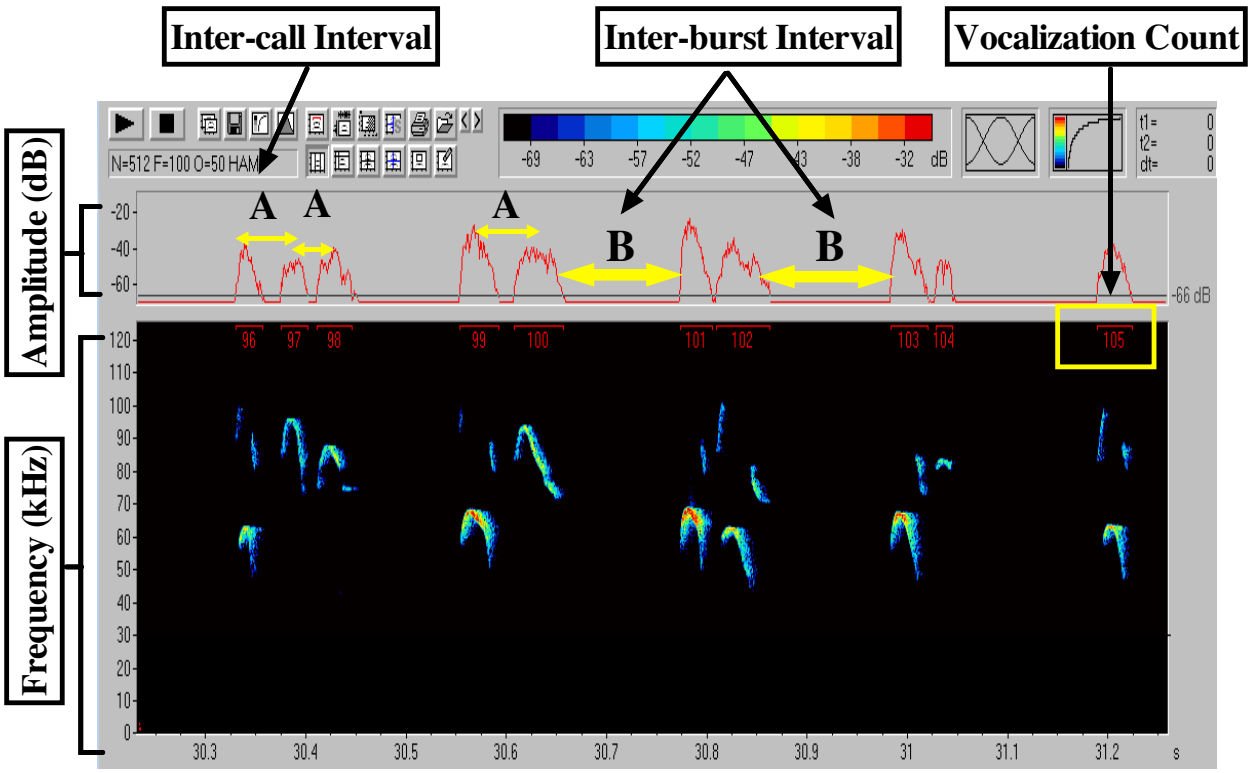

Figure 2.1 Screenshot of Ultrasonic Vocalization Analysis depicting Intercall and Interburst Interval. Maternally isolated USVs are visualized and analyzed using Avisoft Sound Analysis Software. Examples of the intercall interval are depicted as "A" and examples of the interburst interval are depicted as "B." Time window is approximately one second.

Open Field Assay (PND 21):

Activity was measured (weaning age) in a 20" x20" x20" plexiglass box in 200 lux lighting. Movement was recorded using an overhead CCV camera for 10 minutes. Total distance traveled was analyzed offline using tracking analysis software (Noldus, Ethovision XT).

Hindlimb Clasp Assay (PND 30):

Animals were suspended by their tail 10 cm above the lab bench (measured from the tip of the tail) for 20 seconds. Each animal received two trials, with 10-minute inter-trial intervals. Trials were recorded with a CCV camera and scored offline by an experimenter blind to genotype. Clasping behavior was defined by movement of the hindlimb(s) curling inward toward the belly of the animal. The total time spent clasping across two trials was averaged and severity score was determined as follows: 0.0 (0 seconds clasping), 0.5 (<1 second clasping), 1.0 (between 1 and 5 seconds), 1.5 (between 5 and 10 seconds clasping) and 2.0 (> 10 seconds clasping).

Audiogenic Stimulus Assay (PND 30):

Animals were habituated to testing environment (plexiglass cylinder 10" diameter, 12" height) for 5 minutes. Audiogenic stimulus was performed by scraping the metal bars of a cage top approximately 15" above test subject. The stimulus lasted 45 seconds or until tonic-clonic seizure was observed visually. Following cessation of the stimulus the latency to recover was recorded. Recovery was called when any of the four paws were lifted from the ground, including walking, grooming or stretch attending behaviors.

EEG/EMG Surgeries:

Mouse EMG/EEG 3-Channel headmounts and accessories for subdural cortical EEG recordings were purchased from Pinnacle, Inc. (Model No. 8201, 8202, 8206). On PND 28, animals were anesthesized with continuous flow of 1% Isoflourane. Headmounts were glued on to the cranium and pilot holes for screws were made using a 25-gauge needle. Steel screws were set into four fixed locations on the headmount, with two recording electrodes over the posterior left and right cortex and two reference electrodes in the left and right frontal cortex. Screws were electrically coupled to the headmount through quick setting epoxy applied underneath the screw head. Dental glue was applied to keep headmount in place and screws isolated from external noise. Two single wire electrodes for EMG recordings were implanted in a small pocket of the nuchal muscles. Animals were injected with 1% Flouxetine at the end of surgery and monitored daily while receiving two doses of Flouxetine every 24 hours for 3 days following surgery. EEG and EMG activity was measured on day 5 following surgery.

Electroencephalographic Recordings (PND 35):

Mice were acutely anesthetized in Isoflourane to minimize anxiety during the process of connecting the headmount to the preamplifier. EEG/EMG recording started when recovery of movement was observed and data was collected continuously for three hours (sampling rate 400 Hz). Data used for analysis started one hour after recording start time. See SI methods for details regarding surgery procedure and spiking analysis.

EEG Spiking Analysis*:*

Raw EEG files were converted to the generic .edf format (EDF browser v1.22, Teunis van Beelen, Netherland) and then imported into Matlab (Mathworks Inc., 2011a) for analysis. Fast Fourier transformation of .edf files were processed and visualized using a custom program in Matlab developed by Dr. Gary Yellen, HMS. EEG signals were transformed to frequency domain and power in frequency bands of 2-4Hz, 4-8Hz, 8-12Hz, 12-20Hz, and 20-80Hz. For the power spectrum, the amount of EEG in a band is quantified in units of microvolts squared. Using spectrogram analysis we found that the spikes in EEG possessed harmonics throughout the 4-80Hz range, which reliably caused an increase in power in the 20-80Hz range. Since the majority of power during normal brain activity occurs in the lower frequency bands (<20Hz), these small "bumps" in power in the higher frequency bands (20-80Hz) caused by spiking activity, were easy to differentiate. A spiking event was recorded when a change in power > 10dB occurred in the 20-80Hz frequency band. We chose to use a power threshold (dB) instead of amplitude (υV) threshold due to variance in voltage baselines. Spiking events were recorded manually while visually scanning EEG files offline in 10-second window intervals. Our EEG spike analysis was validated against an automated seizure detection algorithm (1). Our results were very consistent with this independent mode of analysis and exhibited a high correlation (r = 0.97) between both approaches (Figure 2.2).

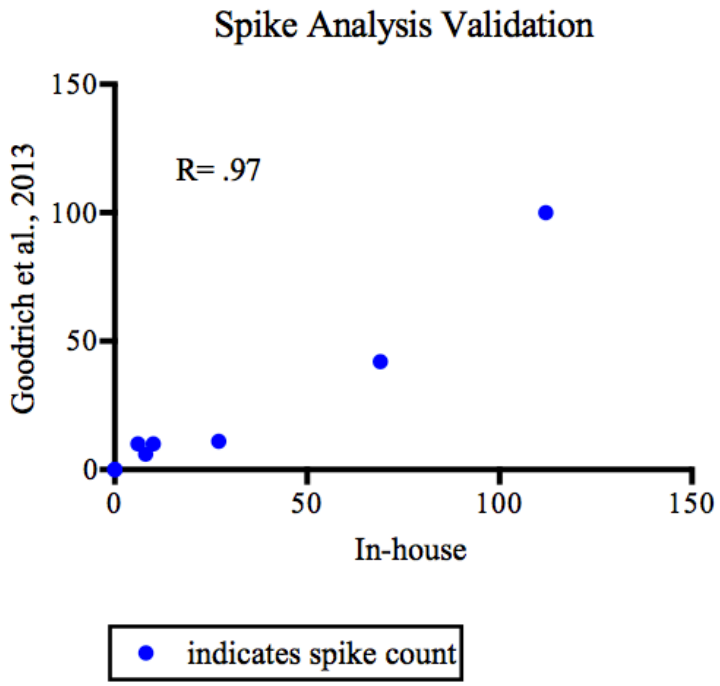

Figure 2.2 Validation of spiking analysis for EEG recordings The total number of spiking events were quantified manually in-house. To validate our analysis, a subset of EEG files (WT n=3, AS n=3) were analyzed with an automated spike detection program. Pearson's correlation was used for statistical analysis[26].

Protein Extraction/ Western Blot:

Freshly dissected mouse hippocampi or cultured cells (plated E16.5 and stimulated DIV7) were collected and dounce homogenized in RIPA buffer (50 mM Tris pH 8.0, 150 mM NaCl, 1% Triton X-100, 0.5% Sodium Deoxycholate, 0.1% SDS, 5 mM EDTA, 10 mM NaF, complete protease inhibitor cocktail tablet (Roche), 1 mM sodium orthovanadate, 1 mM b-glycerophosphate). For western blots, samples were boiled for 5 min in SDS sample buffer, resolved by SDS PAGE, transferred to nitrocellulose, and immunoblotted. Antibodies were diluted 1:1000 in 3% BSA with Sodium Azide and never used more than 3 times for immunoblotting. Antibodies are as follows: αARC (gift from Dr. Paul Worley); αE6AP (Sigma), αNPAS4 (in-house), αB2-ACTIN (Sigma), αGAPDH (Abcam). For quantification, each sample was ran in triplicate and normalized to a loading control.

2.4 Results

Overview of behavioral analysis

For the studies described below, we classified mice less than postnatal day 42 (<PND 42) as juvenile, and mice older than postnatal day 42 (>PND 42) as adults. We assessed AS phenotypes using two different mouse strains, pure B6 [B6] and F1 Hybrids of B6:129 [Hybrid], unless otherwise noted. In all cases the experiments were carried out using both male and female mice at an approximately 1:1 ratio. The time window for behavioral characterization extends from PND 3 to PND 35.

AS mice display an altered developmental time course of ultrasonic vocalizations

Ultrasonic vocalizations (USVs) produced by mouse pups when they are isolated from their mother have been suggested to be a means by which the pups seek parental care. Notably, this form of communication is disrupted in various mouse models of autism [27-29]. To determine if there is a defect in USV production in AS mice we recorded and quantified USVs emitted by wildtype [WT] and AS littermates while isolated from their homecage for four minutes. We found that throughout early postnatal development, the frequency and amplitude of USVs are similar between WT and AS mice (Figure 2.3 *A* and *B*). In addition, the intercall and interburst interval between USVs was unperturbed in AS mice (Figure 2.3 *C* and *D*). These data suggest the robust structural and temporal features of USV production are largely intact in AS mice.

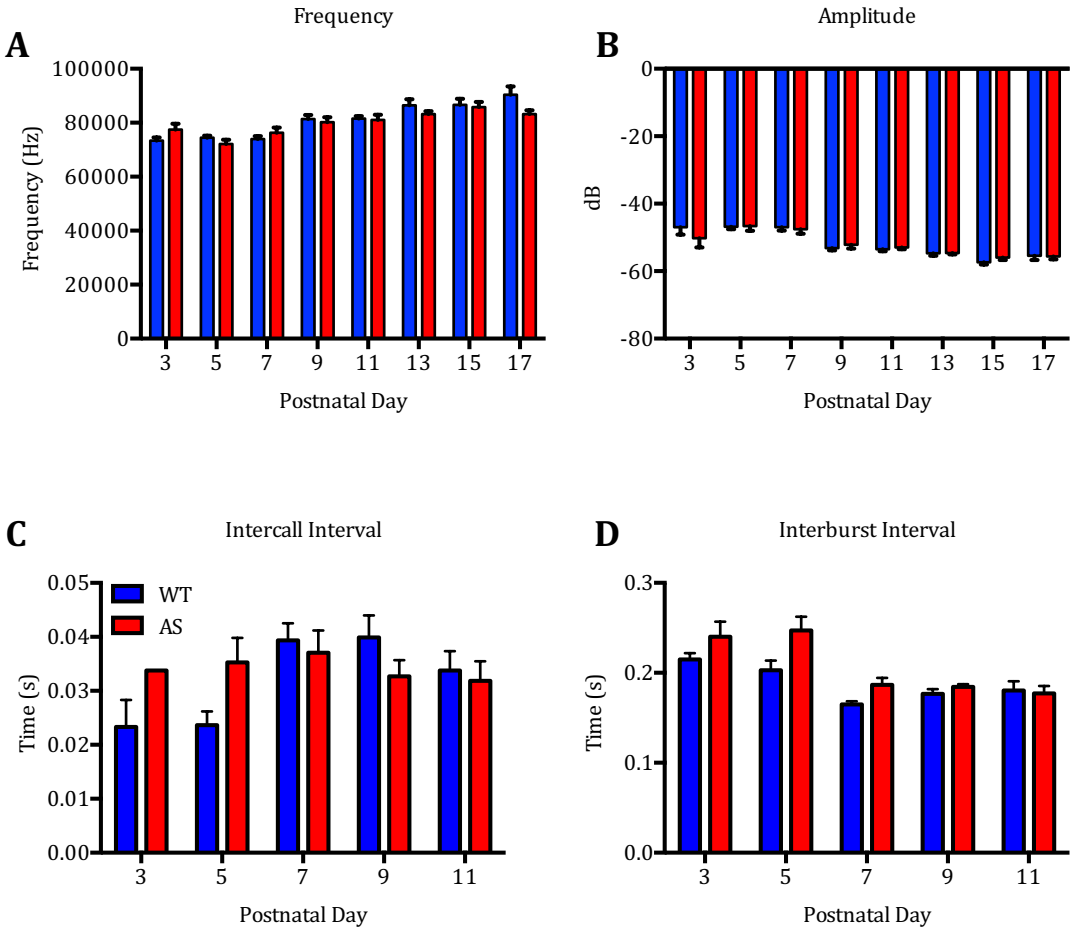

Figure 2.3 Structural and temporal features of ultrasonic vocalizations in AS mice are indistinguishable from WT littermates.

(A) Average frequency of vocalizations (WT n=8, AS n=9)

(B) Average amplitude of vocalizations (WT n=8, AS n=9)

(C) Average intercall interval (WT n=8, AS n=9)

(D) Average Interburst interval (WT n=8, AS n=9).

Statistics for (A-D): Two-way, non-repeating measures ANOVA; Bonferroni multiple comparisons correction.

In contrast, we found a significant difference in the total number of USVs emitted by AS mice (Figure 2.4 *A-C*). As in previous studies [30], we found that WT mice display a highly stereotyped time-course of USV production, with a peak in the total number of calls produced on PND 7 and a drastic reduction by PND 15. We found that AS mice produce a larger number of USVs relative to WT mice between PND 13-PND 17. Similar findings were obtained when the AS mutation was crossed to three different background strains of mice.

To determine whether disruption of the maternally inherited, neuronally expressed *Ube3a* gene is the cause of the altered USVs, we performed the USV assay using mice in which the paternal *Ube3a* gene, rather than the maternally inherited gene, is mutated (termed PAT mice). Because the paternally derived *Ube3a* gene is not expressed in neurons, PAT mice might be predicted not to display a USV phenotype since neurons in these mice express the wild type *Ube3a* gene inherited from their mother. We found that USV production in PAT mice is indistinguishable from that of their WT littermates (Figure 2.4 *D*).

Variables inherent in our experimental design could account for the increase in USV production in AS mice. One possibility is that the increase in USV production is due to improper or insufficient care of AS mouse pups by their mother [31]. To address this possibility we weighed AS and WT pups immediately after USV testing on each day. We found that AS and WT littermates show no differences in weight gain throughout early development (Figure 2.5 *A-C*) suggesting that the pups have access to maternal care, irrespective of genotype. Previous studies have shown that postnatal handling of mouse pups can modify emotional circuits, reducing anxiety-like behaviors and stress responses in adulthood [32,33].

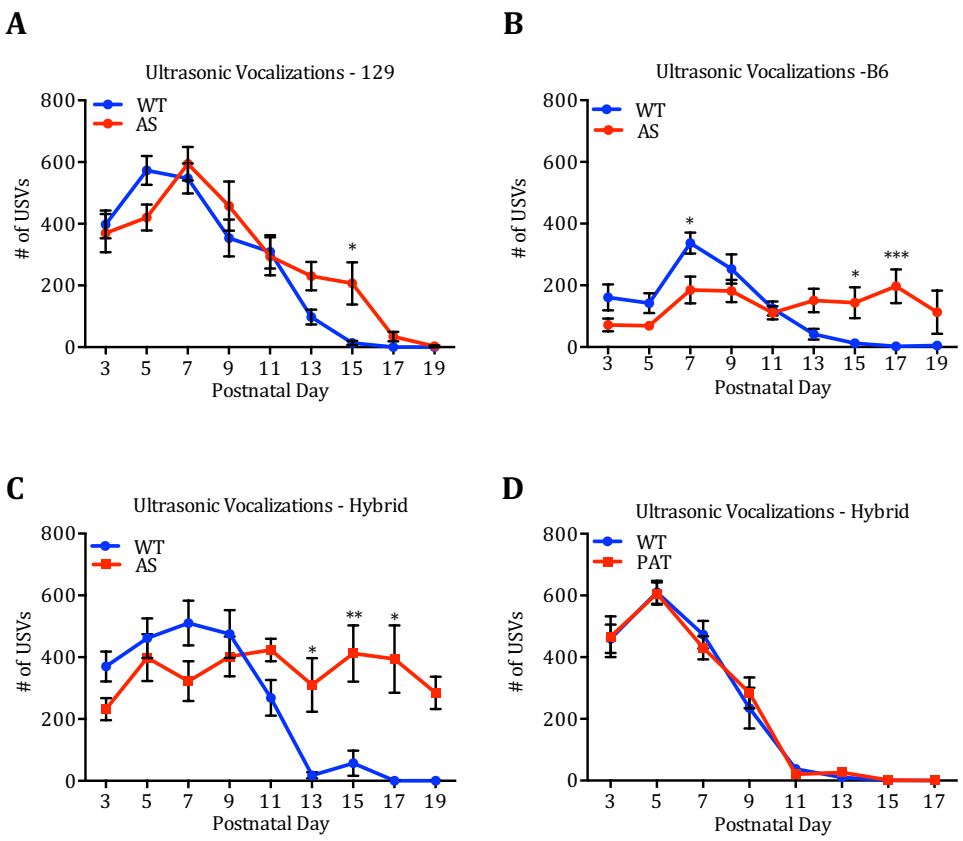

Figure 2.4 Loss of the maternally inherited *Ube3a* gene leads to abnormal ultrasonic vocalization (USV) production. The total number of USVs emitted from maternally isolated mouse pups throughout postnatal development.

(A-C) WT and AS littermates are compared on a 129 (n: WT=12; AS=15), B6 (n: WT=15; AS=18) and Hybrid (n: WT=24; AS=22) genetic background, *respectively*.

(D) Mutation of the paternal copy of *Ube3a* [PAT mice] does not lead to changes in USV production (n: WT=11; PAT=13).

Statistics for (A-D): Two-way, non-repeating measures ANOVA; Bonferroni correction for multiple comparisons. *Indicates $p<.05$, **$p<.01$, ***$p<.0001$. Error bars represent SEM.

However, when USV production was monitored on PND 16 with AS and WT mice that had experienced no prior investigator handling, we found that AS mice still produced significantly more USVs than their WT littermates **(**Figure 2.5 *D* and *E*). This suggests that repetitive handling is not likely an explanation for the observed phenotype.

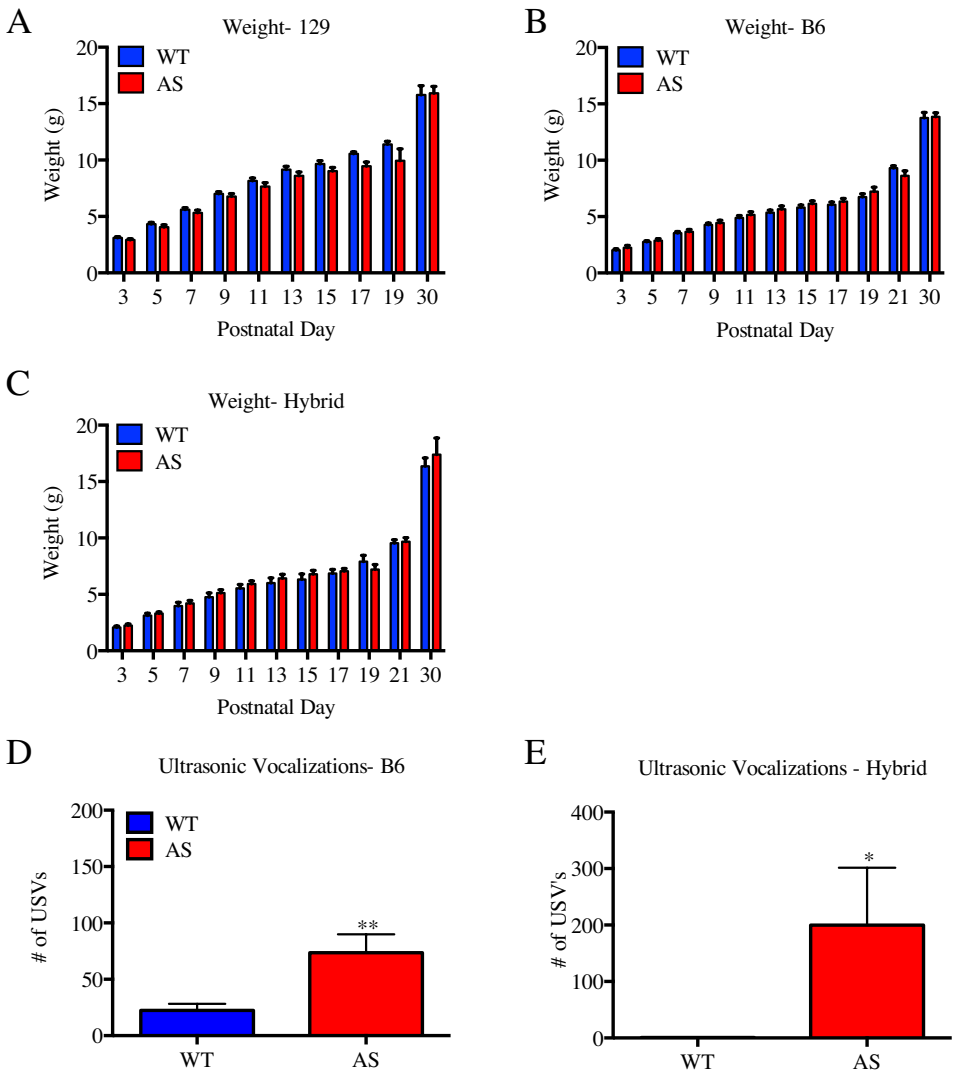

Figure 2.5 USV phenotype in AS mice is not due to differences in postnatal weight or repetitive handling.

Figure 2.5 (Cont'd)

(A-C) Weight of WT and AS littermates during early postnatal development are compared on a 129 background (WT n=11; AS n=7), B6 background (WT n=19, AS n=15), and hybrid background (WT n=11, AS n=10), *respectively*.

(D-E) USVs measured from naïve WT and AS mice at PND 16 as done previously (see Figure 2.2 A-D). AS mice exhibited significantly more USVs than WT littermates on a B6 background (WT n=13; AS n=15) and hybrid background (WT n=7; AS n=5).

Statistics for (A-C): Two-way, non-repeating measures ANOVA; Bonferroni multiple comparisons correction.

Statistics for (D-E): Unpaired two-tailed t-test. *Indicates $p<.05$, **$p<.01$. Error bars represent SEM.

Early postnatal motor deficits in AS mice

To assess motor coordination during early postnatal development we tested locomotor activity of AS and WT mice at PND 21 using the open field assay**.** In this assay, mice are allowed to freely explore an arena for 10 minutes while movement of the mice is recorded and then analyzed using motion tracking software. This analysis revealed that AS mice travel significantly less than their WT littermates (Figure 2.6).

We next assayed WT and AS mice for the presence of the hindlimb clasp, a behavior that is considered to be a general indication of an impaired motor response circuit**.** At PND 30, AS mice have a pronounced hindlimb clasp phenotype compared to WT mice (Figure 2.6 *B*). We next considered the possibility that the hindlimb clasp response might manifest itself earlier than PND 30 since other deficits in AS mice occurred at earlier times during development than previously appreciated. We found that hindlimb clasp behavior occurs in both WT and AS mice as early as PND 13; interestingly, the frequency of this behavior is dramatically increased within the population of AS mice at a similar time to the onset of USV abnormalities (Figure 2.7 *A* and *B)*.

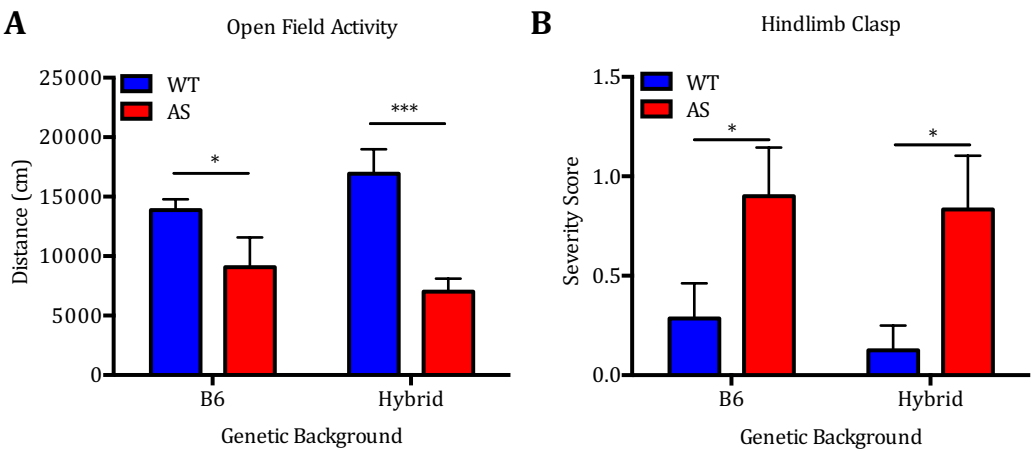

Figure 2.6 Young AS mice have abnormal motor activity compared to WT littermates in open field arena and hindlimb clasp assay.

(A) Total distanced traveled in an open field arena at PND 21 is compared between WT and AS littermates on a B6 (n: WT=11; AS=4) and Hybrid (n: WT=9, AS=10) genetic background.

(B) Hindlimb clasp behavior is compared between WT and AS littermates at PND 30 on a B6 (n: WT=7; AS=5) and Hybrid (n: WT=7; AS=6) genetic background. Severity score for hindlimb clasp was determined by the average time spent clasping during two 20-second trials (see Methods).

Statistics for (A-B): WT and AS littermates on B6 or Hybrid backgrounds were analyzed individually with an unpaired, two-tailed t-test prior to plotting on a single graph.

*Indicates $p<.05$. Error bars represent SEM.

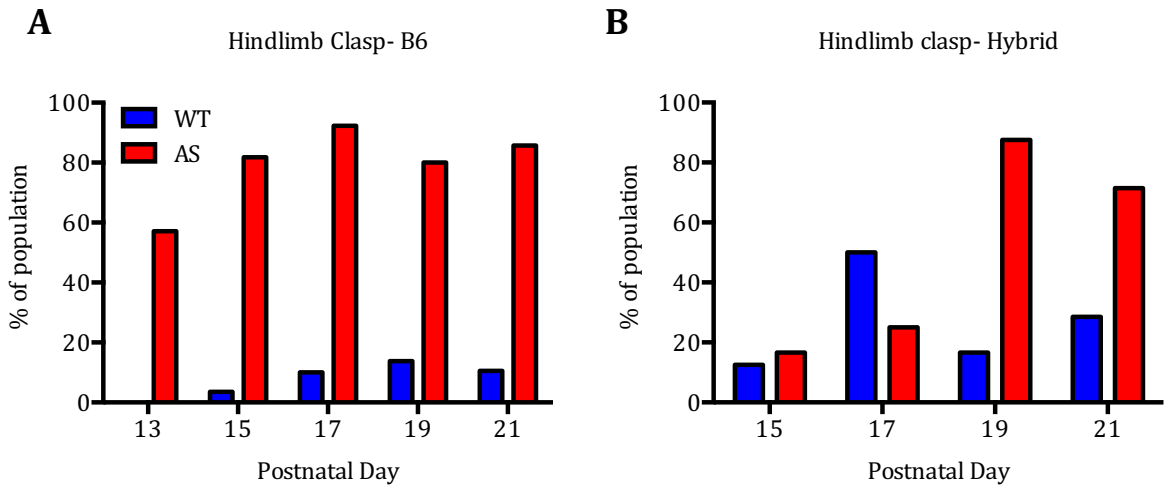

Figure 2.7: AS mice have increased frequency of hindlimb clasping in early development when compared to WT littermates. Hindlimb clasp activity compared between WT and AS mice from PND 3 through PND 21.

(A) B6 genetic background (WT n= 5-16; AS n= 7-9).

(B) Hybrid genetic background (WT n=9; AS n=7-10).

Juvenile AS mice have an enhanced seizure-like response to audiogenic stimulus and abnormal cortical EEGs

Seizures in AS occur as early as six months of age, and often precede clinical diagnosis of AS in humans. The susceptibility to seizures has been studied in adult AS mice (>PND 42) using an audiogenic stimulus assay [6,11]. Previous studies indicate that adult mice on a pure B6 background are more resistant to seizure induction than other strains, such as 129, however juvenile mice have not been investigated [34]. In our pilot experiments using the audiogenic stimulus assay at PND 25, we found that 60% of WT mice on a 129 background exhibited debilitating tonic-clonic seizures that led to death. The high frequency of fatal seizures observed in the 129 WT population may limit our ability to detect differences in seizure activity between WT and AS mice. Thus, we focused on mice in the B6 background, which are known to have less severe seizures. Pilot experiments using B6 mice revealed that none of our WT mice exhibited seizure-induced death and the mice ceased moving and displayed freezing behavior when the audiogenic stimulus was terminated (referred to in this paper as a "seizure-like" response). Thus, we were able to quantify the seizure-like response of these mice by measuring the latency with which these mice regain motor activity when the audiogenic stimulus is discontinued. This analysis revealed that young AS mice take a significantly longer time to recover following the cessation of the audiogenic stimulus (Figure 2.8 *A* and *B*).

In humans with AS, seizure progression is quite variable with age. While seizures are first observed in early childhood, they are typically less prevalent in older children but can reappear in adults [23]. Therefore, we asked if the response of WT and AS mice to an audiogenic stimulus changes as the mice mature. Using the audiogenic stimulus protocol,

we found that in contrast to our observations with young mice, during adulthood (PND 42-90) there is no significant difference between WT and AS mice in their latency to recover from an audiogenic stimulus (Fig. 2.8 *C*). The average WT latency to recover from the audiogenic stimulus does not change as WT mice mature, suggesting that as AS mice mature, their ability to recover from an audiogenic stimulus improves.

To investigate further the neurological basis of the enhanced seizure susceptibility in AS mice, we used subdural electroencephalographic recordings (EEGs) to measure basal cortical activity. Electrodes were implanted in mice in the posterior cortex on PND 25 and recordings were performed between ages PND 30 to PND 35. Basal brain activity in AS mice was indistinguishable from their WT littermates, however, AS mice possessed infrequent high amplitude "spiking" events. These high amplitude (>200μV) spikes occurring within the 4-8 Hz range have been observed in the hippocampus and cortex of adult AS mice and qualitatively described [20]. We quantified spiking activity (see Methods) and found AS mice have significantly more spiking events compared to WT littermates (Figure 2.11). Thus, abnormal EEG activity can be observed in AS mice as early as PND 30.

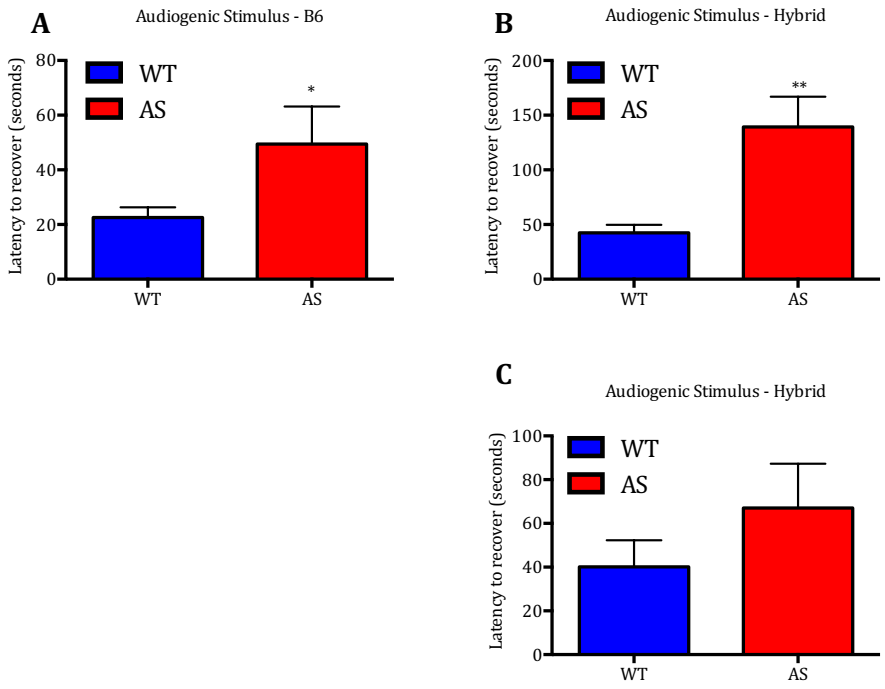

Figure 2.8: AS mice have an enhanced latency to recover from an audiogenic stimulus.

(A-B) Total time to recover motor activity following an audiogenic stimulus between AS mice and WT littermates on a B6 background (n: WT=7; AS=5) and Hybrid background (n: WT=7; AS=8).

(C) Audiogenic stimulus phenotype in AS mice becomes less robust in adulthood. WT and AS mice were subject to the audiogenic stimulus assay throughout the adult period PND 42- 90. Latency to recover was indistinguishable between WT and AS mice littermates (WT n= 8; AS n=10).

Statistics: Unpaired, two-tailed t-test. *Indicates $p<.05$, **$p<.01$. Error bars represent SEM.

Lowering the level of *ARC* rescues abnormal brain activity in AS mice

Having identified strain-independent and robust behavioral deficits, we next asked if it was possible to reverse these phenotypes by decreasing the expression of neuronal proteins whose expression has been suggested to be up-regulated in the AS mouse. Towards this end we focused our attention on ARC and EPHEXIN5 [E5] two proteins that regulate synapse number and/or function [8,9,35,36]. To reduce the level of ARC expression in AS mice, we mated Ube3a$^{m+/p-}$ females with males that are heterozygous for a knockout allele for *ARC* [ARC$^{+/-}$]. This cross produces four genotypes: Ube3a$^{m-/p+}$ mice [AS mice], Ube3a$^{m-/p+}$ mice that also have the ARC$^{+/-}$ allele [AS-ARC$^{+/-}$ mice] as well as WT mice and ARC$^{+/-}$ mice for littermate comparison. To confirm that the expression of *ARC* is reduced using this genetic approach, we quantified *ARC* mRNA levels using qPCR analysis on all four genotypes. As *ARC* is an activity-regulated gene [37], we induced its expression by exposing mice to an enriched environment for one hour prior to harvesting hippocampal mRNA. We found that ARC$^{+/-}$ mice, both in the WT and AS background, display an approximately 50% reduction in the level of *ARC* mRNA expression (Figure 2.9). By contrast, the expression of other activity-regulated genes (i.e., *Fos, Bdnf* and *Npas4*) was not reduced in ARC$^{+/-}$ mice, suggesting that the decrease in *ARC* mRNA expression is a direct consequence of the mutation of *ARC*, and is not due to a global change in activity-regulated gene networks (Figure 2.9).

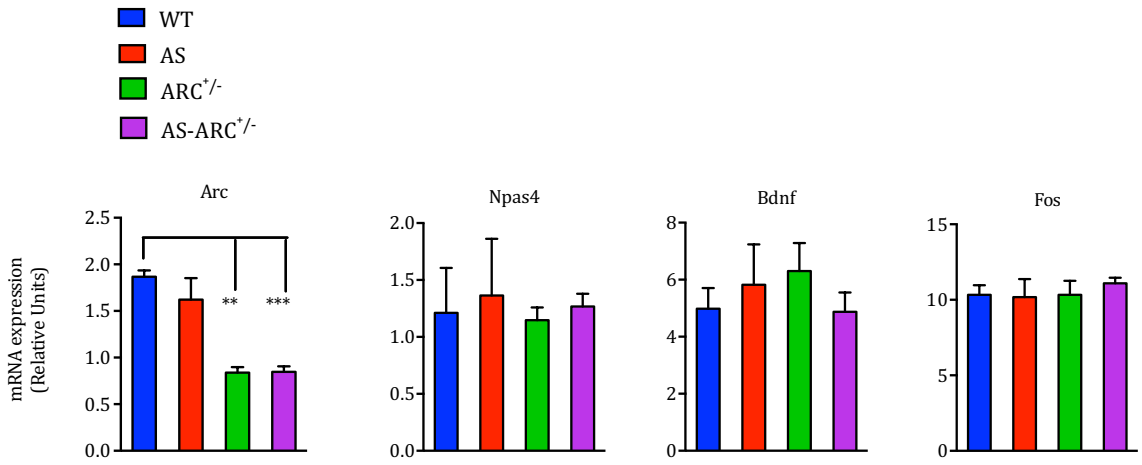

Figure 2.9: Heterozygosity of ARC allele leads to 50% reduction in ARC mRNA levels. Following exposure to an enriched environment, ARC$^{+/-}$ and AS-ARC$^{+/-}$ mice have reduced *ARC* mRNA expression compared to WT littermates. *ARC* heterozygosity does not affect induction levels of other known immediate-early genes *Fos, Bdnf* and *Npas4.* Relative Units reflects Ct values normalized to Tubulin. (n: WT=2; AS=4; ARC$^{+/-}$=8; AS-ARC$^{+/-}$=4). Statistics: Two-way ANOVA; Bonferroni correction for multiple comparisons. **Indicates $p<.01$, ***$p<.001$. Error bars represent SEM.

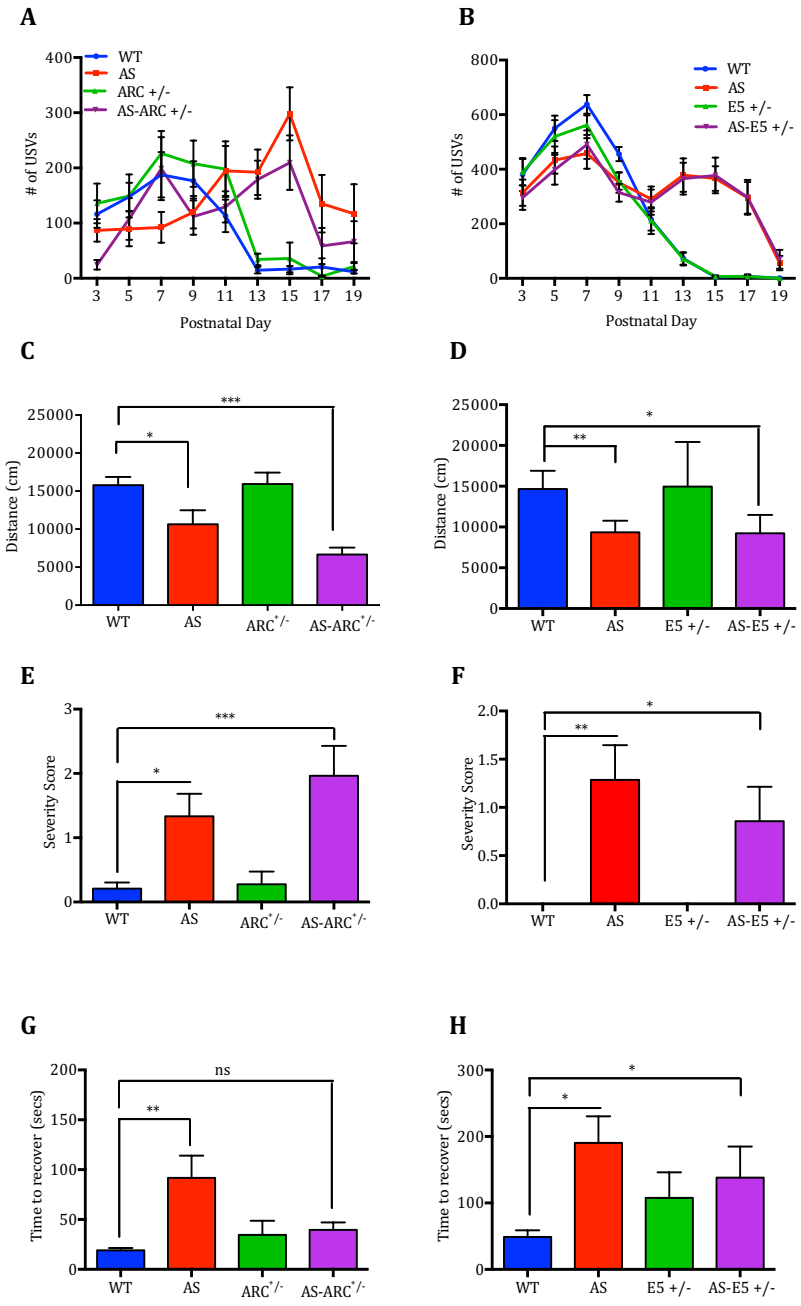

Figure 2.10 Lowering levels of *ARC*, but not *Ephexin5*, rescues audiogenic stimulus phenotype in AS mice, but not USV or motor deficits.

(A-H) Behavioral analysis of progeny generated from *Ube3a* x *ARC* (**Left**) and *Ube3a* x *E5* (**Right**) genetic interaction.

Figure 2.10 (Cont'd)

(A-B) Total number of USVs emitted during maternal isolation throughout postnatal development (*Ube3a* x *ARC*: WT=16; AS=18; $ARC^{+/-}$=13; AS-$ARC^{+/-}$=10 /*Ube3a* x *E5*: WT=17; AS=16; $E5^{+/-}$=19; AS-$E5^{+/-}$=17).

(C-D) Total distance traveled in open field arena at PND21. (*Ube3a* x *ARC*: WT=13; AS=6, $ARC^{+/-}$=5; AS-$ARC^{+/-}$=5 /*Ube3a* x *E5*: WT=7; AS=3; $E5^{+/-}$=4; AS-$E5^{+/-}$=5)

(E-F) Hindlimb clasp severity measured at PND 30 (*Ube3a* x *ARC*: WT=12; AS=12; $ARC^{+/-}$=10; AS-$ARC^{+/-}$=7 /*Ube3a* x *E5*: WT=9; AS=7; $E5^{+/-}$=7; AS-$E5^{+/-}$=7)

(G-H) Latency to recover motor activity following audiogenic stimulus at PND 30 (*Ube3a* x *ARC*: WT=12; AS=13; $ARC^{+/-}$=10; AS-$ARC^{+/-}$=7 /*Ube3a* x *E5*: WT=9; AS=7; $E5^{+/-}$=7; AS-$E5^{+/-}$=7) Statistics for (A-H): Two-way ANOVA; Bonferroni correction for multiple comparisons. *Indicates $p<.05$, **$p<.01$ ***$p<.001$. Error bars represent SEM.

We next asked if reducing the level of ARC or E5 expression reverses the defects in USV production, motor function, and seizure-related activity that we detect in AS mice. We found that reducing the level of ARC or E5 expression has no effect on the number of USVs in the AS mice (Figure 2.10 A and B), does not modify the hypoactivity observed in the open field assay (Figure 2.10 C and D), and does not reverse the pronounced hindlimb clasp observed in AS mice (Figure 2.10 E and F).

Given that ARC regulates surface AMPA receptor expression at excitatory synapses, and consequently influences neuronal excitability, and E5 has been shown to restrict the number of excitatory synapses, we considered the possibility that an increase in the level of ARC and/or E5 might underlie the seizure-related phenotypes in AS mice. To investigate seizure activity under conditions where ARC or E5 levels are reduced, we exposed mice to an audiogenic stimulus as described above and assessed the time it took for the mice to regain mobility after the stimulus was terminated. We found that reducing the level of ARC expression in AS mice completely reverses their enhanced response to the audiogenic stimulus. By contrast reducing the level of E5 expression had no effect on the response of AS mice to the audiogenic stimulus (Figure 2.10 G and H). To assess directly the effect of reducing ARC expression on the seizure-like activity observed in AS mice EEG recordings were performed. This analysis revealed that reducing ARC mRNA expression completely reverses the increased spiking frequency observed in AS mice (Figure 2.11).

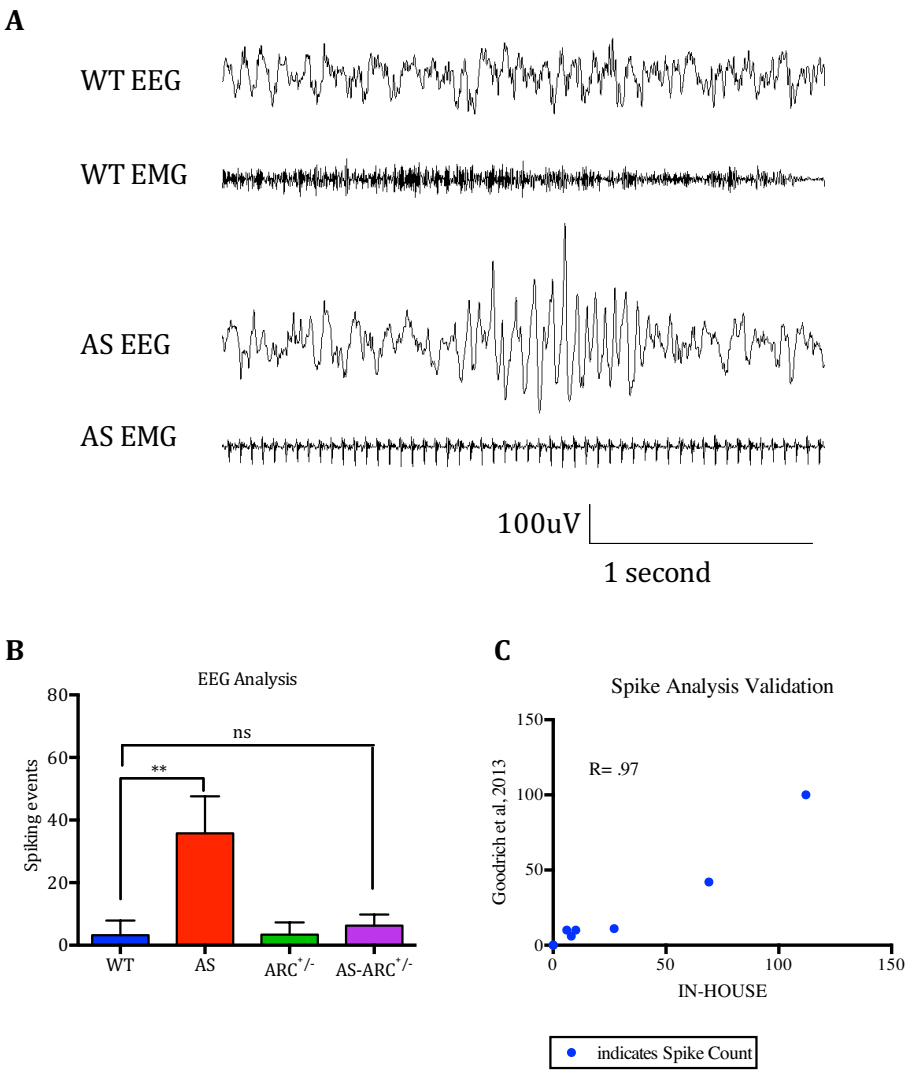

Figure 2.11 AS mice have significantly more large amplitude spiking events compared to WT mice and this phenotype can be reversed by lowering levels of *ARC.*

(A) Representative EEG from WT and AS mice at PND 30. High amplitude (~ 200μV), 4-8 Hz spiking events are depicted in the AS EEG trace. Note: Simultaneous EMG recording shows immobility of AS mouse during spiking activity.

Figure 2.11 (Cont'd)

(B) Quantification of spiking activity from progeny of UBE3A x ARC genetic interaction (n: WT=9; AS=9; $ARC^{+/-}$=13; AS-$ARC^{+/-}$=7). Statistics: Two-way ANOVA; Bonferroni correction for multiple comparisons. **Indicates p<.01. Error bars represent SEM.

(C) Validation of spiking analysis for EEG recordings. Total number of spiking events was measured manually (See Supplemental Methods) in-house. To validate of our analysis, a subset of EEG files (WT n=3, AS n=4) were analyzed with an automated spike detection program (1). Pearson's correlation was used for statistical analysis. R = 0.97

References

1. Angelman H: 'Puppet' children. A report on 3 cases. Develop. Med. Child Neurol. 7, 1965

2. Tan WH, Bacino CA, Skinner SA, et al: Angelman syndrome: Mutations influence features in early childhood. Am J Med Genet A 155A:81-90, 2011

3. Tatsuya Kishino MLJW: UBE3A/E6-AP mutations cause Angelman Syndrome. Nature Genetics, 1997

4. Robert D. Nicholls JHMK, Merlin G. Butlet, Susan Karam & Marc Lalande: Genetic imprinting suggested by maternal heterodisomy in non-deletion Prader-Willi syndrome. Nature 342:281-284, 1989

5. j Cayton-Smith LL: Angelman Syndrome: a review of the clinical and genetic aspects. Journal of Medical Genetics 40:87-95, 2003

6. Yong-hui Jiang DA, Urs Albrecht, Coleen M. Atkins, Jeffrey L. Noebels, Gregor Eichele, J. David Sweatt and Arthur L. Beaudet: Mutation of the Angelman Ubiquitin Ligase in Mice Causes Increased Cytoplasmic p53 and Deficits of Contextual Learning and Long-Term Potentiation. Neuron 21:799-811, 1998

7. Jon M. Huibregtse MSaPMH: A cellular protein mediates association of p53 with the E6 oncoprotein of human papillomavirus types 16 or 18. The EMBO Journal 10:4129-4135, 1991

8. Greer PL, Hanayama R, Bloodgood BL, et al: The Angelman Syndrome protein Ube3A regulates synapse development by ubiquitinating arc. Cell 140:704-16, 2010

9. Margolis SS, Salogiannis J, Lipton DM, et al: EphB-mediated degradation of the RhoA GEF Ephexin5 relieves a developmental brake on excitatory synapse formation. Cell 143:442-55, 2010

10. Kaphzan H, Buffington SA, Jung JI, et al: Alterations in intrinsic membrane properties and the axon initial segment in a mouse model of Angelman syndrome. J Neurosci 31:17637-48, 2011

11. van Woerden GM, Harris KD, Hojjati MR, et al: Rescue of neurological deficits in a mouse model for Angelman syndrome by reduction of alphaCaMKII inhibitory phosphorylation. Nat Neurosci 10:280-2, 2007

12. Egawa K, Kitagawa K, Inoue K, et al: Decreased tonic inhibition in cerebellar granule cells causes motor dysfunction in a mouse model of Angelman syndrome. Sci Transl Med 4:163ra157, 2012

13. Baudry M, Kramar E, Xu X, et al: Ampakines promote spine actin polymerization, long-term potentiation, and learning in a mouse model of Angelman syndrome. Neurobiol Dis 47:210-5, 2012

14. Daily JL, Nash K, Jinwal U, et al: Adeno-associated virus-mediated rescue of the cognitive defects in a mouse model for Angelman syndrome. PLoS One 6:e27221, 2011

15. Meng L, Person RE, Huang W, et al: Truncation of Ube3a-ATS unsilences paternal Ube3a and ameliorates behavioral defects in the Angelman syndrome mouse model. PLoS Genet 9:e1004039, 2013

16. Huang HS, Allen JA, Mabb AM, et al: Topoisomerase inhibitors unsilence the dormant allele of Ube3a in neurons. Nature 481:185-9, 2012

17. Dindot SV, Antalffy BA, Bhattacharjee MB, et al: The Angelman syndrome ubiquitin ligase localizes to the synapse and nucleus, and maternal deficiency results in abnormal dendritic spine morphology. Hum Mol Genet 17:111-8, 2008

18. Yashiro K, Riday TT, Condon KH, et al: Ube3a is required for experience-dependent maturation of the neocortex. Nat Neurosci 12:777-83, 2009

19. Riday TT, Dankoski EC, Krouse MC, et al: Pathway-specific dopaminergic deficits in a mouse model of Angelman syndrome. J Clin Invest 122:4544-54, 2012

20. Miura K, Kishino T, Li E, et al: Neurobehavioral and electroencephalographic abnormalities in Ube3a maternal-deficient mice. Neurobiol Dis 9:149-59, 2002

21. Heck DH, Zhao Y, Roy S, et al: Analysis of cerebellar function in Ube3a-deficient mice reveals novel genotype-specific behaviors. Hum Mol Genet 17:2181-9, 2008

22. Huang HS, Burns AJ, Nonneman RJ, et al: Behavioral deficits in an Angelman syndrome model: effects of genetic background and age. Behav Brain Res 243:79-90, 2013

23. Pelc K, Boyd SG, Cheron G, et al: Epilepsy in Angelman syndrome. Seizure 17:211-7, 2008

24. Thibert RL, Larson AM, Hsieh DT, et al: Neurologic manifestations of Angelman syndrome. Pediatr Neurol 48:271-9, 2013

25. Damien Colasa JW, Patrice Fortc, Denise Salvertc, Nicole Sardaa: Sleep disturbances in Ube3a maternal-deficient mice modeling Angelman syndrome. Neurobiology of Disease 20:471-478, 2005

26. Goodrich GS, Kabakov AY, Hameed MQ, et al: Ceftriaxone treatment after traumatic brain injury restores expression of the glutamate transporter, GLT-1, reduces

regional gliosis, and reduces post-traumatic seizures in the rat. J Neurotrauma 30:1434-41, 2013

27. Esposito G, Yoshida S, Ohnishi R, et al: Infant calming responses during maternal carrying in humans and mice. Curr Biol 23:739-45, 2013

28. Rodriguiz RM, Colvin JS, Wetsel WC: Neurophenotyping genetically modified mice for social behavior. Methods Mol Biol 768:343-63, 2011

29. Scattoni ML, Crawley J, Ricceri L: Ultrasonic vocalizations: a tool for behavioural phenotyping of mouse models of neurodevelopmental disorders. Neurosci Biobehav Rev 33:508-15, 2009

30. Martin E Hahn LK, Louis Weinrb, Andrew Henry, Norman Schanz and Evelyn M. Hahn.: Genetic and Developmental Influences on Infant Mouse Ultrasonic Calling. II. Developmental Patterns in the Calls of Mice 2-12 Days of Age. Behavior Genetics 28:315-325, 1998

31. Lavooy MEHaMJ: A Review of the Methods of Studies on Infant Ultrasound Production and Maternal Retrievel in Small Rodents. Behavior Genetics 35:31-51, 2005

32. Michael B. Hennessy JL, Edna L. Loe, Seymour Levine: Maternal Behavior, Pup Vocalizations, and Pup Temperature Changes Following Handling in Mice of 2 Inbred Strains. Developmental Psychobiology 13:573-584, 1980

33. Crabbe JC: Genetics of Mouse Behavior: Interactions with Laboratory Environment. Science 284:1670-1672, 1999

34. Jr. JLFaFHS: Audiogenic Seizures in Eleven Mouse Strains. The Journal of Heredity

35. Cao C, Rioult-Pedotti MS, Migani P, et al: Impairment of TrkB-PSD-95 signaling in Angelman syndrome. PLoS Biol 11:e1001478, 2013

36. Simone Kühnle BM, Konstantin Matentzoglu and Martin Scheffner: Role of the ubiquitin ligase E6AP/UBE3A in controlling levels of the synaptic protein Arc. PNAS 110:8888-8893, 2013

37. Shepherd JD, Bear MF: New views of Arc, a master regulator of synaptic plasticity. Nat Neurosci 14:279-84, 2011

CHAPTER 3

Discussion

3.1 Summary of findings

The primary goal of this dissertation is to test the hypothesis that deregulation of UBE3A substrates contribute to the clinical phenotype of AS. I test this hypothesis by genetically reducing the expression of UBE3A substrates in a mouse model of AS and then evaluating these mice in clinically relevant behavioral assays. If reduction of a specific substrate results in the modification or reversal of a clinically relevant phenotype, this would provide evidence that the substrate contributes directly the behavioral disorder in AS.

The experiments proposed in this approach require clinically relevant behavioral phenotypes to be present in the AS mouse model. However, the behavioral phenotype of the AS mouse model, as described in previous studies, is not convincing as a model of the human disorder; the learning and memory phenotypes are not robust and motor and seizure phenotypes are sensitive to the background strain and gender[1-9]. Additionally, core features of the human disorder, such as communication deficits, had not been yet been investigated. Thus, the extent to which the AS mouse model can recapitulate features of the human disorder emerged as a gap in knowledge at the time of this study. In order to test the UBE3A substrate hypothesis, it required that I directly address this gap in knowledge.

I hypothesized that the inability to discover robust behavioral abnormalities in the AS mouse is a consequence of behavioral testing during a late period in development, beyond the age of sexual maturity. A feature of AS in humans is that

this disorder is first manifested during early childhood, suggesting that analyzing behaviors in juvenile AS mice would be advantageous[10-12]. I test this hypothesis by evaluating Wildtype [WT] and AS mice in clinically relevant behavioral paradigms during juvenile development (<42 days old).

Conclusions regarding the juvenile AS mouse model hypothesis

The findings from this study suggest that a juvenile AS mouse is a valid model of the human disorder (Figure 3.1). During the juvenile period (<42 days old) the AS mouse can be characterized by communication deficits, movement disorder, susceptibility to seizures and an abnormal EEG. The communication and motor deficits have coincident onset during the first two weeks of postnatal life, as demonstrated by a prolonged production of ultrasonic vocalizations (USVs) and pronounced hindlimb clasp at postnatal day [PND] 11 and 13. The AS mouse also displays hypoactivity and motor spasms during juvenile development as demonstrated by reduced locomotor activity in the open field arena at PND 21 and a hindlimb clasp at PND 30. Lastly, the AS mouse has an enhanced response to the audiogenic stimulus at PND 30 and an abnormal EEG that is present are early as PND 35. Thus, the behavioral phenotype of a juvenile AS mouse recapitulates features of the human disorder; including communication and movement disorder, seizures and an abnormal EEG. These phenotypes are present when the mutation of the maternal *UBE3A* gene is introduced on three different background strains of mice and are insensitive to gender. Thus, the juvenile AS mouse model can be useful

for addressing fundamental questions related to the biology of AS and for testing candidate molecular and/or genetic therapeutic approaches.

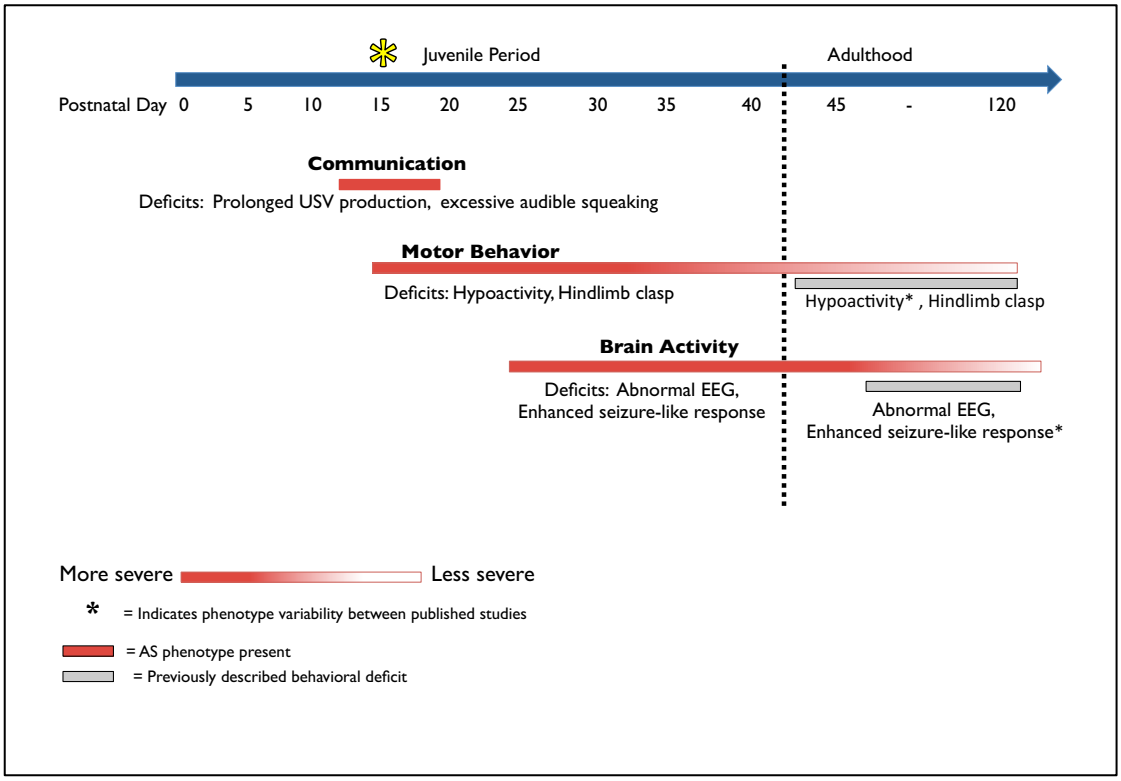

Figure 3.1 Summary of behavioral findings from WT and AS mice

The findings from this dissertation are merged with some behavioral data from previous published studies. Red bars indicate newly identified phenotypes in the Juvenile AS mouse model; Gray bars represent those phenotypes that have a correlate found in adulthood; Black asterisks mark previously described adult behavioral phenotypes that have varied between studies. The yellow star indicates the time point where coincident onset of communication and motor phenotypes is observed.

Conclusions regarding the UBE3A substrate hypothesis

With these clinically relevant phenotypes in hand, I next tested the hypothesis that deregulation of UBE3A substrates contribute to the clinical phenotype of AS. I found that reducing the expression levels of ARC or Ephexin5 (E5) in the AS mouse does not modify the USV phenotype, hypoactivity or hindlimb clasp. However, reducing the levels of ARC is able to reverse the enhanced response to an audiogenic stimulus and the abnormal EEG. The rescue of these abnormalities is specific to ARC in that reducing the level of E5 did not modify these phenotypes.

These behavioral data support the hypothesis that deregulation of the UBE3A substrate ARC does contribute to the clinical phenotype of AS. For this to be true, it requires that ARC is indeed, a bonafide substrate of UBE3A. In previous studies, ARC has been shown to exhibit UBE3A-dependent ubiquitination and degradation and the levels of ARC have been shown to be up-regulated in AS mice[13-15]. However, it has also been proposed that ARC is not a substrate of UBE3A, but instead, a downstream target of UBE3A's transcriptional co-activator function[16]. The activity-regulated ARC gene can be induced in mouse embryonic fibroblasts from stimulation by extracellular estrogen. Knockdown of UBE3A in this context leads to enhancement of ARC mRNA induction, suggesting that UBE3A normally functions as a co-repressor of the ARC gene. The authors propose that the increase in ARC protein in AS is a secondary consequence from increased ARC mRNA expression. However, in contrast to both of these models, by quantitative measurements I have been unable to detect a statistically significant difference in the level of ARC mRNA or ARC protein in brains or neuronal extracts when WT and AS mice are compared

(Figure 3.2). Thus, the status of ARC as a bonafide substrate of UBE3A remains an open question. The molecular mechanism by which UBE3A and ARC interact to modify the behavioral and physiological phenotype is not clear.

In light of these findings, I am unable to claim that I have formally tested the UBE3A substrate hypothesis. It is possible that ARC is not a direct substrate of UBE3A and that the reduction in ARC levels in AS-ARC$^{+/-}$ mice leads to an attenuation of seizure-like activity because UBE3A and ARC regulate a common cellular process, such as controlling the surface expression of AMPA receptors[16] (Figure 3.3). It is also possible that a reduction in ARC levels in AS-ARC$^{+/-}$ mice might lead to an attenuation of seizure-like activity through non cell-autonomous, circuit level adaptations within the brain. It will be important in the future to determine the locus of ARC expression in AS mice in an effort to understand how the decrease in ARC expression attenuates seizure-like activity.

Indeed, several proteins have been shown to be up-regulated in the AS brain that are not thought to be targets of UBE3A. Further, reduction of these proteins in the AS mouse has been shown to rescue physiological deficits. Examples of such proteins include (but are not limited to); NAV1.6 (sodium channel 1.6), ANK-3 (ankyrin-G), alpha1-NaKA (alpha-1 subunit of Na/K-ATPase) and phosphorylated CAMKII (calmodulin-dependent protein kinase II)[1,7]. The axonal initial segmental proteins, NAV1.6, ANK-3 and alpha1-Na/KA and α1-NaKA, are important for regulating the intrinsic properties of the neuronal membrane, and deregulation of these proteins are thought to contribute to the altered resting membrane potential, threshold potential and action potential amplitude in AS neurons.

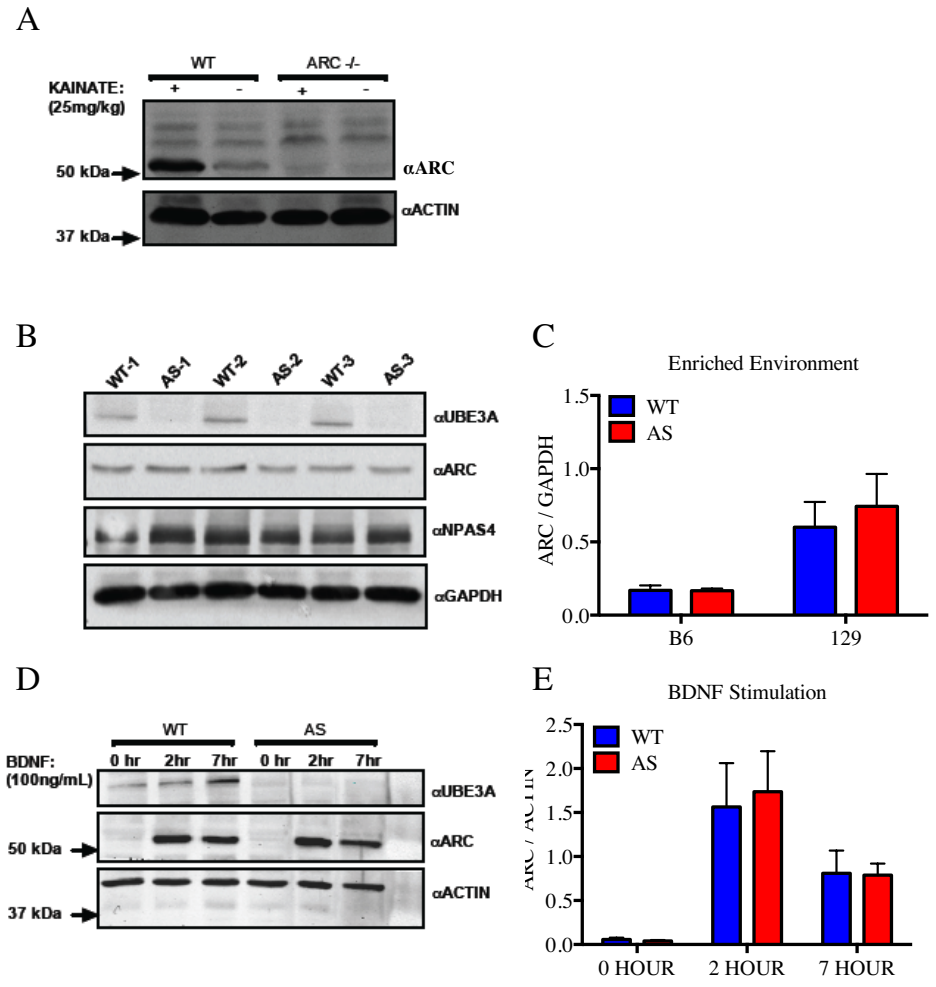

Figure 3.2 ARC protein levels are unchanged between WT and AS mice. ARC protein levels in AS and WT mice were analyzed in different contexts.

(A) Western blot with validation of ARC antibody. Wildtype (*ARC* +/+) and ARC Knockout (*ARC* -/-) mice were exposed to Kainic Acid (25mg/kg) for two hours. Hippocampal lysates were prepared and analyzed using Western immunoblotting with anti-ARC antibodies (provided by Dr. Paul Worley). Note prominent band at 50 kDa appears with stimulation and is absent in the ARC -/- lysate.

Figure 3.2 (Cont'd)

(B) Representative western blot from WT and AS littermates exposed to 2 hours of Enriched Environment. Hippocampal lysates were immunoblotted with αUBE3A, αARC, αNPAS4 and αGAPDH.

(C) Quantification of Fig. S6*B* western blot shows no statistical difference between ARC in AS and WT mice. ARC levels normalized to GAPDH. (WT n=3; AS n=3). (D) Representative blot of WT and AS cortical neuronal cultures stimulated for 0, 2, or 7 hours with 100ng/ml Brain-Derived Neurotrophic Factor (BDNF). (WT n=3; AS n=3).

(E) Quantification of Fig. S5.*D* reveals no difference in ARC protein levels between WT and AS mice. (C,E) Whole cell lysates were quantified using Bradford Assay and ran in triplicate for quantification. 50ug of protein was loaded for western blot analysis and protein levels were normalized to GAPDH or ACTIN loading control. One-way ANOVA was used for statistical analysis.

Interestingly, reduction in the levels of these axon-initial segment proteins *in vivo* in the AS mouse results in reversal of these deficits in neuronal physiology and LTP. Thus, an alternative approach to the UBE3A substrate hypothesis is to focus on identifying deregulated proteins in AS that have important roles in neuronal development and function. If ARC is not a direct substrate of UBE3A, the implications from the findings in this dissertation are relevant for considering treatments and alternative therapeutic approaches for AS.

In conclusion, in this dissertation, I demonstrate that a juvenile AS mouse exhibits clinically relevant, strain-independent behavioral phenotypes early in life. The characterization of these behavioral defects in AS mice may facilitate identification of the neuronal circuits that are disrupted in AS, and provide a path towards the development of pharmacological or genetic therapies for treating this debilitating disorder.

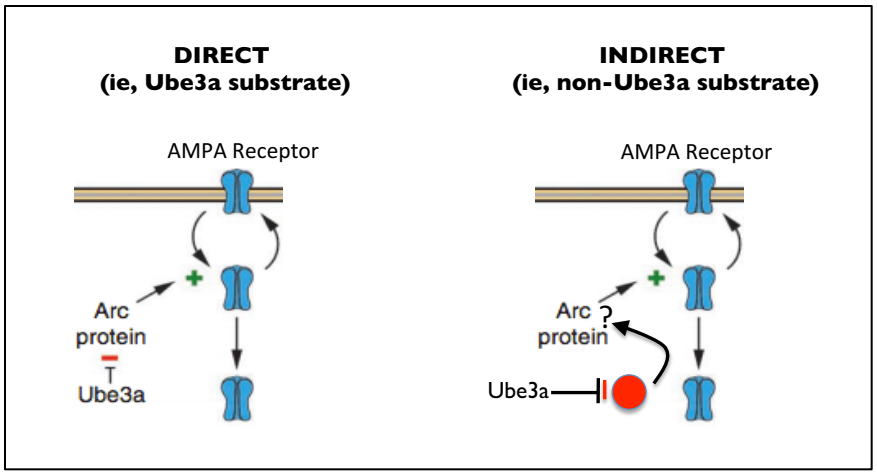

Figure 3.3 Two potential models to explain ARC mediated rescue of seizure-like activity and an abnormal EEG

Model on left: ARC is a direct substrate of UBE3A. In this model, UBE3A can regulate ARC protein levels through UBE3A-dependent ubiquitination and degradation, or, alternatively, UBE3A may directly regulate the endocytic functions of ARC through a different type of UBE3A-dependent ubiquitination event. In this model, deregulation of ARC as a substrate directly contributes to the phenotypes in AS.

Model on right: It is possible that ARC is not a direct substrate of UBE3A and that the reduction in ARC levels in AS-ARC$^{+/-}$ mice leads to an attenuation of seizure-like activity because UBE3A and ARC regulate a common cellular process, such as controlling the surface expression of AMPA receptors. The rescue is a result of an indirect interaction between UBE3A and ARC and an unknown protein or set of proteins that may exist within the postsynaptic membrane.

3.2 Implications for therapeutic approaches in AS

Seizures have been reported in 90% of children with AS that have a 15q11 deletion and greater than 50% of children that have mutations specifically within the *UBE3A* gene [17-19]. In all cases, the EEGs of individuals with AS have been found to be abnormal [20]. Although EEGs are not necessarily identical between different people, a hallmark of the EEG defect in humans with AS is the occurrence of abnormal bouts of high amplitude and low frequency (2-3 Hz) delta waves early in life. While certain features of the EEG abnormality that we detect in AS mice are specific to mice, the phenotype is observed in multiple strains of mice across multiple brain regions. This suggests that the EEG is a reliable way to monitor the abnormal brain activity that accompanies AS and therapies for treating AS might be tested for their efficacy in reversing the EEG phenotype. In addition, rescue of these abnormalities by reducing the levels of ARC provide a promising lead for treating these deficits in humans with AS. In support of this idea, reducing levels of ARC through a small-molecule CN2097 is able to reverse the LTP deficits in the hippocampus of AS mice. In this context, the increased levels of ARC are reduced indirectly through modification of the ARC-PSD95-BDNF-TRKB signaling complex in the postsynaptic membrane[15].

The analysis of behavior in juvenile AS mice revealed that, as in humans, behavioral deficits in AS mice emerge early in life. AS mice appear normal at birth and show no obvious defects in brain anatomy [21]. However, as the brain begins to mature, a significant defect in communication and motor abilities is observed.

Previous studies have suggested that visual experience modifies the development of neural circuits in young AS mice, and that in the absence of visual stimulation neural circuit defects fail to develop[21]. Thus, UBE3A is likely required for the postnatal period of activity-dependent refinement of the neuronal circuits in the brain.

The developmental time course of USV production in WT mice, specifically the robust suppression of this behavior at PND 13 – 15, suggests that a critical period may exist for the development of USV circuits in early postnatal development. This might involve the inhibition of motor circuits that facilitate USV production. Given that the defect in USV production in AS mice becomes apparent at PND 13 when WT mice are beginning to suppress USV production, I speculate that the persistence of USVs in AS mouse pups could reflect a defect in sensory-dependent neural circuit maturation. A similar defect in the development of inhibitory circuits could underlie the emergence of the hindlimb clasp phenotype in AS mice, as this phenotype is first detected at the same time during post-natal development that USV production becomes abnormal.

From these observations, it is a possibility that treating AS requires therapeutic intervention during this early postnatal period development (<3 years of age). Findings from mouse models of other monogenic disorders, such as Rett Syndrome, suggest that the behavioral abnormalities of these disorders are reversible, even when treated during the adult postnatal period[22,23]. However, the symptoms in Rett Syndrome are different in their onset and progression; the motor and speech abnormalities in AS appear earlier in development and are characterized by a failure to develop, whereas in Rett Syndrome, these skills are acquired

normally and then subsequently lost[24]. Taken together, these data suggest there may a distinct developmental time window during with AS can be treated.

Indeed, a recent study showed that re-instatement of UBE3A protein during early development, but not late development, resulted in rescue of juvenile AS phenotypes including anxiety, epilepsy and repetitive behaviors[25]. The biology that gates the developmental boundaries for UBE3A rescue of phenotypes is not known and warrants further investigation. Interestingly, the increased susceptibility of seizures was not reversed in a juvenile AS mouse model when *UBE3A* was reinstated in early development. This provides further evidence that UBE3A and ARC are likely working indirectly to modify the enhanced brain activity phenotypes in AS mice.

3.3 UBE3A, Angelman Syndrome and Autism Spectrum Disorder

In support of our findings with AS mice, a previous study reported the presence of abnormal USVs and cortical EEGs in a strain of mice (15q11-q13 deletion mice) that contain a 1.6 Mb deletion in chromosome 15q11 that is found in the majority of humans with AS [26]. In addition to disrupting *UBE3A* function, this deletion knocks out expression of a large number of genes, including *CYFIP1, NIPA1, NIPA2, GCG5, WHCD1l1, GOLGA8E*, and a *GABA* receptor cluster. Given the nature of this deletion, it was not clear if the abnormal USVs and cortical EEGs observed in 15q11-q13 deletion mice are due specifically to the loss of *UBE3A* or to disruption of additional genes in the 15q11-q13 locus. Our findings with AS mice provide strong

support for the conclusion that the defects in USV production and cortical EEGs are specifically due to the disruption of *UBE3A*. By comparing the effect of deleting the maternally inherited versus the paternally inherited allele of *UBE3A* on USV production we are able to conclude that the USV defect is likely due to the loss of *UBE3A* specifically in neurons. Identification of the particular neuronal subtypes that underlie these defects will require the selective disruption or replacement of *UBE3A* in defined neural subtypes.

A common clinical phenotype between AS and Autism Spectrum Disorder (ASD) is the robust impairment of communicative behaviors in early development[27-29]. This is especially true for nonverbal behavior, or significant delay in the acquisition of speech, that is observed among children with these disorders. In addition, individuals with copy number variations in the genomic locus 15q11.2-13, also display nonverbal behavior and delay in speech[27]. A common genetic perturbation that exists among all of these conditions is mutation of UBE3A[30]. Thus, a role as emerged for UBE3A in the development of communication circuits in early development. In the absence of these monogenic neurodevelopmental disorders, such AS or 15q11.2-13 Dup, this link between UBE3A and language development would have otherwise gone unappreciated. I conclude that the juvenile AS mouse model recapitulates the robust impairment of communication behavior in humans and future studies could use this mouse model to elucidate the UBE3A-dependent pathways that give rise to these communication deficits.

References

1. Kaphzan H, Buffington SA, Jung JI, et al: Alterations in intrinsic membrane properties and the axon initial segment in a mouse model of Angelman syndrome. J Neurosci 31:17637-48, 2011

2. Grier MD, Carson RP, Lagrange AH: Toward a Broader View of Ube3a in a Mouse Model of Angelman Syndrome: Expression in Brain, Spinal Cord, Sciatic Nerve and Glial Cells. PLoS One 10:e0124649, 2015

3. Huang HS, Burns AJ, Nonneman RJ, et al: Behavioral deficits in an Angelman syndrome model: effects of genetic background and age. Behav Brain Res 243:79-90, 2013

4. Jana NR: Understanding the pathogenesis of Angelman syndrome through animal models. Neural Plast 2012:710943, 2012

5. Mabb AM, Judson MC, Zylka MJ, et al: Angelman syndrome: insights i nto genomic imprinting and neurodevelopmental phenotypes. Trends Neurosci 34:293-303, 2011

6. Yong-hui Jiang DA, Urs Albrecht, Coleen M. Atkins, Jeffrey L. Noebels, Gregor Eichele, J. David Sweatt and Arthur L. Beaudet: Mutation of the Angelman Ubiquitin Ligase in Mice Causes Increased Cytoplasmic p53 and Deficits of Contextual Learning and Long-Term Potentiation. Neuron 21:799-811, 1998

7. van Woerden GM, Harris KD, Hojjati MR, et al: Rescue of neurological deficits in a mouse model for Angelman syndrome by reduction of alphaCaMKII inhibitory phosphorylation. Nat Neurosci 10:280-2, 2007

8. Mulherkar SA, Sharma J, Jana NR: The ubiquitin ligase E6-AP promotes degradation of alpha-synuclein. J Neurochem 110:1955-64, 2009

9. Heck DH, Zhao Y, Roy S, et al: Analysis of cerebellar function in Ube3a-deficient mice reveals novel genotype-specific behaviors. Hum Mol Genet 17:2181-9, 2008

10. Angelman H: 'Puppet' children. A report on 3 cases. Develop. Med. Child Neurol. 7, 1965

11. Williams CA: The behavioral phenotype of the Angelman syndrome. Am J Med Genet C Semin Med Genet 154C:432-7, 2010

12. Williams CA, Driscoll DJ, Dagli AI: Clinical and genetic aspects of Angelman syndrome. Genet Med 12:385-95, 2010

13. Greer PL, Hanayama R, Bloodgood BL, et al: The Angelman Syndrome protein Ube3A regulates synapse development by ubiquitinating arc. Cell 140:704-16, 2010

14. Sun J, Zhu G, Liu Y, et al: UBE3A Regulates Synaptic Plasticity and Learning and Memory by Controlling SK2 Channel Endocytosis. Cell Rep 12:449-61, 2015

15. Cao C, Rioult-Pedotti MS, Migani P, et al: Impairment of TrkB-PSD-95 signaling in Angelman syndrome. PLoS Biol 11:e1001478, 2013

16. Simone Ku¨hnle BM, Konstantin Matentzoglu and Martin Scheffner: Role of the ubiquitin ligase E6AP/UBE3A in controlling levels of the synaptic protein Arc. PNAS 110:8888-8893, 2013

17. Tan WH, Bacino CA, Skinner SA, et al: Angelman syndrome: Mutations influence features in early childhood. Am J Med Genet A 155A:81-90, 2011

18. Pelc K, Boyd SG, Cheron G, et al: Epilepsy in Angelman syndrome. Seizure 17:211-7, 2008

19. Yum MS, Lee EH, Kim JH, et al: Implications of slow waves and shifting epileptiform discharges in Angelman syndrome. Brain Dev 35:245-51, 2013

20. Vendrame M, Loddenkemper T, Zarowski M, et al: Analysis of EEG patterns and genotypes in patients with Angelman syndrome. Epilepsy Behav 23:261-5, 2012

21. Yashiro K, Riday TT, Condon KH, et al: Ube3a is required for experience-dependent maturation of the neocortex. Nat Neurosci 12:777-83, 2009

22. Gadalla KK, Bailey ME, Cobb SR: MeCP2 and Rett syndrome: reversibility and potential avenues for therapy. Biochem J 439:1-14, 2011

23. Lang M, Wither RG, Colic S, et al: Rescue of behavioral and EEG deficits in male and female Mecp2-deficient mice by delayed Mecp2 gene reactivation. Hum Mol Genet 23:303-18, 2014

24. Cianfaglione R, Clarke A, Kerr M, et al: A national survey of Rett syndrome: age, clinical characteristics, current abilities, and health. Am J Med Genet A 167:1493-500, 2015

25. Silva-Santos S, van Woerden GM, Bruinsma CF, et al: Ube3a reinstatement identifies distinct developmental windows in a murine Angelman syndrome model. J Clin Invest 125:2069-76, 2015

26. Jiang YH, Pan Y, Zhu L, et al: Altered ultrasonic vocalization and impaired learning and memory in Angelman syndrome mouse model with a large maternal deletion from Ube3a to Gabrb3. PLoS One 5:e12278, 2010

APPENDIX

Appendix A: Work resulting from collaborations

1. Margolis SS, Salogiannis J, Lipton DM, Mandel-Brehm C, Wills ZP, Mardinly AR, Hu L, Greer PL, Bikoff JB, HO HY, Soskis MJ, Sahin M Greenberg ME. (2010) EphB-mediated degradation of the RhoA GEF Ephexin5 relieves a developmental brake on excitatory synapse formation. Cell 143(3):442-55

2. Wills ZP, Mandel-Brehm C, Mardinly AR, McCord AE, Giger RJ, Greenberg ME. (2012) The nogo receptor family restricts synapse number in the developing hippocampus. Neuron 73(3):466-81

3. Mardinly AR, Spiegel I, Tzeng CP, Bazinet JE, Mandel-Brehm C, Harmin DA, Greenberg ME. (2014) Unique experience-induced gene programs in interneuron subtypes shapes cortical circuits. Nature (In review)

Published in final edited form as:
Cell. 2010 October 29; 143(3): 442–455. doi:10.1016/j.cell.2010.09.038.

EphB-mediated degradation of the RhoA GEF Ephexin5 relieves a developmental brake on excitatory synapse formation

Seth S. Margolis[1,3], **John Salogiannis**[1,3], **David M. Lipton**[1], **Caleigh Mandel-Brehm**[1], **Zachary P. Wills**[1], **Alan R. Mardinly**[1], **Linda Hu**[1], **Paul L. Greer**[1], **Jay B. Bikoff**[1], **Hsin-Yi Henry Ho**[1], **Michael J. Soskis**[1], **Mustafa Sahin**[2], and **Michael E. Greenberg**[1,‡]

[1] Department of Neurobiology, Harvard Medical School, 220 Longwood Avenue, Boston MA 02115, USA

[2] F.M. Kirby Neurobiology Center, Departments of Neurology, Children's Hospital Boston, Harvard Medical School, Boston, MA 02115, USA

Abstract

The mechanisms that promote excitatory synapse formation and maturation have been extensively studied. However, the molecular events that limit excitatory synapse development so that synapses form at the right time and place and in the correct numbers are less well understood. We have identified a RhoA guanine nucleotide exchange factor, Ephexin5, which negatively regulates excitatory synapse development until EphrinB binding to the EphB receptor tyrosine kinase triggers Ephexin5 phosphorylation, ubiquitination, and degradation. The degradation of Ephexin5 promotes EphB-dependent excitatory synapse development and is mediated by Ube3A, a ubiquitin ligase that is mutated in the human cognitive disorder Angelman syndrome and duplicated in some forms of Autism Spectrum Disorders (ASDs). These findings suggest that aberrant EphB/Ephexin5 signaling during the development of synapses may contribute to the abnormal cognitive function that occurs in Angelman syndrome and, possibly, ASDs.

Introduction

A crucial early step in the formation of excitatory synapses is the physical interaction between the developing presynaptic specialization and the postsynaptic dendrite (Jontes et al., 2000; Ziv and Smith, 1996). This step in excitatory synapse development is thought to be mediated by cell surface membrane proteins expressed by the developing axon and dendrite and appears to be independent of the release of the excitatory neurotransmitter glutamate (reviewed in Dalva et al., 2007). Several recent studies have revealed an important role for Ephrin cell surface-associated ligands and Eph receptor tyrosine kinases in this early cell-cell contact phase that is critical for excitatory synapse formation (Dalva et al., 2000; Ethell et al., 2001; Henkemeyer et al., 2003; Kayser et al., 2006; Kayser et al., 2008; Lai and Ip, 2009; Murai et al., 2003). Ephs can be divided into two classes, EphA and EphB, based on their ability to bind the ligands EphrinA and EphrinB, respectively (reviewed in Flanagan and Vanderhaeghen, 1998). EphBs are expressed postsynaptically on the surface of developing dendrites, while their cognate ligands, the EphrinBs, are expressed

‡To whom correspondence should be addressed: Harvard Medical School, Department of Neurobiology, Goldenson Bldg. 420, 220 Longwood Avenue, Boston, MA 02115, Phone: 617-432-1772, FAX: 617-734-7557, Michael_Greenberg@hms.harvard.edu.
[3]These authors contributed equally to this work

on both the developing axon and dendrite (Grunwald et al., 2004; Grunwald et al., 2001; Lim et al., 2008). When an EphrinB encounters an EphB on the developing dendrite, EphB becomes autophosphorylated, thus increasing its catalytic kinase activity (reviewed in Flanagan and Vanderhaeghen, 1998). This leads to a cascade of signaling events including the activation of guanine nucleotide exchange factors (GEFs) Tiam, Kalirin, and Intersectin, culminating in actin cytoskeleton remodeling that is critical for excitatory synapse development (reviewed in Klein, 2009). Consistent with a role for EphBs in excitatory synapse development, EphB1/EphB2/EphB3 triple knockout mice have fewer mature excitatory synapses *in vivo* in the cortex, and hippocampus (Henkemeyer et al., 2003; Kayser et al., 2006). In addition, the disruption of EphB function postsynaptically in dissociated hippocampal neurons leads to defects in spine morphogenesis and a decrease in excitatory synapse number (Ethell et al., 2001; Kayser et al., 2006). Conversely, activation of EphBs in hippocampal neurons leads to an increase in the number of dendritic spines and functional excitatory synapses (Henkemeyer et al., 2003; Penzes et al., 2003). These findings indicate that EphBs are positive regulators of excitatory synapse development.

While there has been considerable progress in characterizing the mechanisms by which EphBs promote excitatory synapse development, it is not known if there are EphB-associated factors that restrict the timing and extent of excitatory synapse development. We hypothesized that neurons might have evolved mechanisms which act as checkpoints to restrict EphB-mediated synapse formation, and that the release from such synapse formation checkpoints might be required if synapses are to form at the correct time and place and in appropriate numbers.

We considered the possibility that likely candidates to mediate the EphB-dependent restriction of excitatory synapse formation might be regulators of RhoA, a small G protein that functions to antagonize the effects of Rac (Tashiro et al., 2000). In previous studies we identified a RhoA GEF, Ephexin1 (E1), which interacts with EphA4 (Fu et al., 2007; Sahin et al., 2005; Shamah et al., 2001). E1 is phosphorylated by EphA4 and is required for the EphrinA-dependent retraction of axonal growth cones and dendritic spines (Fu et al., 2007; Sahin et al., 2005). While E1 does not appear to interact with EphB, E1 is a member of a family of five closely related GEFs. Of these GEFs, Ephexin5 (E5) (in addition to E1) is highly expressed in the nervous system. Therefore, we hypothesized that E5 might function to restrict the EphB-dependent development of excitatory synapses by activating RhoA.

In this study we report that EphB interacts with E5, that E5 suppresses excitatory synapse development by activating RhoA, and that this suppression is relieved by EphrinB activation of EphB during synapse development. Upon binding EphrinB, EphB catalyzes the tyrosine phosphorylation of E5 which triggers E5 degradation. We identify Ube3A as the ubiquitin ligase that mediates E5 degradation, thus allowing synapse formation to proceed. As *UBE3A* is mutated in Angelman syndrome and duplicated in some forms of Autism Spectrum Disorders (ASDs), these findings suggest a possible mechanism by which the mutation of Ube3A might lead to cognitive dysfunction (Jiang et al., 1998; Kishino et al., 1997). Specifically, we provide evidence that in the absence of Ube3A, the level of E5 is elevated and propose that this may lead to the enhanced suppression of EphB-mediated excitatory synapse formation, thereby contributing to Angelman syndrome and, possibly, ASDs.

Results

Ephexin5 interacts with EphB2

To identify mechanisms that restrict the ability of EphBs to promote an increase in excitatory synapse number, we searched for RhoA guanine nucleotide exchange factors (GEFs) that specifically activate RhoA signaling, are expressed in the same population of

neurons that express EphB, are expressed at the same time during development as EphB, and interact with EphB. Structure-function studies of GEFs identified amino acid residues in the activation domain of Rho family GEFs that specifically identify the GEFs as activators of RhoA rather than Rac or Cdc42. Applying this criterion, fourteen GEFs were identified that specifically activate RhoA (Rossman et al., 2005). Of these GEFs we found by in situ hybridization that E5 has a similar expression pattern to EphB in the hippocampus (Fig 1A). These findings raised the possibility that E5 might mediate the effect of EphB on developing synapses.

We asked if E5 interacts physically with EphB. We transfected HEK293T (293) cells with plasmids encoding Myc-tagged E5, E1, or a vector control together with Flag-tagged EphB2 or EphA4 and asked if these proteins co-immunoprecipitate. Extracts were prepared from the transfected 293 cells and EphA4 or EphB2 immunoprecipitated with Flag antibodies. The immunoprecipitates were subjected to SDS polyacrylamide gel electrophoresis (SDS-PAGE) and blotted with anti-Myc antibody (α-Myc). We found that E5 co-immunoprecipitates with EphB2 but not with EphA4 (Fig 1B). The relatively weak E5 interaction with EphA4 is consistent with published experiments (Ogita et al., 2003). By contrast, E1 is co-immunoprecipitated by EphA4 but not EphB2 (Shamah et al., 2001). These findings suggest that E5 interacts preferentially with EphB2.

To extend this analysis we investigated whether EphB2 interacts with E5 in neurons. Neurons from embryonic day 16 (E16) mouse brains were lysed in RIPA buffer and the lysates incubated with affinity purified anti-C-terminal E5 (α-C-E5) or control (IgG) antibodies. The immunoprecipitates were then resolved by SDS-PAGE and immunoblotted with affinity purified anti-N-terminal E5 (α-N-E5) or EphB2 (α-EphB2) antibodies (Fig 1C). This analysis revealed that endogenous, neuronal EphB2 is immunoprecipitated by α-C-E5 but not IgG. Moreover, using lysates from brains of wild type or E5 knockout mice (*E5*$^{-/-}$, see Fig S1), we find that α-C-E5 immunoprecipitates EphB2 only from brain lysates when E5 is present (Fig 1D). Taken together, these findings suggest that EphB interacts with Ephexin5 in neurons.

As an independent means of assessing if EphB and E5 interact with one another, we used immunofluorescence microscopy to determine if these two proteins co-localize in neurons. Cultured mouse hippocampal neurons were transfected with a plasmid expressing green fluorescent protein (GFP). The GFP-expressing neurons were imaged and quantified for the co-localization of EphB2 and E5 puncta by staining with α-C-E5 and α-EphB2. This analysis revealed that EphB2 and E5 co-localize along dendrites (Fig 1E). We find that 40% of EphB staining overlaps with α-C-E5 staining early during the development of excitatory synapses. After eight days in vitro (DIV) the overlap of EphB with E5 within neuronal dendrites decreases to below the level that would be detected by random chance. This change suggests that EphB interacts with E5 early during development, possibly to inhibit EphB synapse formation.

Ephexin5 is a guanine nucleotide exchange factor that activates RhoA

To determine if E5 activates RhoA, we transfected 293 cells with a control plasmid or a plasmid that drives the expression of Myc-tagged mouse E5. We prepared extracts from the transfected cells and incubated the extracts with a GST-fusion protein that includes the Rhotekin-Binding Domain (GST-RBD), a protein domain that selectively interacts with active (GTP-bound) but not inactive (GDP-bound) RhoA. Following SDS-PAGE of the proteins in the extract that bind to GST-RBD, RhoA binding to GST-RBD was measured by immunoblotting with α-RhoA antibodies. We found that cells expressing E5 exhibited higher levels of activated RhoA compared to cells transfected with a control plasmid, indicating that E5 activates RhoA (Fig 2A).

When a similar series of experiments were performed using a GST-fusion Pak-Binding Domain (GST-PBD) which specifically interacts with active forms of two other Rho GTPases, Rac1 and Cdc42, we found that E5 does not induce the binding of GST-PBD to Rac1 or Cdc42. In contrast, E1-expressing cells displayed enhanced binding of Rac1 and Cdc42 to GST-PBD. We conclude that E5 activates RhoA but not Rac1 or Cdc42 (Fig S2A).

To determine whether E5 activation of RhoA requires the GEF activity of E5, we generated a mutant form of E5 in which its GEF activity is impaired. To identify the residues required for Ephexin5 guanine nucleotide exchange activity we compared its Dbl-homology (DH) domain to the DH domain of other RhoA-specific GEFs (Snyder et al., 2002). We identified within the α5 helix of E5's DH domain three amino acids that are conserved in other GEFs that, like E5, activate RhoA but not Rac1 and Cdc42 (Fig S2B). To generate a form of E5 predicted to be inactive as a GEF, we mutated these three conserved amino acids (L562, Q566, and R567) to alanine (E5-LQR). Using the GST-RBD pull down assay we found that although E5-WT and E5-LQR are expressed at similar levels, the E5-LQR mutant is significantly impaired relative to WT in its ability to activate RhoA (Fig 2B). As a control, we mutated other conserved residues within the α5 DH region to alanine (Q547, S548, R555, and L556). When we tested this mutant we observed no defect in RhoA activation, suggesting that the E5-LQR mutation specifically disrupts the GEF activity of E5 and that the inability of the LQR mutant to activate RhoA is not a general consequence of disrupting the α5 region of Ephexin5 (Fig S2C). Taken together, these findings indicate that E5 requires an intact conserved GEF domain to promote RhoA activity in 293 cells, suggesting that E5 functions as a RhoA GEF.

We next asked if E5 expression affects RhoA activity in the brain. We lysed P3 whole brains from wild type or *E5*$^{-/-}$ mice and performed a GST-RBD pull down assay. This analysis revealed a significant decrease in RhoA activation in brain extracts from *E5*$^{-/-}$ mice compared to wild type mice, suggesting that E5 is required to maintain wild type levels of RhoA activity in the brain (Fig 2C).

Ephexin5 negatively regulates excitatory synapse number

Our findings indicate that E5 interacts with EphB, a key regulator of excitatory synapse development. Thus, we asked whether E5 plays a role in the development of excitatory synapses. We generated two short hairpin RNA constructs that each knocks down E5 protein levels when expressed in 293 cells or cultured hippocampal neurons (Fig S3A–S3B). These shRNAs were introduced into cultured hippocampal neurons together with a plasmid that drives expression of green fluorescent protein (GFP) to allow detection of the transfected cells. We found by staining with α-N-E5 antibodies that the E5 shRNAs (E5-shRNA), but not scrambled hairpin control shRNAs (ctrl-shRNA), efficiently knocked down E5 expression in the transfected neurons (Fig S3C).

By staining with antibodies that recognize pre- and post- synaptic proteins or by visualizing dendritic spines in GFP transfected neurons we observed a significant increase in the number of excitatory synapses and dendritic spines that are present on the E5-shRNA-expressing neurons compared to neurons expressing ctrl-shRNAs (Fig 3A and 3B). By contrast, we failed to detect a significant change in dendritic spine length or width under these conditions (Fig S3D). These findings suggest that E5 functions to restrict spine/excitatory synapse number but has no significant effect on spine morphology. Consistent with these conclusions, we found that overexpression of E5 in hippocampal neurons leads to a decrease in the number of excitatory synapses that are present on the E5-overexpressing neurons (Fig 3C). This ability of E5 to negatively regulate excitatory synapse number requires its RhoA GEF activity, as overexpression of E5-LQR had no effect on synapse number (Fig 3D).

To assess the effect of reducing E5 levels on the functional properties of excitatory synapses, we recorded miniature excitatory postsynaptic currents (mEPSCs) from cultured hippocampal neurons transfected with E5-shRNA or ctrl-shRNA. We observed an increase in the frequency and amplitude of mEPSCs on neurons expressing E5-shRNA compared to ctrl-shRNA (Fig 3E). This suggests that E5 acts postsynaptically to restrict excitatory synapse function. The increase in mEPSC frequency could be due to an increase in presynaptic vesicle release onto the transfected neuron or an increase in the number of excitatory synapses that are present on the transfected neuron. We favor the latter possibility since our transfection protocol selectively reduces E5 levels postsynaptically and also because the increase in synapse number is most consistent with the increase in co-staining of pre- and post-synaptic markers that we observe when the level of E5 is reduced. The possibility that E5 functions postsynaptically is further supported by immunofluorescence staining experiments demonstrating that E5 is enriched in dendrites relative to axons (Fig S1F).

As an independent means of assessing the importance of E5 in the control of excitatory synapse number, we cultured hippocampal neurons from $E5^{-/-}$ mice or their wild type littermates for 10 days *in vitro* and then, following transfection of a GFP-expressing plasmid into these neurons, quantified the number of excitatory synapses present on the transfected neuron at DIV14. We observed a three-fold increase in the number of synapses that are present on $E5^{-/-}$ neurons compared to $E5^{+/-}$ neurons (Fig 4A). Taken together with the E5-shRNA knockdown and E5 overexpression analyses, these findings suggest that E5 acts postsynaptically to reduce excitatory synapse number.

We next asked if E5 regulates synapse number in the context of an intact developing neuronal circuit using conditional E5 ($E5^{fl/fl}$) animals (see Fig S1). Upon introduction of Cre recombinase into $E5^{fl/fl}$ cells, exons 4–8 of the *E5* gene are excised resulting in a cell that no longer produces E5 protein (data not shown). Organotypic slices were prepared from the hippocampus of the $E5^{fl/fl}$ mice or their wild type littermates. Using the biolistic transfection method, a plasmid expressing Cre recombinase was introduced into a low percentage of neurons in the slices. We found that introduction of a Cre-expressing plasmid into $E5^{fl/fl}$ neurons in the hippocampal slice led to a significant increase in the density of dendritic spines present on the Cre-expressing neurons (Fig 4B). By contrast, expression of Cre in neurons of a wild type hippocampal slice has no effect on dendritic spine density. The length and width of dendritic spines analyzed in these experiments showed no significant difference between wild type and $E5^{-/-}$ neurons (Fig S4). Thus, elimination of E5 expression in neurons in the context of an intact neuronal circuit leads to an increase in the number of dendritic spines.

To assess the role of E5 in hippocampal circuit development *in vivo*, we performed acute slice physiology experiments in the CA1 region of the hippocampus from wild type or $E5^{-/-}$ mice. We find that relative to wild type neurons, in $E5^{-/-}$ CA1 pyramidal neurons there are more frequent excitatory events that have larger amplitude (Fig 4C). A possible explanation for these findings is that when E5 function is disrupted during in vivo development more excitatory synapses form resulting in more excitatory post-synaptic events. To test this possibility, we used array tomography to quantify the number of excitatory synapses that form in the CA1 stratum radiatum of wild type and $E5^{-/-}$ mice. We observed a ~2-fold increase in the number of excitatory synapses within the CA1 region of the $E5^{-/-}$ hippocampus compared to wild type mice (Fig 4D). Specifically, the number of juxtaposed synapsin and PSD-95 puncta was quantified and considered a measurement of the number of excitatory synapses that form within the CA1 region of the hippocampus *in vivo*. This analysis revealed a significant increase in the number of PSD-95 puncta but no change in the number of synapsin puncta density (Fig 4D). This suggests that the increase in excitatory

synapse number in the stratum radiatum of $E5^{-/-}$ mice is likely due to the absence of E5 post-synaptically and that when E5 is present within dendrites it functions to negatively regulate synapse number *in vivo*. On the basis of these results, we conclude that a key function of E5 is to restrict excitatory synapse number during the development of neuronal circuits.

Ephexin5 restricts EphB2 control of excitatory synapse formation

We next considered the possibility that the ability of E5 to restrict excitatory synapse number might be controlled by EphB2 signaling. To test this idea, we asked whether reducing EphB2 signaling eliminates the increase in excitatory synapse number detected when E5 levels are knocked down by expression of E5-shRNA. To block EphB2 activation, we introduced into neurons a kinase dead version of EphB2 (EphB2-KD) which has been previously shown to block EphB2 signaling (Dalva et al., 2000). As described above, expression of E5-shRNA in neurons leads to a significant increase in the number of synapses that are present on the E5-shRNA-expressing neuron. However, this increase was reversed if the E5-shRNA was co-transfected with a plasmid that drives expression of EphB2-KD, but was not affected by co-transfection of a control plasmid (Fig 4E). These findings suggest that the increase in excitatory synapse number that occurs when E5 levels are reduced requires EphB signaling. Consistent with this conclusion, we find that if we overexpress wild type EphB2 in neurons more synapses are present on the EphB-expressing neuron. However, this effect is reduced if E5 is overexpressed in neurons together with EphB (Fig 4F). It is possible that the ability of overexpressed E5 to suppress the synapse-promoting effect of EphB2 reflects independent actions of these two signaling molecules. However, given that EphB2 and E5 interact with one another in neurons, the most likely interpretation of these results is that E5 functions directly to restrict the synapse-promoting effects of EphB2. If this were the case, we would predict that for EphB2 to positively regulate excitatory synapse development it would be necessary to inactivate and/or degrade E5.

EphB mediates phosphorylation of Ephexin5 at tyrosine-361

We considered the possibility that since EphB2 is a tyrosine kinase it might inhibit the GEF activity or expression of the E5 protein by catalyzing the tyrosine phosphorylation of E5. In support of this possibility, stimulation of dissociated mouse hippocampal neurons with EB1 for 15 minutes led to an increase in the level of E5 tyrosine phosphorylation as detected by probing immunoprecipitated E5 with the pan-anti-phosphotyrosine antibody, 4G10 (Fig 5A).

We have previously shown that EphrinA1 stimulation of cultured neurons leads to the tyrosine phosphorylation of E1 at tyrosine 87 (Sahin et al., 2005). On the basis of this finding we hypothesized that exposure of neurons to EphrinB1 (EB1) might promote the phosphorylation of the analogous tyrosine residue (Y361) on E5 (Fig 5B) and that phosphorylation at this site might lead to E5 inactivation. To address this possibility, we overexpressed EphB2 in 293 cells together with wild type E5 or a mutant form of E5 in which Y361 is converted to a phenylalanine (E5-Y361F). Lysates were prepared from the transfected cells and after SDS-PAGE were immunoblotted with 4G10 (Fig 5C). We found that in the presence of EphB2, E5-WT, but not E5-Y361F, becomes tyrosine phosphorylated. These findings suggest that EphB2 catalyzes the tyrosine phosphorylation of E5 primarily at Y361.

To show definitively that E5 Y361 is tyrosine phosphorylated, we generated E5 phospho-Y361 antibodies (α-pY361). To demonstrate that these antibodies specifically recognizes the Y361-phosphorylated form of E5, we immunoblotted cell lysates prepared from 293 cells that express EphB2 and either E5-WT or E5-Y361F with α-pY361. This analysis

demonstrated that the α-pY361 bind to wild type E5 but not E5-Y361F (Fig 5C). Furthermore, using α-pY361 we found that when wild type EphB2, but not a kinase dead or cytoplasmic truncated version of EphB2, is expressed in 293 cells together with E5, E5 becomes phosphorylated at Y361 (Fig S5A). In contrast, when EphA4 or EphA2 were expressed in 293 cells we detected little to no phosphorylation of E5 at Y361 (Fig S5B). These findings suggest that EphB2, but not EphAs, promote E5 Y361 phosphorylation (pY361).

We also found by immunoblotting with the α-pY361 that E5 is phosphorylated at Y361 in the hippocampus of wild type but not $E5^{-/-}$ mice (Fig S5C), and that EB1 stimulation of cultured hippocampal neurons leads to E5 Y361 phosphorylation (Fig 5D). By immunofluorescence microscopy we detect punctate α-pY361 staining along the dendrites of EB1-treated wild type neurons, but less staining in untreated neurons (Fig 5E). This result suggests that E5 becomes newly phosphorylated at Y361 upon exposure of hippocampal neurons to EB1.

EphB2-mediated degradation of Ephexin5 is kinase and proteasome dependent

We asked if EB1 stimulation of E5 Y361 phosphorylation leads to a change in E5 activity or expression. To investigate this possibility we asked if EphB suppresses E5-dependent RhoA activation in a phosphorylation-dependent manner. We transfected 293 cells with E5 in the presence or absence of EphB2 and measured RhoA activity using the RBD pull down assay (Fig 5F). We found that E5-dependent RhoA activation was reduced in 293 cells expressing EphB2 and E5 compared to cells expressing E5 alone. These findings are consistent with the possibility that EphB2-mediated tyrosine phosphorylation of E5 either leads to a suppression of E5's ability to activate RhoA, or alternatively might trigger a decrease in E5 protein expression resulting in a decrease in RhoA activation. We found this latter possibility to be the case (Fig 5F, E5 loading control). Furthermore, when we compared lysates from the brains of wild type or $EphB2^{-/-}$ mice, we observed that E5 phosphorylation at Y361 is decreased while the levels of E5 expression are increased in the lysates from $EphB2^{-/-}$ mice (Fig 5G). These data suggest that EphB2 functions to phosphorylate and degrade E5.

Consistent with the idea that E5 expression is destabilized in the presence of EphB, we observed that in the dendrites of cultured hippocampal neurons overexpressing EphB2, endogenous E5 expression levels are reduced compared to control transfected neurons or neurons transfected with a kinase dead version of EphB2 (Fig S6A and B). When neurons were exposed to EB1 compared to EA1 for 60 minutes, we found by immunoblotting of neuronal extracts, or immunofluorescence staining with α-N-E5, that exposure to EB1 leads to a decrease in E5 expression (Fig 6A). The lack of complete loss of E5 expression by western blot may be due to the fact that EB1 stimulation leads to dendritic and not somatic loss of E5 expression. Moreover, immunofluorescence staining revealed a loss of E5 puncta specifically within the dendrites of EB1-stimulated neurons, consistent with the possibility that EB1/EphB-mediated degradation of E5 relieves an inhibitory constraint that suppresses excitatory synapse formation on dendrites. In support of this idea, we find by immunoblotting of extracts from mouse hippocampi that endogenous E5 protein levels are highest at postnatal day 3 prior to the time of maximal synapse formation and then decrease as synapse formation peaks in the postnatal period (Fig S6C). Northern blotting revealed that this decrease in E5 protein is not due to a change in the level of E5 mRNA expression (Fig S6C). Given that E5 protein levels decrease dramatically during the time period P7-P21 when synapse formation is maximal, these findings suggest that E5 may need to be degraded prior to synapse formation.

We asked whether EphB-mediated degradation of E5 could be reconstituted in heterologous cells. When EphB and Myc-tagged E5 were co-expressed in 293 cells we observed a

significant decrease in E5 protein expression in the presence of EphB2. The presence of EphB2 had no effect on the level of expression of a related GEF, E1 (Fig 6B). We asked whether EphB-mediated degradation of E5 depends upon Y361 phosphorylation. We found that in 293 cells overexpressing Myc-tagged E5, the co-expression of EphB2, but not EphB2-KD, resulted in a significant decrease in E5 levels (Fig 6C). This suggests that EphB tyrosine kinase activity is required for E5 degradation. The EphB-mediated reduction in E5 levels is dependent on Y361 phosphorylation, as EphB2 expression had no effect on the level of E5 Y361F expression (Fig 6D). This suggests that the phosphorylation of E5 at Y361 triggers E5 degradation.

We considered the possibility that the Y361 phosphorylation-dependent decrease in E5 protein levels might be due to EphB-dependent stimulation of E5 proteasomal degradation. Consistent with this possibility we found that addition of the proteasome inhibitor lactacystin to 293 cells leads to a reversal of the EphB-dependent decrease in E5 protein levels, as measured by an increase in total ubiquitinated E5 (Fig S6D). In addition, in neuronal cultures the EB1 induced decrease in E5 protein expression is blocked if the proteasome inhibitor lactacystin is added prior to EB1 addition (Fig 6E). Notably, in the presence of lactacystin, E5 is ubiquitinated, further supporting the idea that E5 is degraded by the proteasome.

To test whether E5 is ubiquitinated in the brain, we incubated wild type or $E5^{-/-}$ brain lysates with α-C-E5 and after immunoprecipitation and SDS-PAGE, probed with α-ubiquitin antibodies. This analysis detected the presence of ubiquitinated species in α-C-E5 immunoprecipitates prepared from wild type but not $E5^{-/-}$ brain lysates (Fig 6F). These findings indicate that E5 is ubiquitinated in the brain.

EphB2-mediated degradation of Ephexin5 requires Ube3A

During proteasome-dependent degradation of proteins, specificity is conferred by E3 ligases or E2 conjugating enzymes that recognize the substrate to be degraded. The E3 ligase binds to the substrate and catalyzes the addition of polyubiquitin side chains to the substrate thereby promoting degradation via the proteasome (Hershko and Ciechanover, 1998). We considered several E3 ligases that have recently been implicated in synapse development as candidates that catalyze E5 degradation. One of these E3 ligases, Cbl-b, has previously been implicated in the degradation of EphAs and EphBs (Fasen et al., 2008; Sharfe et al., 2003). A second E3 ligase, Ube3A, has been shown to regulate synapse number. To determine if Ube3A and/or Cbl-b catalyze E5 degradation we first asked if either of these E3 ligases interacts with and degrades E5 in 293 cells. When these E3 ligases were epitope-tagged and expressed in 293 cells together with E5 we found that E5 co-immunoprecipitates with Ube3A but not with Cbl-b (Fig 7A). The co-immunoprecipitation of Ube3A with E5 was specific in that Ube3A was not co-immunoprecipitated with two other neuronal proteins, E1 or the transcription factor MEF2. In a previous study we have shown that Ube3A binds to substrates via a Ube3A binding domain (hereafter referred to as UBD (Greer et al., 2010). Using protein sequence alignment programs, ClustalW and ModBase, we identified a UBD in E5, providing further support for the idea that E5 might be a substrate of Ube3A (Fig S7A). Consistent with this hypothesis, we found that the level of E5 expression is reduced in 293 cells co-transfected with Ube3A compared to cells co-transfected with Cbl-b (Fig S7B).

We asked if EB1/EphB-mediated E5 degradation in neurons is catalyzed by Ube3A. To inhibit Ube3A activity we introduced into neurons a dominant interfering form of Ube3A (dnUbe3A) that contains a mutation in the ubiquitin ligase domain rendering Ube3A inactive. We have previously shown that even though dnUbe3A is catalytically inactive it still binds to E2 ligases and to its substrates and functions in a dominant negative manner to block the ability of wild type Ube3A to ubiquitinate its substrates (Greer et al., 2010). We

found that when introduced into 293 cells dnUbe3A binds to E5 (Fig 7A). We also found by immunofluorescence microscopy that when overexpressed in neurons, dnUbe3Ablocks EB1/EphB stimulation of E5 degradation (Fig 7B). EB1/EphB stimulation of E5 degradation was also attenuated when Ube3A expression was knocked down by a shRNA that specifically targets the Ube3A mRNA (Fig 7B (Greer et al., 2010)). Notably, the presence of the dnUbe3A did not affect E5 expression in neurons in the absence of EphrinB stimulation, suggesting that EphrinB stimulation of E5 Y361 phosphorylation may be required for Ube3A-mediated degradation of E5 (Fig S7C).

To determine if Ube3A-dependent degradation of E5 might be relevant to the etiology of Angelman syndrome we asked if the absence of Ube3A in a mouse model of Angelman syndrome affects the level of E5 expression in the brain. We compared the level of E5 protein expression in the brains of wild type mice to that expressed in the brains of mice in which the maternally inherited Ube3A was disrupted ($Ube3A^{m-/p+}$). Because the paternally inherited copy of Ube3A is silenced in the brain due to imprinting, the level of Ube3A expression in $Ube3A^{m-/p+}$ neurons is very low. We found that the level of E5 expression in the brains of $Ube3A^{m-/p+}$ mice was significantly higher than that detected in the brains of wild type mice (Fig 7C). Moreover, the level of ubiquitinated E5 in brains of $Ube3A^{m-/p+}$ mice was significantly reduced compared to the brains of litter mate controls (Fig 7D). In addition we found that when neurons from wild type and $Ube3A^{m-/p+}$ brains were cultured and then treated with EB1 the level of E5 protein was reduced upon EB1 treatment in wild type but not in $Ube3A^{m-/p+}$ neurons (Fig 7E). Taken together, these findings suggest that in response to EB treatment E5 is tyrosine phosphorylated by an EphB-dependent mechanism, and that this leads to E5 degradation by a Ube3A-dependent mechanism. If E5 degradation is disrupted due to a loss of Ube3A as occurs in Angelman syndrome the result is an increase in E5 expression and a disruption of the proper control of excitatory synapse number during brain development.

Discussion

Previous studies have revealed a role for EphrinB/EphB signaling in the development of excitatory synapses (Klein, 2009). However, the regulatory constraints that temper EphB-dependent synapse development so that excitatory synapses form at the right time and place, and in the correct number were not known. In this study we identify a RhoA GEF, E5, which functions to restrict EphB-dependent excitatory synapse development. E5 interacts with EphB prior to EphrinB binding, and by activating RhoA serves to inhibit synapse development. The binding of EphrinB to EphB as synapses form triggers the phosphorylation and degradation of E5 by a Ube3A-dependent mechanism. The reduction in E5 expression may allow EphB to promote excitatory synapse development by activating Rac and other proteins at the synapse.

The findings that E5 functions to restrict excitatory synapse number suggests that, even though EphBs promote excitatory synapse development, there are constraints on the activity of EphB so that synapse number is effectively controlled. There are several steps in the process of synapse development where E5 may function to restrict synapse number. One possibility is that E5 functions early in development as a barrier to excitatory synapse formation by activating RhoA and restricting the motility or growth of dendritic filopodia that are the sites of contact by the presynaptic neuron. For example, by inhibiting dendritic filopodia formation or motility, E5 may decrease the number of contacts the filopodia make with the presynaptic neuron, thus resulting in the formation of fewer synapses. An alternative possibility is that E5 functions to restrict synapse number later in development perhaps to counterbalance the positive effects of EphB on Rac that promote dendritic spine

development. An additional possibility is that E5 functions after excitatory synapse development as a regulator of synapse elimination.

Our analyses of E5 function are most consistent with the possibility that E5 functions early in the process of synapse development. First, we find that E5 is expressed, active, and bound to EphB prior to synapse formation. Second, the interaction of EphrinB with EphB, a process that is thought to be an early step in excitatory synapse development, triggers the degradation of E5. Third, our preliminary time-lapse imaging studies suggest that E5 is localized to newly formed filopodia prior to synapse development where it appears to restrict filopodia motility and growth (Margolis et al. unpublished). Thus, E5 might function as an initial barrier to synapse formation until it is degraded upon EphrinB binding to EphB.

It is possible that through its interaction with EphB, E5 marks the sites where synapses will form, and that the degradation of E5 is a critical early step in excitatory synapse development. While the mechanisms by which E5 is degraded are not fully understood, our studies suggest that the phosphorylation of the N-terminus of E5 at Y361 triggers the Ube3A-mediated proteasomal degradation of E5. One possibility is that prior to pY361 the N- and C-terminal portions of E5 interact, thereby protecting E5 from degradation. The phosphorylation of E5 at Y361 may relieve this inhibitory constraint allowing for E5 ubiquitination and degradation. A similar mechanism has been shown to regulate the activation of the Rac GEF Vav, (Aghazadeh et al., 2000)). During EphrinA/EphA signaling it has been proposed that Vav-mediated endocytosis of the EphrinA/EphA complex may allow the conversion of the initial adhesive interaction between EphrinA and EphA-expressing cells into a repulsive interaction that results in growth cone collapse and axon repulsion. It is possible that E5 has a related function during EphB signaling at synapses. Typically the EB/EphB interaction is thought to be repulsive. This has been documented in studies of EphB's role in the process of axon guidance (Egea and Klein, 2007; Flanagan and Vanderhaeghen, 1998). However, during synapse development the EphrinB/EphB interaction is thought to result in synapse formation, a process that requires an interaction between the developing pre- and post-synaptic specialization. One possibility is that when EphrinB and EphB mediate the interaction between the incoming axon and the developing dendrite, the interaction is facilitated by the degradation of E5 by Ube3A. Since E5 is a RhoA GEF, its presence might initially lead to repulsion between the incoming axon and the dendrite. However, the EphB-dependent degradation of E5 might convert this initial repulsive interaction into an attractive one.

The finding that Ube3A is the ubiquitin ligase that controls EphB-mediated E5 degradation is of interest given the role of Ube3A in human cognitive disorders such as Angelman syndrome and autism. The absence of Ube3A function in Angelman syndrome would be predicted to result in an increase in E5 protein expression, and thus a decrease in EphB-dependent synapse formation. Consistent with this possibility, we find in a mouse model for Angelman syndrome that the level of E5 protein expression is elevated and that in response to EphrinB treatment E5 is not degraded. Likewise, several studies have indicated that synapse development and function is disrupted in these mice (Jiang et al., 1998; Yashiro et al., 2009).

The recent finding that the Ube3A gene lies within a region of chromosome 15 that is sometimes duplicated in autism raises the possibility that altered levels of Ephexin5 and the resulting defects in excitatory synapse restriction might also be a mechanism relevant to the etiology of autism (Glessner et al., 2009). If this is the case, a possible therapy for treating autism might be to reduce the level of Ube3A activity, and thus increase the level of Ephexin5 expression. It is important to consider that in addition to Ephexin5, Ube3A regulates the abundance of other synaptic proteins. Nevertheless, the ultimate effect of the

aberrant expression of Ephexin5 and other Ube3A substrates on synapse development and function will require further study. It seems likely that such studies will provide further understanding of the development of human cognitive function and new insights into how this process goes awry in disorders such as Angelman syndrome and autism.

Experimental Procedures

DNA Constructs

Details of DNA constructs can be found in supplementary section.

Generation of *E5*$^{-/-}$ Mice

An E5 targeting vector was electroporated into 129 J1 ES cells, and positive clones were identified by Southern hybridization with two separate probes (See supplementary section).

Antibodies

Details of antibodies can be found in supplementary section.

Mice, Cell culture, Transfections, and Ephrin stimulations

Ube3a knockout mice were previously described (Greer et al., 2010). EphB2 knockout mice were previously described (Kayser et al., 2008). 293T cells were cultured in DMEM and transfected using the calcium phosphate method. Organotypic slice cultures were prepared from P6 mouse brains and biolistically transfected. Acute slices were prepared from P12-14 mice. Dissociated neurons were cultured in Neurobasal Medium supplemented with B27 and transfected using the Lipofectamine method. For details on cell culture, transfections and Ephrin stimulations see supplementary section.

Cell lysis, immunoprecipitations, GEF pulldown assays and western blots

Whole rat or mouse brains or cultured cells were collected and homogenized in RIPA buffer. For immunoprecipitations, lysed cells were centrifuged and supernatants were incubated with appropriate antibody for 2 hours at 4°C, followed by addition of Protein-A or Protein-G beads (Santa Cruz Biotechnology) for 1 hour, and washed three times with ice-cold RIPA buffer. For the α-PY361 detection experiment in 293T cells, samples were boiled in SDS buffer to disrupt the E5/EphB2 interaction and diluted 1:5 in 1.25X RIPA buffer prior to immunoprecipitation of E5-Myc. RBD and PBD pulldown assays were conducted according to the manufacture's suggestions (Upstate Cell Signaling Solutions). For details see supplementary section.

In situ hybridization

To generate probes for *in situ* hybridization, mouse E5 and EphB2 cDNA were subcloned into pBluescript II SK (+). Bluescript plasmids containing E5 or EphB2 cDNA were linearized using the restriction enzyme BssHII. Sense and antisense probes were generated using DIG RNA labeling mix (Roche) according to manufacturer's instructions. Full-length DIG-labeled probes were subjected to alkaline hydrolysis as described in supplementary section.

Immunocytochemistry

Neurons were paraformaldehyde fixed in PBS. For measuring synapse density, fixed neurons were incubated with α-PSD-95 and α-Synapsin antibodies followed by α-Cy3 and α-Cy5 antibodies to visualize the primary antibodies. For protein co-localization experiments fixed neurons were similarly treated using α-EphB2 antibodies and α-N-E5

antibodies or α-pY361-E5. For over-expression studies fixed neurons were incubated using α-Myc or α-Flag antibodies to visualize overexpressed E5-Myc or EphB2-Flag protein in the context of the GFP-labeled neurons. For details see supplementary section.

Synapse Assay, Image analysis and quantification

Images were acquired on a Zeiss LSM5 Pascal confocal microscope and spine and synapse analysis was performed as previously described (see supplementary section).

Ube3A Knockout Cultures

Dissociated hippocampal neurons from Ube3A knockout and wild-type mice were prepared as previously described (Greer et al., 2010).

Array Tomography

Array tomography was performed as previously described (Micheva and Smith, 2007) with modifications as described in the supplementary section.

Electrophysiology

Electrophysiology was performed using standard methods (see supplementary section).

Supplementary Material

Refer to Web version on PubMed Central for supplementary material.

Acknowledgments

We thank M. Thompson, Y. Zhou, and H. Ye for assistance in generating mice; E. Griffith, J. Zieg, S. Cohen, I. Spiegel, M. Andzelm, and the Greenberg lab for critical discussions. This work was supported by National Institute of Neurological Disorders and Stroke grant RO1 5R01NS045500 (M.E.G); NRSA Training grant 5T32AG00222-15 (S.S.M.); Edward R. and Anne G. Lefler postdoctoral fellowship (S.S.M.).

References

Aghazadeh B, Lowry WE, Huang XY, Rosen MK. Structural basis for relief of autoinhibition of the Dbl homology domain of proto-oncogene Vav by tyrosine phosphorylation. Cell. 2000; 102:625–633. [PubMed: 11007481]

Dalva MB, Takasu MA, Lin MZ, Shamah SM, Hu L, Gale NW, Greenberg ME. EphB receptors interact with NMDA receptors and regulate excitatory synapse formation. Cell. 2000; 103:945–956. [PubMed: 11136979]

Dalva MB, McClelland AC, Kayser MS. Cell adhesion molecules: signalling functions at the synapse. Nat Rev Neurosci. 2007; 8:206–220. [PubMed: 17299456]

Egea J, Klein R. Bidirectional Eph-ephrin signaling during axon guidance. Trends Cell Biol. 2007; 17:230–238. [PubMed: 17420126]

Ethell IM, Irie F, Kalo MS, Couchman JR, Pasquale EB, Yamaguchi Y. EphB/syndecan-2 signaling in dendritic spine morphogenesis. Neuron. 2001; 31:1001–1013. [PubMed: 11580899]

Fasen K, Cerretti DP, Huynh-Do U. Ligand binding induces Cbl-dependent EphB1 receptor degradation through the lysosomal pathway. Traffic. 2008; 9:251–266. [PubMed: 18034775]

Flanagan JG, Vanderhaeghen P. The ephrins and Eph receptors in neural development. Annu Rev Neurosci. 1998; 21:309–345. [PubMed: 9530499]

Fu WY, Chen Y, Sahin M, Zhao XS, Shi L, Bikoff JB, Lai KO, Yung WH, Fu AK, Greenberg ME, et al. Cdk5 regulates EphA4-mediated dendritic spine retraction through an E1-dependent mechanism. Nat Neurosci. 2007; 10:67–76. [PubMed: 17143272]

Greer PL, Hanayama R, Bloodgood BL, Mardinly AR, Lipton DM, Flavell SW, Kim TK, Griffith EC, Waldon Z, Maehr R, et al. The Angelman Syndrome protein Ube3A regulates synapse development by ubiquitinating arc. Cell. 2010; 140:704–716. [PubMed: 20211139]

Grunwald IC, Korte M, Wolfer D, Wilkinson GA, Unsicker K, Lipp HP, Bonhoeffer T, Klein R. Kinase-independent requirement of EphB2 receptors in hippocampal synaptic plasticity. Neuron. 2001; 32:1027–1040. [PubMed: 11754835]

Grunwald IC, Korte M, Adelmann G, Plueck A, Kullander K, Adams RH, Frotscher M, Bonhoeffer T, Klein R. Hippocampal plasticity requires postsynaptic ephrinBs. Nat Neurosci. 2004; 7:33–40. [PubMed: 14699416]

Henkemeyer M, Itkis OS, Ngo M, Hickmott PW, Ethell IM. Multiple EphB receptor tyrosine kinases shape dendritic spines in the hippocampus. J Cell Biol. 2003; 163:1313–1326. [PubMed: 14691139]

Hershko A, Ciechanover A. The ubiquitin system. Annu Rev Biochem. 1998; 67:425–479. [PubMed: 9759494]

Jiang YH, Armstrong D, Albrecht U, Atkins CM, Noebels JL, Eichele G, Sweatt JD, Beaudet AL. Mutation of the Angelman ubiquitin ligase in mice causes increased cytoplasmic p53 and deficits of contextual learning and long-term potentiation. Neuron. 1998; 21:799–811. [PubMed: 9808466]

Jontes JD, Buchanan J, Smith SJ. Growth cone and dendrite dynamics in zebrafish embryos: early events in synaptogenesis imaged in vivo. Nat Neurosci. 2000; 3:231–237. [PubMed: 10700254]

Kayser MS, McClelland AC, Hughes EG, Dalva MB. Intracellular and trans-synaptic regulation of glutamatergic synaptogenesis by EphB receptors. J Neurosci. 2006; 26:12152–12164. [PubMed: 17122040]

Kayser MS, Nolt MJ, Dalva MB. EphB receptors couple dendritic filopodia motility to synapse formation. Neuron. 2008; 59:56–69. [PubMed: 18614029]

Kishino T, Lalande M, Wagstaff J. UBE3A/E6-AP mutations cause Angelman syndrome. Nat Genet. 1997; 15:70–73. [PubMed: 8988171]

Klein R. Bidirectional modulation of synaptic functions by Eph/ephrin signaling. Nat Neurosci. 2009; 12:15–20. [PubMed: 19029886]

Lai KO, Ip NY. Synapse development and plasticity: roles of ephrin/Eph receptor signaling. Curr Opin Neurobiol. 2009; 19:275–283. [PubMed: 19497733]

Lim BK, Matsuda N, Poo MM. Ephrin-B reverse signaling promotes structural and functional synaptic maturation in vivo. Nat Neurosci. 2008; 11:160–169. [PubMed: 18193042]

Micheva KD, Smith SJ. Array tomography: a new tool for imaging the molecular architecture and ultrastructure of neural circuits. Neuron. 2007; 55:25–36. [PubMed: 17610815]

Murai KK, Nguyen LN, Irie F, Yamaguchi Y, Pasquale EB. Control of hippocampal dendritic spine morphology through ephrin-A3/EphA4 signaling. Nat Neurosci. 2003; 6:153–160. [PubMed: 12496762]

Ogita H, Kunimoto S, Kamioka Y, Sawa H, Masuda M, Mochizuki N. EphA4-mediated Rho activation via Vsm-RhoGEF expressed specifically in vascular smooth muscle cells. Circ Res. 2003; 93:23–31. [PubMed: 12775584]

Penzes P, Beeser A, Chernoff J, Schiller MR, Eipper BA, Mains RE, Huganir RL. Rapid induction of dendritic spine morphogenesis by trans-synaptic ephrinB-EphB receptor activation of the Rho-GEF kalirin. Neuron. 2003; 37:263–274. [PubMed: 12546821]

Rossman KL, Der CJ, Sondek J. GEF means go: turning on RHO GTPases with guanine nucleotide-exchange factors. Nat Rev Mol Cell Biol. 2005; 6:167–180. [PubMed: 15688002]

Sahin M, Greer PL, Lin MZ, Poucher H, Eberhart J, Schmidt S, Wright TM, Shamah SM, O'Connell S, Cowan CW, et al. Eph-dependent tyrosine phosphorylation of ephexin1 modulates growth cone collapse. Neuron. 2005; 46:191–204. [PubMed: 15848799]

Shamah SM, Lin MZ, Goldberg JL, Estrach S, Sahin M, Hu L, Bazalakova M, Neve RL, Corfas G, Debant A, et al. EphA receptors regulate growth cone dynamics through the novel guanine nucleotide exchange factor ephexin. Cell. 2001; 105:233–244. [PubMed: 11336673]

Sharfe N, Freywald A, Toro A, Roifman CM. Ephrin-A1 induces c-Cbl phosphorylation and EphA receptor down-regulation in T cells. J Immunol. 2003; 170:6024–6032. [PubMed: 12794130]

Snyder JT, Worthylake DK, Rossman KL, Betts L, Pruitt WM, Siderovski DP, Der CJ, Sondek J. Structural basis for the selective activation of Rho GTPases by Dbl exchange factors. Nat Struct Biol. 2002; 9:468–475. [PubMed: 12006984]

Tashiro A, Minden A, Yuste R. Regulation of dendritic spine morphology by the rho family of small GTPases: antagonistic roles of Rac and Rho. Cereb Cortex. 2000; 10:927–938. [PubMed: 11007543]

Yashiro K, Riday TT, Condon KH, Roberts AC, Bernardo DR, Prakash R, Weinberg RJ, Ehlers MD, Philpot BD. Ube3a is required for experience-dependent maturation of the neocortex. Nat Neurosci. 2009; 12:777–783. [PubMed: 19430469]

Ziv NE, Smith SJ. Evidence for a role of dendritic filopodia in synaptogenesis and spine formation. Neuron. 1996; 17:91–102. [PubMed: 8755481]

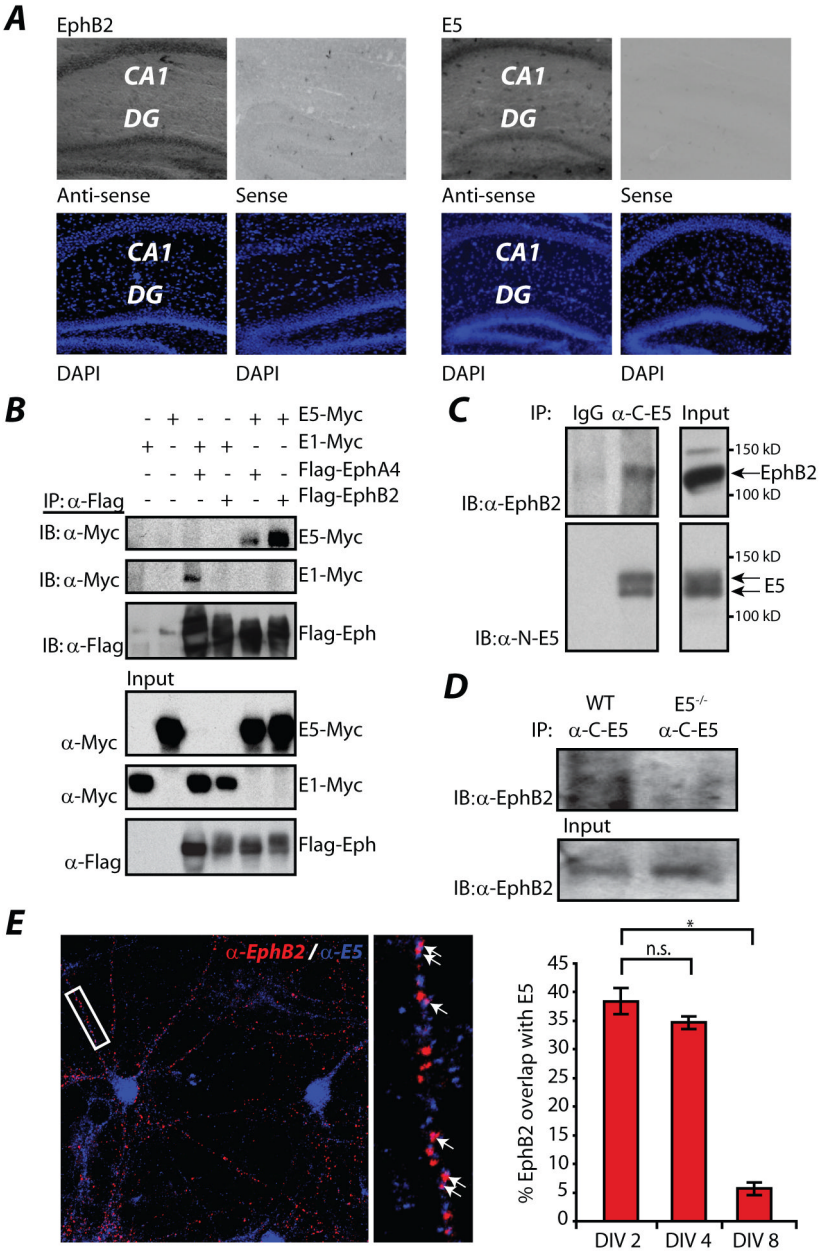

Figure 1. Ephexin5 interacts with EphB2

A) E5 and EphB2 are expressed in the CA1 region and dentate gyrus (DG) of the hippocampus at P12. Adjacent 100 nm mouse brain sections were stained for E5 or EphB2 using digoxigenin-labeled RNA probes to the anti-sense strand or sense strand as a control (top). Lower panels show nuclear staining with DAPI.

B) Immunoprecipitation with α-Flag from 293 cell lysates previously transfected with various combinations of overexpressing plasmids containing E1-Myc, E5-Myc, Flag-EphB2, and/or Flag-EphA4, followed by immunoblotting with α-Myc or α-Flag. Input protein levels shown (bottom).

C) Immunoprecipitation of mouse cortical lysates with IgG or α-C-E5, followed by immunoblotting with α-EphB2 or α-N-E5 (left). Input protein levels shown (right).

D) Immunoprecipitation of WT or $E5^{-/-}$ mouse whole brain lysates with α-C-E5 followed by immunoblotting with α-EphB2. Input EphB2 levels shown (bottom).
E) Dissociated rat hippocampal neurons were stained using α-N-E5 (Blue) and α-EphB2 (Red). A representative image of overlapped EphB2 and E5 is shown (left). White rectangle outlines magnified dendritic region (right) showing examples of EphB2/E5 co-localization (arrows). In three independent experiments, quantification of overlapped EphB2/E5 puncta was determined at DIV2, DIV4 and DIV8 and is represented as percent of EphB2 overlapped with E5 (right). Error bars ±SEM; *p <0.05, non-significant (n.s.).
See also Figure S1.

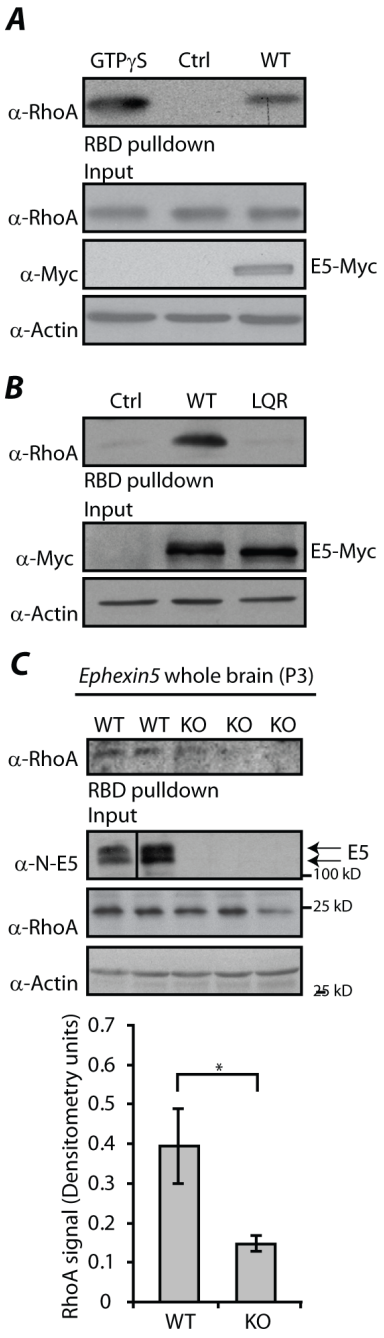

Figure 2. Ephexin5 is a GEF that activates RhoA

A) Lysates from 293 cells transfected with empty vector (Ctrl) or E5-Myc overexpressing vector (WT) were assayed for endogenous RhoA activity using the RBD pulldown assay and analyzed by immunoblotting with an antibody to RhoA (top). GTPγS lane is a positive control for inducing RhoA activity. Increased endogenous RhoA activity is demonstrated by presence of α-RhoA signal in RBD pulldown lanes. Input protein levels and α-Actin loading control are shown (Bottom).

B) Lysates from 293 cells transfected with empty vector (Ctrl), E5-Myc (WT) or LQR mutant of E5-Myc (LQR) were assessed for RhoA activity as measured by RBD assay described in (A). Input protein levels and α-Actin loading control are shown (Bottom).

C) Presence of E5 is critical for wild type levels of endogenous RhoA signaling *in vivo.* P3 mouse whole brain lysates from WT or $E5^{-/-}$ (KO) littermates were subjected to RBD pulldown assays as described in (A). A representative immunoblot is shown (left). From three experiments, blinded to condition, the quantification of α-RhoA signal was normalized to input RhoA signal (Right). Error bars ±SEM; *p<0.05.
See also Figure S2.

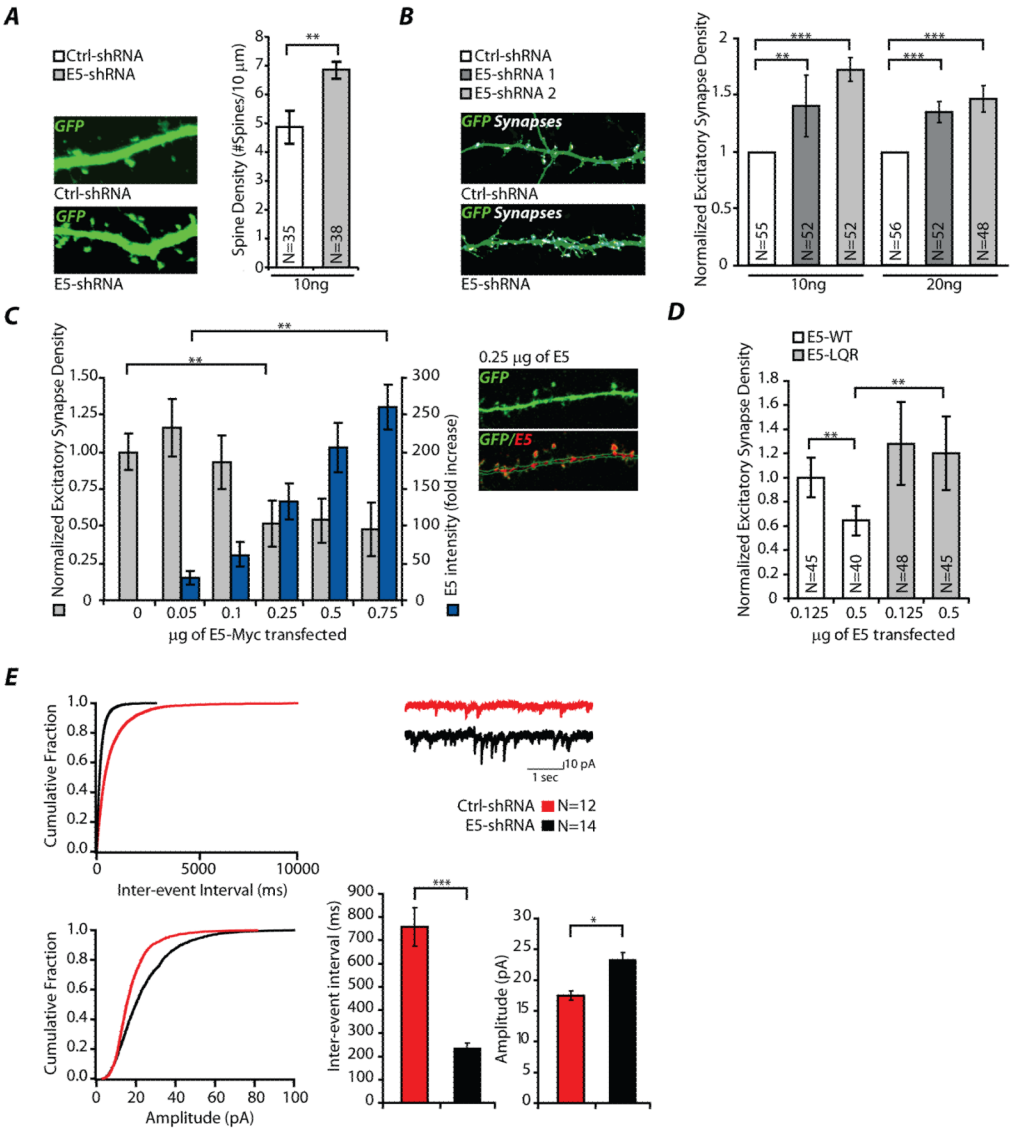

Figure 3. Ephexin5 negatively regulates excitatory synapse number

A) 10 ng of E5-shRNA or Ctrl-shRNA was co-transfected with GFP into rat hippocampal neurons at DIV14. At DIV18 dendritic spines were measured as described in methods. Representative image illustrates dendritic spines. N indicates number of neurons assessed. Error bars ±SEM; **p < 0.01, ANOVA.

B) 10 ng or 20 ng of two different E5-shRNA or Ctrl-shRNA constructs was co-transfected with GFP into rat hippocampal neurons at DIV10. At DIV14 excitatory synapses were measured as described in methods. Representative image illustrates quantified synapse puncta (White). Error bars ±SEM; **p < 0.01, ***p<0.005, ANOVA.

C) DIV10 rat hippocampal neurons were co-transfected with GFP and increasing concentrations of E5-Myc or control plasmid. At DIV 14 excitatory synapses (gray bars) and exogenous E5 expression (blue bars) were measured as described in methods. Representative image illustrates localization of E5-Myc on transfected neuron (Red). Error bars ±SEM; **p < 0.01, ANOVA.

D) Neurons were transfected with E5-Myc (E5-WT) or E5-LQR-Myc (E5-LQR) and quantified as in (C). Error bars ±SEM; **p < 0.01, ANOVA.

E) Quantification of mEPSC inter-event interval and amplitude from hippocampal neurons transfected as in (B) with 20 ng of shRNA. Cumulative distribution plots, bar graphs and representative traces are shown. Error bars are standard deviation of the mean, ***$p<0.005$, *$p<0.05$.
See also Figures S3, and S1.

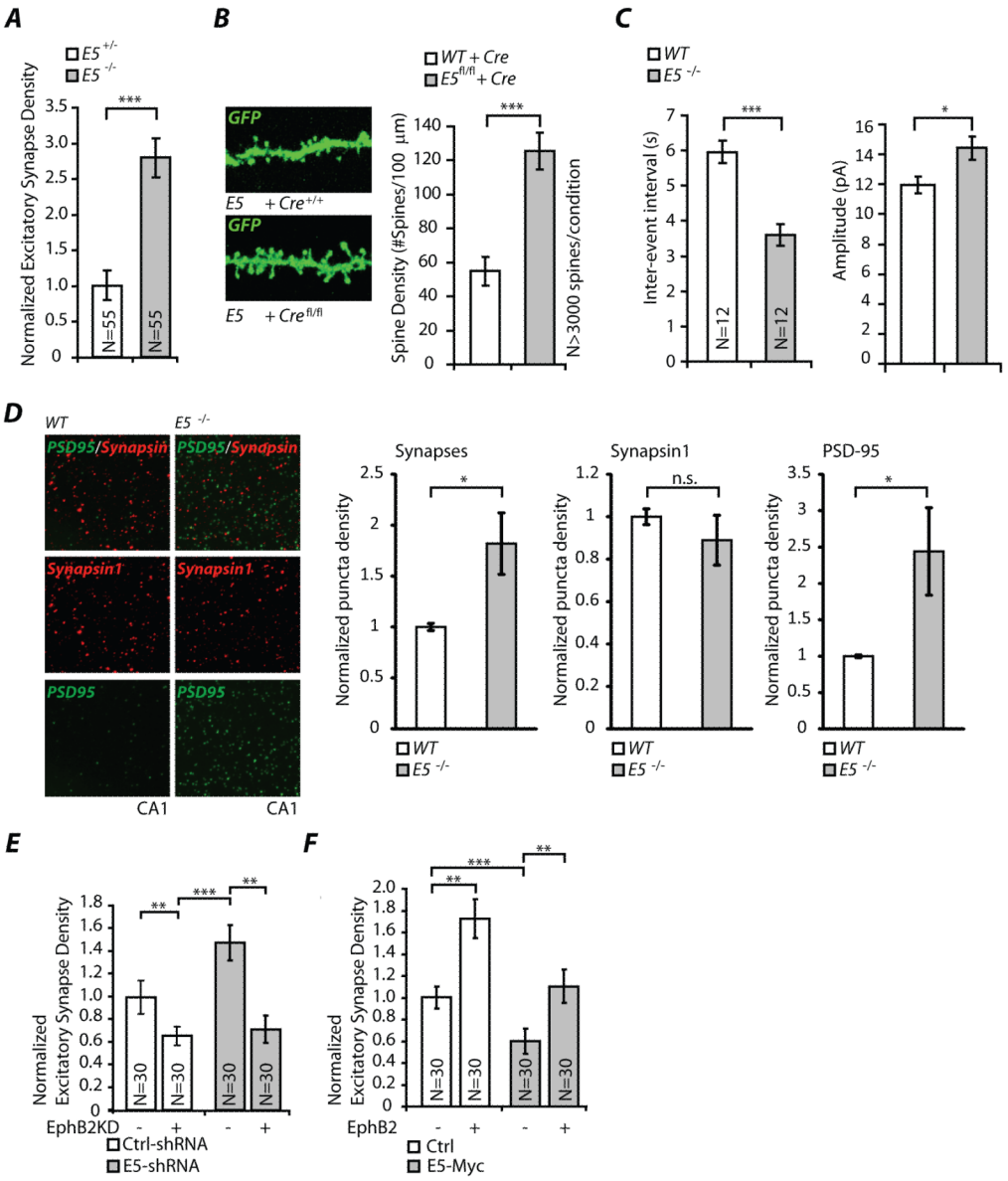

Figure 4. Ephexin5 restricts EphB2 control of excitatory synapse formation

A) E16 hippocampi from E5$^{+/-}$ or E5$^{-/-}$ mice were dissected and dissociated for culture. At DIV10 dissociated neurons were transfected with GFP. At DIV14 neurons were fixed, stained and, excitatory synapses were measured as described in methods. Error bars ±SEM; ***p < 0.005, ANOVA.

B) Organotypic slices from WT or E5$^{fl/fl}$ mice were biolistically transfected with Cre-recombinase (Cre) and dendritic spines were quantified as described in methods. Representative images are shown (left). Error bars ±SEM; ***p < 0.005, KS test.

C) Quantification of mEPSC inter-event interval and amplitude from acute hippocampal brain slices prepared from P12-P14 WT or E5$^{-/-}$ mice. Error bars are standard deviation of the mean; ***p<0.005, *p<0.05.

D) Hippocampi from three independent littermate pairs consisting of P12 WT and E5$^{-/-}$ mice were prepared as described in methods for quantification of synapses, Synapsin1 and PSD-95 using array tomography. Error bars ±SEM; *p < 0.05, Mann-Whitney U-Test.

E) Increase in excitatory synapse number following loss of E5 requires EphB2 signaling. At DIV10, control plasmid (−) or EphB2KD plasmid (+) were co-expressed in dissociated mouse hippocampal neurons with GFP and either Ctrl-shRNA or E5-shRNA. At DIV14 excitatory synapses were measured as described in methods. Error bars ±SEM; **p < 0.01, ***p<0.005, ANOVA.

F) E5 can suppress an EphB2-mediated increase in excitatory synapse number. At DIV10, control plasmid (-) or EphB2-expressing plasmid (+) were co-expressed in dissociated mouse hippocampal neurons with GFP and either control (Ctrl) plasmid or E5-Myc plasmid. At DIV14 excitatory synapses were measured as described in methods. Error bars ±SEM; **p < 0.01, ***p<0.005, ANOVA.

See also Figures S4, and S1.

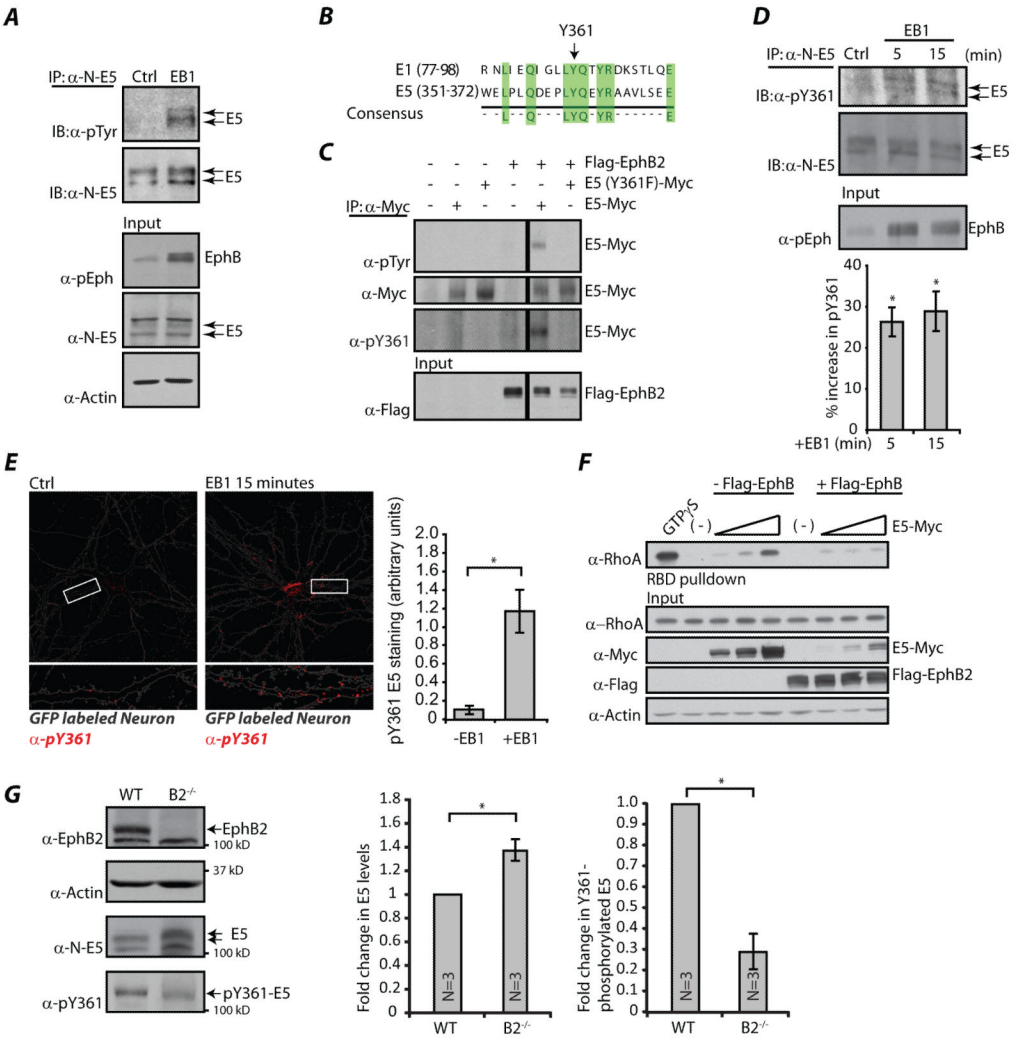

Figure 5. EphB2 mediates phosphorylation of Ephexin5 at tyrosine-361

A) Dissociated mouse hippocampal neurons were stimulated with either α-Fc IgG (Ctrl) or pre-clustered Fc-EB1 for 15 minutes. Neuronal lysates were immunoprecipitated with α-N-E5, followed by immunoblotting for pan-phosphotyrosine (α-pTyr) or E5 with α-N-E5. EB1 stimulation was determined by immunoblotting neuronal lysates for phospho-Eph (pEph). Input protein levels and α-Actin loading control are shown (Bottom).

B) E5-Y361 is a conserved residue with E1-Y87 (Sahin et al., 2005).

C) Immunoprecipitation with α-Myc from 293 cell lysates previously transfected with various combinations of overexpressing plasmids containing E5-Myc, E5 (Y361F)-Myc and/or EphB2-Flag, followed by immunoblotting with α-pTyr, α-Myc, α-pY361 or α-Flag. Input EphB2 levels are shown (bottom).

D) Neurons were treated and lysates prepared as in part A followed by immunoblotting with α-pY361 or α-N-E5. Representative immunoblot with input phospho-Eph (pEph) levels is shown (top). Quantification of three independent experiments is shown as a percent increase in pY361 over Ctrl stimulation (bottom). Error bars ±SEM; *p<0.05.

E) Dissociated rat hippocampal neurons were transfected with GFP (gray) and stimulated as in part A, followed by fixing and staining for endogenous phosphorylated E5 using α-pY361 (Red). Representative image shown (left). White rectangle outlines magnified dendritic

region showing examples of phospho-E5 staining (left bottom). Four independent experiments were imaged and analyzed for pY361 (bar graph). Error bars ±SEM; *p<0.05.
F) Lysates from 293 cells transfected with empty vector (-) or increasing concentrations of E5-Myc with or without Flag-EphB2 were assessed for endogenous RhoA activity by RBD assay (previously described). GTPγS lane is a positive control for inducing RhoA. Input protein levels and α-Actin loading control are shown (Bottom).
G) WT and EphB2$^{-/-}$ (B2$^{-/-}$) brain lysates were immunoblotted with α-EphB2, α-N-E5, α-Actin, or α-pY361 according to methods (left). Quantification of α-N-E5 or α-pY361 signal from three independent experiments is normalized to α-Actin and represented as fold change compared to wild type. Error bars ±SEM; *p<0.05.
See also Figure S5.

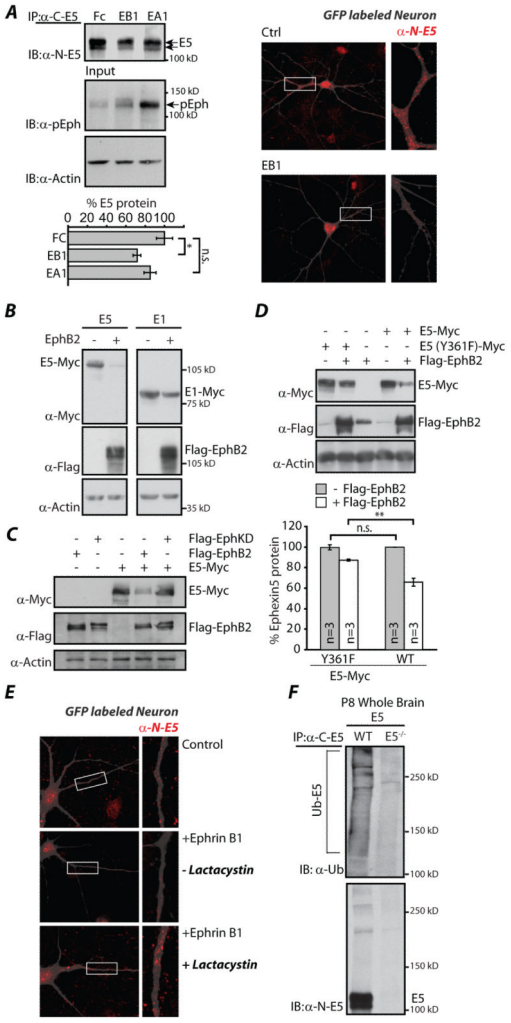

Figure 6. EphB2-mediated degradation of Ephexin5 is kinase and proteasome dependent

A) Dissociated mouse hippocampal neurons were incubated with pre-clustered Fc, Fc-EB1 or Fc-EA1 for 60 minutes, lysed, and immunoprecipitated with α-C-E5 followed by immunoblotting with α-N-E5. Immunoblot of input with α-pEph or α-Actin (loading control) are shown. Western is one representative image and quantification is of three separate experiments with samples normalized to α-Actin (left). Error bars ±SEM; *p<0.05. Right, dissociated mouse hippocampal neurons were transfected with GFP (gray) and stimulated with either pre-clustered Fc (Ctrl) or Fc-EB1 (EB1) for 30 minutes, followed by fixing and staining for endogenous E5 using α-N-E5 (Red). White rectangle outlines magnified dendritic region showing examples of E5 staining (right).

B) Lysates from 293 cells previously transfected with various combinations of overexpressing plasmids containing E5-Myc, E1-Myc and/or Flag-EphB2 were immunoblotted with α-Myc, αFlag, or α-Actin (loading control).

C) Lysates from 293 cells previously transfected with various combinations of overexpressing plasmids containing Flag-EphB2, Flag-EphB2KD and/or E5-Myc were immunoblotted with α-Myc, α-Flag, or α-Actin (loading control).

D) Lysates from 293 cells previously transfected with various combinations of overexpressing plasmids containing E5-Myc, E5-Y361F-Myc and/or Flag-EphB2 were immunoblotted with α-Myc, α-Flag, or α-Actin (loading control). Representative

immunoblot is shown (top). From three independent experiments E5 levels were quantified and normalized to E5 expression in absence of EphB2-Flag (bottom). Error bars ±SEM; **p<0.01.

E) Dissociated mouse hippocampal neurons transfected with GFP (gray) were stimulated similar to (B) in the absence or presence of lactacystin and immunostained with α-N-E5. White rectangle outlines magnified dendritic region showing examples of E5 staining (right).

F) WT and $E5^{-/-}$ brains were lysed and immunoprecipitated with α-C-E5 followed by immunoblotting with α-ub or α-N-E5.

See also Figure S6.

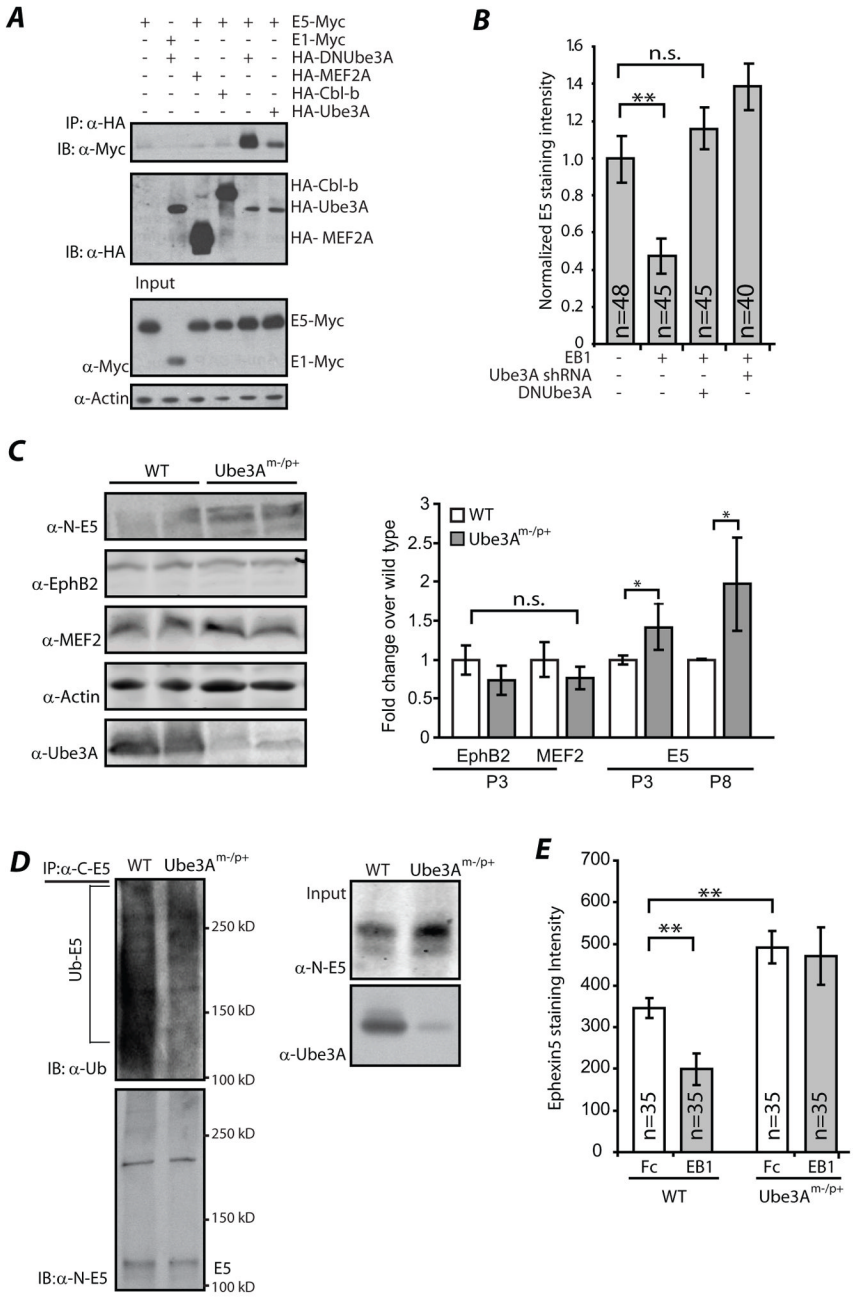

Figure 7. EphB2-mediated degradation of Ephexin5 requires Ube3A

A) Immunoprecipitation with α-HA from 293 cell lysates previously transfected with various combinations of plasmids containing E1-Myc, E5-Myc, HA-DNUbe3A, HA-MEF2A, HA-Cbl-b, and/or HA-Ube3A, followed by immunoblotting with α-HA or α-Myc. Input protein levels and αActin loading control are shown (Bottom).

B) Hippocampal mouse neurons were co-transfected with GFP and control, HA-DNUbe3A or Ube3A-shRNA at DIV10. At DIV14, neurons were incubated with clustered Fc (-) or Fc-EB1 (+) for 30 minutes. Neurons were fixed and stained for E5 with α-N-E5 and quantified according to methods. Quantification is of E5 staining intensity normalized to Fc control. Error bars ±SEM; **p < 0.01, ANOVA.

C) Ube3A wild type and maternal-deficient ($Ube3A^{m-/p+}$) mouse brains were lysed and immunoblotted with α-N-E5, α-EphB2, α-MEF2, α-Actin (loading control), or α-Ube3A (top). Samples were normalized to α-Actin and quantified as described in methods (bottom). Error bars ±SEM; *p<0.05, Mann-Whitney.
D) Brain lysates from WT and $Ube3A^{m-/p+}$ were collected and treated similar to E, immunoprecipitated with α-C-E5 and immunoblotted with α-N-E5 and α-ub. Input protein levels are shown (right).
E) Neurons from WT and $Ube3A^{m-/p+}$ mice were dissociated, cultured and transfected with GFP at DIV10. At DIV14, neurons were incubated with pre-clustered Fc or Fc-EB1 for 30 minutes. Neurons were fixed and stained for E5 with α-N-E5 and quantified according to methods. Error bars ±SEM; **p<0.01.
See also Figure S7.

Published in final edited form as:
Neuron. 2012 February 9; 73(3): 466–481. doi:10.1016/j.neuron.2011.11.029.

The Nogo Receptor Family Restricts Synapse Number in the Developing Hippocampus

Zachary P. Wills[1,2], **Caleigh Mandel-Brehm**[1], **Alan R. Mardinly**[1], **Alejandra E. McCord**[1], **Roman J. Giger**[3,4], and **Michael E. Greenberg**[1,*]

[1]Department of Neurobiology, Harvard Medical School, 220 Longwood Avenue, Boston MA 02115, USA

[2]Department of Neurobiology, University of Pittsburgh, 200 Lothrop Street, Pittsburgh, PA 15213, USA

[3]Department of Cell and Developmental Biology, University of Michigan School of Medicine, 3065 BSRB, 109 Zina Pitcher Place, Ann Arbor, MI 48109-2200, USA

[4]Department of Neurology, University of Michigan School of Medicine, 3065 BSRB, 109 Zina Pitcher Place, Ann Arbor, MI 48109-2200, USA

SUMMARY

Neuronal development is characterized by a period of exuberant synaptic growth that is well studied. However, the mechanisms that restrict this process are less clear. Here we demonstrate that glycosyl-phosphatidylinositol-anchored cell-surface receptors of the Nogo Receptor family (NgR1, NgR2, and NgR3) restrict excitatory synapse formation. Loss of any one of the NgRs results in an increase in synapse number in vitro, whereas loss of all three is necessary for abnormally elevated synaptogenesis in vivo. We show that NgR1 inhibits the formation of new synapses in the postsynaptic neuron by signaling through the coreceptor TROY and RhoA. The NgR family is downregulated by neuronal activity, a response that may limit NgR function and facilitate activity-dependent synapse development. These findings suggest that NgR1, a receptor previously shown to restrict axon growth in the adult, also functions in the dendrite as a barrier that limits excitatory synapse number during brain development.

INTRODUCTION

The establishment of the appropriate number of synaptic connections during development is critical for proper brain function. Failures in this process may underlie neurological disorders including mental retardation, autism, and schizophrenia (Bassell and Warren, 2008; Eastwood, 2004; Südhof, 2008). Recent work has identified several of the cell-cell recognition molecules that promote synapse formation (Dalva et al., 2007), but much less is known about the mechanisms that restrict synapse number to ensure the exquisite specificity in organization of neural circuits that occurs throughout the brain.

Excitatory synaptic development begins as contacts are made between passing axons and dendritic filopodia (Ziv and Smith, 1996), actin-rich protrusions along dendritic shafts. Dendritic filopodia rapidly discriminate between potential partners and appear to stabilize

*Correspondence: michael_greenberg@hms.harvard.edu.

SUPPLEMENTAL INFORMATION

Supplemental Information includes eight figures, two tables, and Supplemental Experimental Procedures and can be found with this article online at doi:10.1016/j.neuron.2011.11.029.

contacts with the appropriate presynaptic axons (Lohmann and Bonhoeffer, 2008). The rapid nature of this process suggests that signaling by cell-surface receptors is likely to be involved in determining when and where synapses form. These cell-surface receptor/ligand complexes include neurexins/neuroligins, EphB/EphrinBs, N-cadherins, and NGL3/LAR, which are thought to contribute to the stabilization of nascent synaptic contacts through recruitment of scaffolding molecules and neurotransmitter receptors (Dalva et al., 2007). It is not known whether analogous mechanisms exist to restrict synapse formation so that synapses form at the right time and place and in the correct number.

We hypothesized that there might be cell-surface receptors that function to restrict one or more steps in the process of synaptic maturation, thereby balancing the process of synapse formation so that synapses form in the correct number. These steps could include determining when and where synaptogenesis begins by preventing the inappropriate recruitment of synaptic components to asynaptic sites, limiting the activity-dependent growth of synapses, or mediating the pruning of weak synaptic contacts during synapse elimination.

We report here the discovery that one subfamily of leucine-rich repeat receptors, the Nogo receptor family, functions to restrict the number of excitatory synapses that form during brain development. Much is known about the function of Nogo Receptor 1 (NgR1) in the adult central nervous system (CNS) (reviewed in Yiu and He, 2006); in contrast, far less is known about Nogo receptor 2 (NgR2) and Nogo receptor 3 (NgR3). NgR1 binds to several ligands, including Nogo-A, MAG, and OMgp, as well as FGF-1 and FGF-2 (Lee et al., 2008). Several of these ligands were isolated from CNS myelin, where they are thought to induce growth-cone collapse and axon retraction following CNS injury, a function suggested to be mediated by NgR1 and several coreceptors, including P75, Lingo, and TROY (reviewed in Yiu and He, 2006). NgR1 signaling in axons has been shown to activate the small GTPase RhoA as well as Rho kinase (ROCK), important cytoskeletal regulatory proteins thought to mediate axon outgrowth inhibition (Niederöst et al., 2002). While there is an emerging appreciation that NgR1 plays a role in restricting dendritic growth and plasticity in several brain regions, the mechanism of this process has not been understood (McGee et al., 2005; Lee et al., 2008, Zagrebelsky et al., 2010, Delekate et al., 2011), nor has the functional role of the various NgR family members during brain development been established.

Here we show that members of the NgR family function in the dendrite to restrict synapse number in vivo. This effect appears to be due to synapse addition, not synapse elimination, and is mediated by RhoA, which reduces overall synapse number in part by constraining dendritic growth, thereby limiting the number of synaptic contacts made during development. Our expression studies show that the NgR family is downregulated by neuronal activity, suggesting a possible mechanism by which the NgR barrier for synapse development is relieved. These findings define a family of cell surface receptors that restrict the number of synaptic connections that form in the mammalian brain and thus ensure the proper development of neural circuits.

RESULTS

The NgR Family Is Dendritically Localized and Inhibits Excitatory Synapse Formation In Vitro

NgR1 was first identified based on its ability to bind Nogo-66, an inhibitor of axon outgrowth (Fournier et al., 2001). However, NgR1 expression is not limited to the axon. Upon examining NgR1 expression in dissociated hippocampal neuron cultures using an NgR1-specific antibody (Figures 1A and 1C, and Figure S1A available online), we found

that NgR1 is expressed from 7 to 18 days in vitro (DIV), a time when the majority of synapses are forming in these cultures (Figure 1B). We used immunocytochemistry to investigate the subcellular distribution of NgR1 and found that it is broadly expressed on dendrites as well as axons (Figure 1D), consistent with biochemical fractionation studies demonstrating that NgR1 is present in both pre- and postsynaptic density fractions (Lee et al., 2008). Experiments using antibodies to specific synaptic proteins revealed that, while NgR1 is in close apposition to synaptic proteins such as PSD95, GluR2, SV2, and GAD67, NgR1 seldom overlaps with these proteins (Figure 1E and quantified in Figure S1B). Whereas PSD95 and GluR2 are expressed in dendritic spines, NgR1 is expressed primarily in the dendritic shaft (outlined in white in Figure $1E_{i-v}$), where it colocalizes with filamentous actin (Figure $1E_v$). These observations suggest that NgR1 is largely excluded from excitatory synapses and instead is concentrated in nonsynaptic sites along the dendritic shaft. Importantly, staining under nonpermeabilizing conditions demonstrates that ~40% of NgR1 is on the cell surface of dendrites (Figures S1C–S1D). Given these findings, we considered the possibility that NgR1 might define regions of dendrites where synaptic development is suppressed.

To assess the function of NgR1 during synapse development, we examined the effect of reducing the expression of NgR1 in cultured hippocampal neurons. Two distinct RNAi-based approaches were used to knockdown NgR1 expression, either direct transfection with short interfering RNA duplexes (siNgR1) or a plasmid encoding a short hairpin RNA to NgR1 (shNgR1) that targets a distinct region of NgR1 mRNA. These RNAis were tested in heterologous cells and primary neuronal cultures, where they selectively reduced NgR1 protein levels while leaving NgR2 and NgR3 expression unaffected (Figures S2A–S2C). To investigate the effect of reducing NgR1 expression on synapse number, hippocampal neurons were cultured, transfected at 9 days in vitro with a plasmid encoding green fluorescent protein (GFP) together with an RNAi to NgR1 or a control RNAi, and fixed 5 days later for staining with antibodies that recognize the pre-synaptic protein synapsin1 (Syn1) and the postsynaptic protein PSD95. To quantify the number of synapses formed on the transfected neuron, we counted the number of apposed Syn1/PSD95 puncta along dendrites of GFP-expressing neurons (see Experimental Procedures). Using this approach we found that knockdown of NgR1 resulted in a significant increase in excitatory synaptic number (Figures 2A–2C; all data are listed in Table S1). Similar results were obtained using alternative sets of synaptic markers (GluR2/Syt1 or NR2B/Syt1) (Figures 2E, 2F, and S2D). Furthermore, we also observed an increase in the average size and intensity of synaptic puncta after NgR1 knockdown (Figures S2E and S2F).

We verified the specificity of the NgR1 RNAi phenotype by testing the ability of an RNAi-resistant form of NgR1 (ResNgR1) to rescue the increase in synapse density observed upon knockdown of NgR1. ResNgR1 was validated in heterologous cells (Figure S1B) and then cotransfected in culture neurons along with shNgR. We found that ResNgR1was sufficient to reverse the increase in synaptic number observed with knockdown of NgR1 (Figure 2D), suggesting that the increase in synapse number in NgR1 RNAi-treated neurons is due to the specific knockdown of NgR1 by RNAi.

NgR1 belongs to a family that includes two highly homologous proteins, NgR2 and NgR3. All three NgRs are expressed at high levels in the dorsal telencephalon during synaptic development (Figure S2G). To investigate whether NgR2 and NgR3 also function as negative regulators of synapse development, we examined the effect of reducing expression of either NgR2 or NgR3 in cultured hippocampal neurons. Short hairpin RNAs to NgR2 (shNgR2) or NgR3 (shNgR3) were validated in heterologous cells (Figure S2H) and then expressed in neurons, where they resulted in a significant increase in excitatory synapse density (Figure S2I). To extend this finding, we acquired knockout mice for *NgR1* (Zheng et

al., 2005), *NgR2*, and *NgR3* (Lexicon Genetics), validated that these animals are null for the respective NgR genes (Figures S5A and S5B), and assessed the contribution of NgR1, NgR2, and NgR3 to synaptic development in cultured hippocampal neurons. These experiments revealed that loss of any single NgR family member ($NgR1^{-/-}$, $NgR2^{-/-}$, or $NgR3^{-/-}$) results in an increase in the number of excitatory synapses relative to littermate controls (Figure 2G). Thus, all three NgR family members have similar functions in restricting synaptic development in vitro, regardless of whether they are removed acutely in individual neurons with RNAi, or constitutively removed throughout neuronal cultures using genetic loss-of-function approaches.

Since eliminating expression of members of the NgR family results in an increase in synapse number, we asked whether overexpression of NgR1 results in a decrease in synapse number. Cultured hippocampal neurons were transfected with varying concentrations of a wild-type NgR1 expression construct (WTNgR1) and synaptic puncta were quantified. When expressed at a low concentration such as that used to rescue the NgR1 shRNA phenotype (100 ng), WTNgR1 had no effect on synapse number; however, a 2-fold higher concentration of WTNgR1 (200 ng) significantly reduced synapse density (Figures 2H and 2I). Similarly, overexpression of WTNgR2 (Figures 2H and 2I) or WTNgR3 (Figure S7A) significantly reduced synapse number. Thus, results from a number of different experiments support that members of the NgR family restrict the number of excitatory synapses that form on hippocampal neurons in culture.

We next asked whether NgR1 inhibits the development of synapses in the context of an intact hippocampal circuit. Hippocampal slices were cultured from wild-type P6 rats and biolistically transfected with GFP alone or GFP along with control RNAi, shNgR1, or WTNgR1 to assess the effect of NgR1 expression on spine formation in a neuronal circuit. Knockdown of NgR1 through the introduction of either shNgR1 or siNgR1 into hippocampal slices for 5 days resulted in a significant increase in the number of dendritic spines relative to control (Figures 3A and 3B), with no effect on spine width or length (Figures 3C and 3D). In contrast, overexpression of WTNgR1 in organotypic hippocampal slices resulted in a substantial reduction in spine number (Figures 3A and 3B). These observations suggest that in an intact neuronal circuit, NgR1 restricts the number of dendritic spines, the sites where the majority of excitatory synapses form.

Our experiments thus far raise the possibility that NgRs either prevent the initiation of new synapses or mediate synapse elimination. To distinguish between these possibilities, we quantified spine addition and elimination over time by repeatedly imaging cultured hippocampal slices that were biolistically transfected with GFP and a control shRNA or shNgR1. We observed that NgR1 knockdown results in a significant increase in spine density following repeated imaging of cultured hippocampal slices (Figures 3E and 3F). A quantification of spines added or eliminated following NgR1 knockdown revealed a significant increase in spine addition but no change in spine elimination (Figures 3G, S3A, and S3B), lending support to the idea that NgR1 functions to suppress the establishment of new synapses rather than by mediating synapse elimination.

NgR1 Functions Postsynaptically

Several NgR1 ligands and coreceptors are expressed on axons and dendrites; thus, the potential exists for NgR1 to signal bidirectionally. To address whether NgR1 functions pre- or postsynaptically, we quantified changes in synapse density observed upon knockdown or overexpression of NgR1 and then deconvolved these same data sets to determine whether there was a change in the number of pre- and/or postsynaptic specializations. This analysis revealed that the effects of NgR1 on synapse density were due to changes in the number of postsynaptic (PSD95 or GluR2) puncta rather than the presynaptic (Syn1 or Syt1) puncta

(Figures 4A–4C; data not shown). Similarly, de-convolution of synapse density measurements following RNAi targeting of NgR2 and NgR3 also revealed a specific increase in PSD95 puncta number, size, and intensity (Figures S2G and S2H). Importantly, simulated modeling studies confirmed that the changes in synapse density following NgR1 knockdown could not be accounted for by random overlap due to increased numbers of postsynaptic puncta (Figures S4B and S4C).

To determine whether changing the level of NgR1 throughout neuronal cultures affects the levels of specific synaptic proteins, we infected neurons with lentiviruses to drive the expression of NgR1 throughout neuronal cultures and found that WTNgR1 overexpression results in a significant reduction in PSD95 protein levels as assessed by quantitative western blotting (Figures 4D and 4E). Moreover, the opposite effect was observed upon NgR1 knockdown, which resulted in a significant increase in both PSD95 and GluR2 levels (Figures 4D, 4E, and S4A). In contrast, the level of Syn1 was unaffected by NgR1 overexpression or knockdown (Figures 4D, 4E, and S4A). Thus, analysis of both single cells and neuronal cultures suggests that NgR1 inhibits the development of excitatory synapses through its action in the postsynaptic cell, where it causes reduced expression of specific postsynaptic proteins. These findings suggest that NgR1 has a cell-autonomous role in the dendrite that is distinct from its previously described function in the axon.

NgR1 Functions Together with a Coreceptor, TROY, to Restrict Excitatory Synapse Number

NgR1 functions by activating intracellular signaling cascades via transmembrane coreceptors such as P75, TROY, and Lingo-1 (Yiu and He, 2006). To investigate whether coreceptor signaling is required for the inhibition of synapse formation by NgR1, we tested the effect of an NgR1 mutant that lacks a co-receptor-binding region (DNNgR1 [Wang et al., 2002a]). Unlike the effect of WTNgR1, overexpression of DNNgR1 did not result in decreased synapse density but rather caused a small but significant increase in synapse density relative to control, presumably due to its ability to sequester ligands away from endogenous NgR1 (Figures 4F and 4G). This finding suggests that NgR1 requires a coreceptor to inhibit synapse development.

Genome-wide RNA sequencing revealed that of the known NgR1 coreceptors, only Lingo-1 and TROY are expressed at appreciable levels in 7 DIV neuronal neurons (data not shown). Since Lingo-1 is largely expressed on axons (Lee et al., 2008), we focused on TROY as a potential NgR1 coreceptor that might function in dendrites to inhibit synapse development.

Immunostaining with protein-specific antisera revealed that TROY is expressed along the dendrites of cultured neurons and overlaps significantly with all NgR family members (Figure S4E). In addition, TROY knockdown (Figures S4E, S4I, S4J, and S8B) caused a significant increase in synapse density in cultured hippocampal neurons (Figure 4H). Together, these findings are consistent with TROY being the coreceptor that mediates the inhibitory effects of NgR1 on synapse development.

To determine whether TROY is required for NgR1-dependent suppression of synapse development, WTNgR1 was overexpressed with or without TROY knockdown (shTROY) and synapse density was quantified. TROY knockdown reversed the reduction in synapse number observed with NgR1 overexpression (Figure 4I). An increase in synapse density was observed, similar to that seen upon TROY knockdown alone. Similar epistasis studies with WTNgR2 and WTNgR3 overexpression revealed that TROY is required for the suppression of synapse development by NgR2 and NgR3 (Figure S4K). Moreover, binding experiments using recombinant TROY protein incubated with heterologous cells expressing different NgR family members show that TROY is capable of binding NgR1 and NgR2, but not

NgR3 (Figure S4F), suggesting that NgR1 and NgR2 may signal through TROY directly. It remains unclear whether the affinity of the NgR3-TROY interaction falls below the detection limit of this assay or whether NgR3 acts through an alternative coreceptor. Taken together, these findings identify TROY as a potential coreceptor for the NgR family that mediates their ability to restrict excitatory synapse number.

The NgR Family Cooperates in Restricting Synaptic Development In Vivo

To address whether the NgR family contributes to synaptic development in vivo, we crossed NgR mutant mice with the GFPM line (Feng et al., 2000), in which a small subset of neurons are genetically labeled with the Thy1-GFP allele, thus enabling visualization of dendritic spines from hippocampal pyramidal neurons. Knockout of any one NgR family member alone was not sufficient to affect the density of dendritic spines in vivo (Figure 5B). Given our previous finding that all three NgR family members play a similar role in limiting synapse development in vitro (Figures 2G and S2I), we hypothesized that these family members might functionally compensate for one another in vivo. To address this possibility, we generated triple knockout mice (*NgRTKO*$^{-/-}$). *NgRTKO*$^{-/-}$ mice were born with the appropriate Mendelian frequencies and appear largely normal, with no obvious defects in formation of the hippocampus. Analysis of GFP-expressing neurons at P18 revealed a significant increase in the number of dendritic spines on CA1 pyramidal neurons in *NgRTKO*$^{-/-}$ mice relative to their triple heterozygous littermate controls (Figures 5A and 5B). These findings are consistent with the idea that the NgR family members function together in vivo to limit the number of excitatory synapses.

To extend this analysis using an independent approach, we performed transmission electron microscopy to visualize the ultrastructural features of excitatory synapses. In micrographs from *NgRTKO*$^{-/-}$ mice, we observed asymmetric synapses of typical morphology, suggesting that the overall structure and vesicle content of excitatory synapses are normal in the absence of NgRs. However, quantification of the number of excitatory synapses in the apical dendritic regions of CA1 revealed that *NgRTKO*$^{-/-}$ mice had a significant increase in the density of excitatory synapses relative to heterozygous littermate controls (Figures 5C and 5D). Furthermore, this effect was not limited to CA1 neurons, since analysis of CA3 neurons also revealed a clear increase in the number of PSDs in *NgRTKO*$^{-/-}$ animals (Figure 5E). Thus, analysis by confocal and electron microscopy suggests that the NgR family functions to limit the number of excitatory synapses in vivo.

To address whether the observed increase in synapse number reflects an increase in functional synapses, we performed whole-cell patch-clamp electrophysiology on CA1 pyramidal neurons from acute hippocampal slices obtained from *NgRTKO*$^{-/-}$ mice and control littermates to quantify the frequency and amplitude of miniature excitatory postsynaptic currents (mEPSCs). This analysis revealed a significant increase in the frequency of mEPSCs in *NgRTKO*$^{-/-}$ mice relative to littermate controls (Figure 5F and S5C), suggesting that the NgR family restricts the development of functional excitatory synapses. Interestingly, there was a small but significant decrease in the amplitude of mEPSCs (Figure 5G and S5D), consistent with the immature spine types observed in *NgR1* knockouts (Lee et al., 2008; Zagrebelsky et al., 2010). Thus, reducing the expression of the NgR family results in an increase in functional synapses that are slightly reduced in strength.

The NgR Family Inhibits Dendritic Growth and Complexity

The question remained as to how NgRs work at a mechanistic level to restrict excitatory synapse number. One possibility was that NgRs limit the formation of new synapses in part by inhibiting dendritic growth, thereby reducing the possibility of contact between axons and dendrites. Therefore, we asked whether loss of NgR family members affects dendritic

branching. Specifically, we analyzed dendritic branch complexity in GFP-expressing neurons by Sholl analysis, which quantifies the number of dendritic branches intersecting concentric circles of increasing radii centered on the cell body (Sholl, 1953). We found that neurons from mice lacking *NgR1* showed a significant increase in dendritic complexity relative to littermate controls, whereas overexpression of WTNgR1 resulted in a decrease in complexity of the dendritic arbor (Figures 6A and 6B; all Sholl data are listed in Table S2). Similarly, there was a significant increase in dendritic complexity and total dendritic length in hippocampal slices upon knockdown of NgR1 (Figure S6). Moreover, this effect was also observed in vivo, where analysis of GFP-expressing CA1 pyramidal neurons from *NgRTKO*$^{-/-}$ animals revealed an increase in both the complexity of basal dendrites (Figures 6C–6E) and total dendritic length (Figure 6F). Taken together, these findings provide evidence that NgR family members inhibit the growth and decrease the complexity of the dendritic arbor and suggest that, in addition to decreasing synapse density, a second way that NgR family members may restrict synapse number is by inhibiting dendritic growth, reducing the overall area for potential synaptic inputs.

NgR1 Restricts Dendritic Growth and Synapse Number through Activation of RhoA

We asked if NgR/TROY limits dendrite and spine/synapse development by inhibiting the polymerization of the actin cytoskeleton, a process that is essential for dendritic and spine growth. Previous studies have shown that RhoA is a critical regulator of actin assembly (Maekawa et al., 1999). To investigate the involvement of RhoA in the inhibition of dendritic growth and synapse development by NgR1, we tested whether NgR1 activates RhoA in hippocampal neurons during synaptic development. Hippocampal neurons were infected with lentivirus expressing WTNgR1, and RhoA activity was assessed using a Rhotekin-binding domain (RBD) assay, which utilizes the Rho-binding domain of Rhoteckin as an affinity reagent to precipitate active Rho (Rho-GTP) from cells. We found that the level of active RhoA was reduced by reduction of NgR1 and elevated upon NgR1 overexpression (Figures 7A and 7B). Thus, NgR1 signaling activates RhoA in hippocampal neurons during synapse formation.

To test whether the inhibitory effect of NgR1 on synapse development is mediated by RhoA, we blocked the activity of RhoA or one of its downstream effectors, ROCK, using selective inhibitors. Treatment of hippocampal cultures with either the Rho inhibitor (C3 Transferase) or the ROCK inhibitor (Y27632) led to a significant increase in synapse number (Figure 7C), suggesting that RhoA signaling acts downstream of NgR1 to restrict synapse number. Further, Rho or ROCK inhibition entirely rescued WTNgR1 suppression of synapse development (Figure 7C). These findings also extended to NgR2, NgR3, and TROY, all of which require Rho and ROCK to suppress synaptic development (Figure S7A). Similarly, inhibition of RhoA or ROCK blocked, albeit not completely, the effect of WTNgR1 overexpression on dendritic growth (Figures 7D, 7E, and S7B). Together, these findings suggest that the NgR family regulates synapse number in part by activating RhoA, potentially restricting actin polymerization that underlies the growth of dendrites and spines.

Neuronal Activity Downregulates the NgR family and TROY

The finding that the NgR family restricts dendritic and spine development raised the possibility that NgR family members function together with TROY as a barrier that limits neural connectivity during development. However, these receptors are highly expressed at a time when neurons are beginning to form synapses, raising the question: what limits the inhibitory effect of NgR family members to allow for synaptogenesis? We hypothesized that stimuli such as neuronal activity that promote dendritic growth and synaptogenesis (Sin et al., 2002; Peng et al., 2009) might trigger the downregulation of the NgR family and/or TROY, thus relieving the barrier to excitatory synapse formation. To test this hypothesis, we

analyzed the expression of NgR1, NgR2, NgR3, and TROY mRNA in response to changes in neuronal activity. Increasing neuronal activity resulted in a significant decrease in the mRNA level in all three NgR family members and TROY (Figures 8C–8F). To confirm these observations at the level of NgR protein expression, GFP-expressing hippocampal neurons were stained with anti-NgR1 antibodies and the total number of NgR1 puncta (cell surface and intracellular) on dendrites was quantified. When neurons were depolarized, either by elevation of levels of potassium chloride, addition of N-methyl-D-aspartic acid (NMDA), or inhibition of GABA receptors with the antagonist bicuculline, the number of NgR1 puncta along dendrites was significantly reduced relative to untreated neurons (Figures 8A and 8B). A similar decrease in TROY and NgR1 protein levels was observed in vivo in response to kainite-induced seizure (Figures 8H and 8I) or enriched environment (Figures S8C and S8D). Conversely, blocking neuronal activity by treatment of neurons with a combination of the NMDA receptor antagonist amino-5-phosphonovaleric acid (APV) and the sodium channel blocker tetrodotoxin (TTX) had the opposite effect, causing a significant increase in the number of dendritic NgR1 puncta (Figures 8A and 8B). Importantly, cell-surface staining confirmed that modulation of neuronal activity altered NgR1 levels present at the cell surface (Figure S8A). While significant levels of the NgR family members persist throughout the period of synaptic development, TROY expression was found to decrease upon the onset of pronounced synaptogenesis (Figure 8G). Thus, neuronal activity and/or reduced expression of the coreceptor TROY may relieve the NgR-dependent barrier to synaptic growth, facilitating synaptogenesis during development and plasticity in the adult.

DISCUSSION

The formation of synaptic connections during development is a highly regulated process that is mediated in part by cell-surface proteins that promote initial contact between developing axons and dendrites. We hypothesized that neural connectivity might also be limited by cell-surface proteins that function to restrict excitatory synapse development so that synapses form at the right time and place and in the correct number. Here we show that the NgR family of proteins serves this important function. Our study suggests that NgRs function along the arbor of dendrites as a barrier that limits synapse formation. Loss of any one member of the NgR family is sufficient to reveal their inhibitory influence in vitro, whereas loss of all three NgRs is required for abnormally elevated excitatory synaptogenesis in vivo. These findings broaden our understanding of NgR1's function, since they identify a dendritic role for receptors whose function was hitherto ascribed mainly to the axon.

At a mechanistic level, NgRs appear to work through the coordinated inhibition of synaptic and dendritic growth. These findings are consistent with those of recent studies of more mature neuronal circuits, demonstrating that both Nogo and the Nogo receptor constrain dendritic growth (Zagrebelsky et al., 2010). The effects of NgR loss on synaptogenesis and dendrogenesis are coupled. Unlike Neuropilin-2, which has a more selective role in regulating the spatial distribution of synapses on a specific region of the dendrite, the primary apical shaft (Tran et al., 2009), the NgR family functions broadly on the dendrite to restrict dendritic growth and limit the number of excitatory synapses that form.

It will be important to identity the ligand or ligands that regulate the activity of the NgR family members in this developmental context. Several ligands have been shown to regulate NgR1 signaling. Recent work provides evidence that Nogo may promote synaptic maturation in more established neuronal circuits (Zagrebelsky et al., 2010; Pradhan et al., 2010). Consistent with these findings, we observe a significant increase in synapse density following Nogo-Fc (Nogo-66) addition to cultured hippocampal neurons (Z. Wills and M. Greenberg, unpublished observations), raising the possibility that Nogo may inhibit rather

than activate NgR in this context. These findings suggest that NgR1 signaling may fulfill multiple roles in synaptogenesis depending on its mechanism of activation and developmental period. Given that Nogo is highly enriched in the PSD (Peng et al., 2004; Raiker et al., 2010), a better understanding of how ligand binding to NgR1 affects its downstream signaling may help to reveal how NgR1 regulates synapse number. It is noteworthy that of the known NgR1 ligands, only MAG can activate NgR2 (Venkatesh et al., 2005), and none have affinity for NgR3. These findings raise the possibility that NgR family members may bind different ligands, allowing each receptor to be tuned to distinct extracellular cues that function in parallel to inhibit synapse formation. Alternatively, these receptors may share a common ligand that remains to be be identified.

NgR1 was originally discovered as a receptor that mediates the inhibition of axon regrowth after injury in the adult (Fournier et al., 2001). More recent studies have also revealed developmental functions of NgR1 in the closure of the critical period in adolescent mice (McGee et al., 2005) and in regulating activity-dependent synaptic strengthening in the hippocampus (Lee et al., 2008). However, robust expression of NgR family members begins in newborn mice (Lee et al., 2008), and its function at this stage of growth was unknown. Our study clarifies this issue by uncovering a role for the NgR family in the early postnatal brain, where it functions in the dendrite to restrict synapse number. What might be the purpose of synaptic restriction by NgR family members? Our live-imaging studies suggest that the NgR family inhibits the formation of new synapses, possibly preventing premature synaptogenesis so that synapses are established at the correct time and place. In addition, the NgR family may provide inhibition to counterbalance prosynaptic factors. Therefore, synapse formation might involve the concurrent activation of signaling pathways that promote synaptogenesis and a relief of inhibition of synapse formation by the NgR family. Consistent with these possibilities, we provide evidence that NgR1 mediates its effects through the activation of RhoA, a GTPase that restricts actin polymerization and thereby limits dendritic growth and spine development (Elia et al., 2006; Sin et al., 2002).

Signaling through RhoA to regulate actin assembly may be a common feature of NgR signaling. Previous work has shown that NgR1 regulates actin dynamics in the axon through TROY, RhoA, and ROCK (Yiu and He, 2006). In the present study, we provide evidence that a similar signaling pathway mediates the effects of NgR1 in the dendrite. While we have found that TROY can bind both NgR1 and NgR2 in heterologous cells (Figures S4E and S4F), future work will be required to demonstrate the presence of a protein complex comprised of these signaling components in developing dendrites. Further, the signals promoting synaptic and dendritic growth may not be identical. Preliminary work suggests that while TROY inhibits synapse development, it does not inhibit dendritic growth (Wills and Greenberg, unpublished data). However, the finding that NgR1 regulates both dendritic and synaptic growth suggests that NgR1 signaling may couple these processes to coordinate neuronal development.

Though our studies were focused on elucidating the developmental function of the NgRs, expression of this family of proteins continues into adulthood, and so it is interesting to speculate that NgR may continue to limit dendritic growth and synapse number in the mature brain. If so, NgR1's dendritic function may be important to consider in the context of neural damage caused by, e.g., injury or stroke, where, it has been suggested, NgR1-mediated inhibition of axonal outgrowth impairs recovery of motor function (Lee et al., 2004; Harvey et al., 2009). Our findings are notable because they raise the possibility that enhanced functional connectivity observed upon blocking NgR1 may be due, at least in part, to increased dendritic growth and elevated synapse formation in postsynaptic neurons.

In addition to its role under pathological circumstances such as injury, it is now clear that Nogo (Delekate et al., 2011) and NgR1 (Lee et al., 2008) have functions in the regulation of neural plasticity. Neural activity causes the downregulation of NgR1, and expression of ectopic NgR1 in the forebrain inhibits memory consolidation (Karlén et al., 2009). These findings imply that NgR1 limits neural connectivity, and in keeping with this idea, mice lacking NgR1 have an abnormal critical period in which ocular dominance plasticity continues abnormally into adulthood (McGee et al., 2005). While these findings suggest that NgR1 constrains plasticity in the brain, it was not known how NgR1 mediates these effects. Results from our study raise the possibility that NgRs limit synaptic plasticity by restricting excitatory synapse development. We speculate that the NgR family functions to limit structural changes in circuitry, from initial circuit formation in the newborn mouse to the closure of the critical period, as well as in the formation of long-term memories and the ability to recover from neural injury. In so doing, the NgR family may ensure wiring fidelity within neural circuits.

EXPERIMENTAL PROCEDURES

Animal Husbandry and Colony Management

NgR1$^{-/-}$ mice have been previously described (Zheng et al., 2005). *NgR2*$^{-/-}$ and *NgR3*$^{-/-}$ mice were obtained from Lexicon Genetics. GFPM mice were obtained from Joshua Sanes (Feng et al., 2000). For more details concerning mouse crosses, genotyping, and knockout validation see Supplemental Information.

DNA Constructs

Details of DNA constructs can be found in the Supplemental Information.

Western Blotting and GEF Pull-Down Assays

For western blotting, hippocampal cultures were collected and homogenized in RIPA buffer. Samples were boiled for 5 min in SDS sample buffer, resolved by SDS-PAGE, transferred to nitrocellulose, and immunoblotted. RBD pull-down assays were conducted according to the manufacturer's suggestions (Upstate Cell Signaling Solutions). For details, see Supplemental Information.

Immunocytochemistry

For immunocytochemistry, neurons were fixed and incubated with the indicated antibodies, as previously described (Tolias et al., 2005). For cell-surface staining of NgR1, anti-NgR1 antibody (1 μg/ml) was added to 14 DIV cultured neurons for 1 hr at 37°C, washed, and fixed as above. For details, see Supplemental Information.

Primary Neuron Cell Cultures

To obtain hippocampal neurons from mutant mice or littermate controls, single-embryo dissections of E16 mouse embryos were performed as previously described (Tolias et al., 2005). Rat hippocampal neurons were prepared from E18 Long-Evans rat embryos (Charles River), as previously described (Xia et al., 1996). Dissociated hippocampal neurons were transfected using the Lipofection method (Invitrogen) according to the manufacturer's suggestions. For details, see Supplemental Information.

Heterologous Cell Culture and Lentiviral Production

HEK293T cells were cultured in DMEM with10% fetal bovine serum and transfected using the calcium phosphate method (Xia et al., 1996). Lentiviruses were produced by co-transfection of HEK293T cells with pLenti-Lox plasmids together with the helper plasmids

Δ8.9 and VSV-G, as previously described (Lois et al., 2002). For details, see Supplemental Information. AP binding studies were carried out in COS cells transfected with GFP alone (CON), WTNgR1, WTNgR2, or WTNgR3 expression constructs. TROY-fc (R&D Systems) was conjugated with anti-fc-AP protein (Venkatesh et al., 2005), then incubated with COS cells for 75 min, washed, fixed, and stained to identify AP activity using BCIP/NBT.

Organotypic Slice Culture

Transverse slices (350 μm) of P5-7 hippocampus were prepared and cultured essentially as described in Stoppini et al. (1991). Slices prepared under sterile conditions were cultured on nylon inserts (0.4 μm pore size, Millicell) in 6-well dishes containing 0.75 ml of antibiotic-free medium (20% horse serum/MEM) and incubated in 5% CO_2 at 37°C. Slice cultures were transfected using a Helios Gene Gun (Biorad) at 8 DIV. Slices were fixed at 13 DIV in 2.5% para-formaldehyde and 4% sucrose and processed for immunohistochemistry.

Confocal Image Analysis and Quantification

All imaging analysis experiments were carried using a Zeiss LSM5 Pascal confocal microscope. For details see Supplemental Information. For live imaging experiments, organotypic rat hippocampal slice cultures were prepared at P5, biolistically transfected with shCON or shNgR1 RNAi constructs at 4 DIV, and cultured for three days (7 DIV) before imaging commenced. Spine-density measurements were carried out in Metamorph. For details, see Supplemental Information.

Electron Microscopy and Analysis

EM analysis was carried out on P18 animals, as described in detail in the Supplemental Information.

Electrophysiology

Electrophysiology was performed using standard methods (see Supplemental Information).

Immunohistochemistry

For immunohistochemistry, P18 mice were fixed with 4% paraformaldehyde in PBS by intracardial perfusion. Brains were sectioned coronally with a vibratome at 100 μm. Immunohistochemistry was performed on slice cultures directly on the nylon culture membrane. See Supplemental Information for details.

RT-PCR

RT-PCR was carried out using standard methodologies. See Supplemental Information for details.

Seizures and Enriched Environment

Seizures were induced for 3 hr in adult C57B6 mice by intraperitoneal injection of kainic acid (Ocean Produce International) at a dose of 25 mg/kg before isolation of the hippocampus. For enriched environment experiments, 6-week-old CD1 male mice were either placed in standard laboratory cages or in cages containing a variety of rodent toys of various shapes and colors (PETCO) for zero to six hours prior to isolation of the hippocampus. Hippocampal tissue was lysed in RIPA lysis buffer and total protein was quantified by BCA assay (Pierce).

Supplementary Material

Refer to Web version on PubMed Central for supplementary material.

Acknowledgments

We thank Mark Wessels and Christina G. Kane for general technical assistance; Sonia Cohen and Paul Greer for preparation of seizure and enriched environment samples, respectively; Athar Malik for reconstructing the shCON RNAi construct targeting firefly luciferase; Marc Tessier-Lavigne for the *NgR1*$^{-/-}$ mice; Zhigang He for WTNgR1, DNNgR1, and WTTROY expression constructs; M. Gee and P. Zhang for assistance with mouse colony management; Sara Vasquez for assistance with neuronal cell cultures; Jesse Gray, T.K. Kim, and David Harmin for RNAseq data (Kim et al., 2010); the MRDDRC Imaging Core (L. Bu); the HMS EM facility (Maria Ericsson); Eric Griffith and Ivo Spiegel for help editing the manuscript; and Sarah Ross for assistance in the writing of this manuscript. This work was supported by National Institute of Neurological Disorders and Stroke grant RO1 5R01NS045500 to M.E.G.

References

Bassell GJ, Warren ST. Fragile X syndrome: loss of local mRNA regulation alters synaptic development and function. Neuron. 2008; 60:201–214. [PubMed: 18957214]

Dalva MB, McClelland AC, Kayser MS. Cell adhesion molecules: signalling functions at the synapse. Nat Rev Neurosci. 2007; 8:206–220. [PubMed: 17299456]

Delekate A, Zagrebelsky M, Kramer S, Schwab ME, Korte M. NogoA restricts synaptic plasticity in the adult hippocampus on a fast time scale. Proc Natl Acad Sci USA. 2011; 108:2569–2574. [PubMed: 21262805]

Eastwood SL. The synaptic pathology of schizophrenia: is aberrant neurodevelopment and plasticity to blame? Int Rev Neurobiol. 2004; 59:47–72. [PubMed: 15006484]

Elia LP, Yamamoto M, Zang K, Reichardt LF. p120 catenin regulates dendritic spine and synapse development through Rho-family GTPases and cadherins. Neuron. 2006; 51:43–56. [PubMed: 16815331]

Feng G, Mellor RH, Bernstein M, Keller-Peck C, Nguyen QT, Wallace M, Nerbonne JM, Lichtman JW, Sanes JR. Imaging neuronal subsets in transgenic mice expressing multiple spectral variants of GFP. Neuron. 2000; 28:41–51. [PubMed: 11086982]

Fournier AE, GrandPre T, Strittmatter SM. Identification of a receptor mediating Nogo-66 inhibition of axonal regeneration. Nature. 2001; 409:341–346. [PubMed: 11201742]

Harvey PA, Lee DH, Qian F, Weinreb PH, Frank E. Blockade of Nogo receptor ligands promotes functional regeneration of sensory axons after dorsal root crush. J Neurosci. 2009; 29:6285–6295. [PubMed: 19439606]

Karlén A, Karlsson TE, Mattsson A, Lundströmer K, Codeluppi S, Pham TM, Bäckman CM, Ogren SO, Aberg E, Hoffman AF, et al. Nogo receptor 1 regulates formation of lasting memories. Proc Natl Acad Sci USA. 2009; 106:20476–20481. [PubMed: 19915139]

Kim TK, Hemberg M, Gray JM, Costa AM, Bear DM, Wu J, Harmin DA, Laptewicz M, Barbara-Haley K, Kuersten S, et al. Widespread transcription at neuronal activity-regulated enhancers. Nature. 2010; 465:182–187. [PubMed: 20393465]

Lee H, Raiker SJ, Venkatesh K, Geary R, Robak LA, Zhang Y, Yeh HH, Shrager P, Giger RJ. Synaptic function for the Nogo-66 receptor NgR1: regulation of dendritic spine morphology and activity-dependent synaptic strength. J Neurosci. 2008; 28:2753–2765. [PubMed: 18337405]

Lee JK, Kim JE, Sivula M, Strittmatter SM. Nogo receptor antagonism promotes stroke recovery by enhancing axonal plasticity. J Neurosci. 2004; 24:6209–6217. [PubMed: 15240813]

Lohmann C, Bonhoeffer T. A role for local calcium signaling in rapid synaptic partner selection by dendritic filopodia. Neuron. 2008; 59:253–260. [PubMed: 18667153]

Lois C, Hong EJ, Pease S, Brown EJ, Baltimore D. Germline transmission and tissue-specific expression of transgenes delivered by lentiviral vectors. Science. 2002; 295:868–872. [PubMed: 11786607]

Maekawa M, Ishizaki T, Boku S, Watanabe N, Fujita A, Iwamatsu A, Obinata T, Ohashi K, Mizuno K, Narumiya S. Signaling from Rho to the actin cytoskeleton through protein kinases ROCK and LIM-kinase. Science. 1999; 285:895–898. [PubMed: 10436159]

McGee AW, Yang Y, Fischer QS, Daw NW, Strittmatter SM. Experience-driven plasticity of visual cortex limited by myelin and Nogo receptor. Science. 2005; 309:2222–2226. [PubMed: 16195464]

Niederöst B, Oertle T, Fritsche J, McKinney RA, Bandtlow CE. Nogo-A and myelin-associated glycoprotein mediate neurite growth inhibition by antagonistic regulation of RhoA and Rac1. J Neurosci. 2002; 22:10368–10376. [PubMed: 12451136]

Peng J, Kim MJ, Cheng D, Duong DM, Gygi SP, Sheng M. Semiquantitative proteomic analysis of rat forebrain postsynaptic density fractions by mass spectrometry. J Biol Chem. 2004; 279:21003–21011. [PubMed: 15020595]

Peng YR, He S, Marie H, Zeng SY, Ma J, Tan ZJ, Lee SY, Malenka RC, Yu X. Coordinated changes in dendritic arborization and synaptic strength during neural circuit development. Neuron. 2009; 61:71–84. [PubMed: 19146814]

Pradhan AD, Case AM, Farrer RG, Tsai SY, Cheatwood JL, Martin JL, Kartje GL. Dendritic spine alterations in neocortical pyramidal neurons following postnatal neuronal Nogo-A knockdown. Dev Neurosci. 2010; 32:313–320. [PubMed: 20938157]

Raiker SJ, Lee H, Baldwin KT, Duan Y, Shrager P, Giger RJ. Oligodendrocyte-myelin glycoprotein and Nogo negatively regulate activity-dependent synaptic plasticity. J Neurosci. 2010; 30:12432–12445. [PubMed: 20844138]

Sholl DA. Dendritic organization in the neurons of the visual and motor cortices of the cat. J Anat. 1953; 87:387–406. [PubMed: 13117757]

Sin WC, Haas K, Ruthazer ES, Cline HT. Dendrite growth increased by visual activity requires NMDA receptor and Rho GTPases. Nature. 2002; 419:475–480. [PubMed: 12368855]

Stoppini L, Buchs PA, Muller D. A simple method for organotypic cultures of nervous tissue. J Neurosci Methods. 1991; 37:173–182. [PubMed: 1715499]

Südhof TC. Neuroligins and neurexins link synaptic function to cognitive disease. Nature. 2008; 455:903–911. [PubMed: 18923512]

Tolias KF, Bikoff JB, Burette A, Paradis S, Harrar D, Tavazoie S, Weinberg RJ, Greenberg ME. The Rac1-GEF Tiam1 couples the NMDA receptor to the activity-dependent development of dendritic arbors and spines. Neuron. 2005; 45:525–538. [PubMed: 15721239]

Tran TS, Rubio ME, Clem RL, Johnson D, Case L, Tessier-Lavigne M, Huganir RL, Ginty DD, Kolodkin AL. Secreted semaphorins control spine distribution and morphogenesis in the postnatal CNS. Nature. 2009; 462:1065–1069. [PubMed: 20010807]

Venkatesh K, Chivatakarn O, Lee H, Joshi PS, Kantor DB, Newman BA, Mage R, Rader C, Giger RJ. The Nogo-66 receptor homolog NgR2 is a sialic acid-dependent receptor selective for myelin-associated glycoprotein. J Neurosci. 2005; 25:808–822. [PubMed: 15673660]

Wang X, Chun SJ, Treloar H, Vartanian T, Greer CA, Strittmatter SM. Localization of Nogo-A and Nogo-66 receptor proteins at sites of axon-myelin and synaptic contact. J Neurosci. 2002; 22:5505–5515. [PubMed: 12097502]

Xia Z, Dudek H, Miranti CK, Greenberg ME. Calcium influx via the NMDA receptor induces immediate early gene transcription by a MAP kinase/ERK-dependent mechanism. J Neurosci. 1996; 16:5425–5436. [PubMed: 8757255]

Yiu G, He Z. Glial inhibition of CNS axon regeneration. Nat Rev Neurosci. 2006; 7:617–627. [PubMed: 16858390]

Zagrebelsky M, Schweigreiter R, Bandtlow CE, Schwab ME, Korte M. Nogo-A stabilizes the architecture of hippocampal neurons. J Neurosci. 2010; 30:13220–13234. [PubMed: 20926648]

Zheng B, Atwal J, Ho C, Case L, He XL, Garcia KC, Steward O, Tessier-Lavigne M. Genetic deletion of the Nogo receptor does not reduce neurite inhibition in vitro or promote corticospinal tract regeneration in vivo. Proc Natl Acad Sci USA. 2005; 102:1205–1210. [PubMed: 15647357]

Ziv NE, Smith SJ. Evidence for a role of dendritic filopodia in synaptogenesis and spine formation. Neuron. 1996; 17:91–102. [PubMed: 8755481]

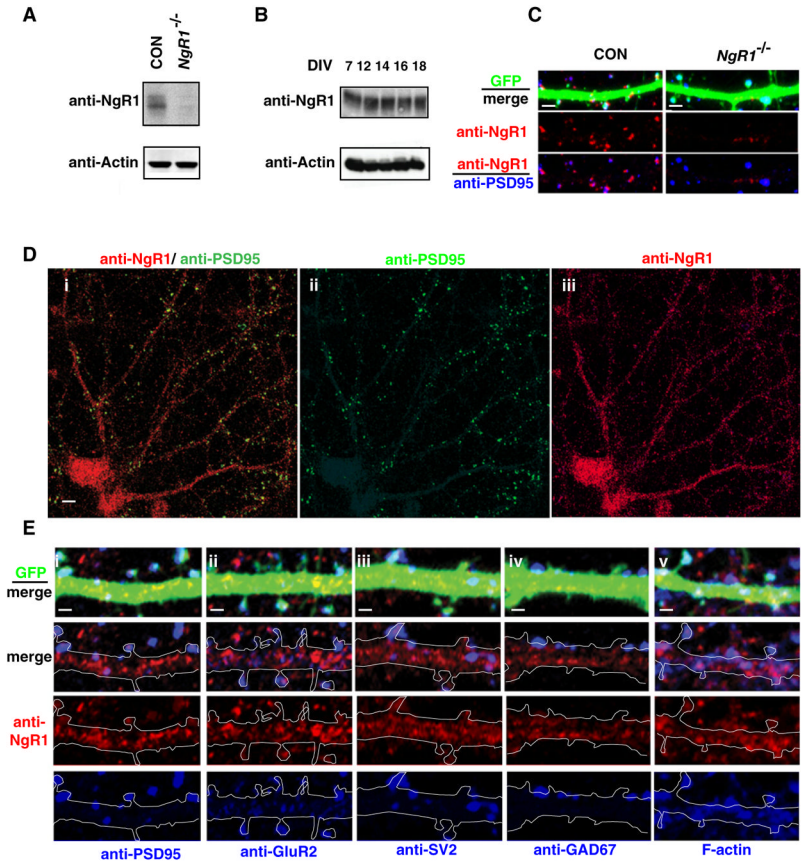

Figure 1. NgR1 Is Expressed on Dendrites of Hippocampal Neurons during Synaptic Development

(A) Specificity of NgR1 antibody in immunoblotting. Lysates from hippocampal neurons (18 DIV) were analyzed by immunoblot using an antibody directed against NgR1. NgR1 protein is expressed in cultures derived from heterozygous *NgR1*$^{+/-}$ embryos (CON) and is selectively lost in neurons derived from *NgR1*$^{-/-}$ embryos. Samples were blotted for actin as a loading control.

(B) Time course of NgR1 expression. Immunoblot analysis of lysates from wild-type hippocampal neurons using an NgR1 antibody demonstrates that NgR1 is highly expressed from 7 to 18 DIV, a time of abundant synapse formation.

(C) Specificity of NgR1 antibody in immunostaining. Hippocampal neurons derived from either heterozygous embryos (CON; *NgR1*$^{+/-}$) or *NgR1* mutant (*NgR1*$^{-/-}$) embryos were transfected with GFP and analyzed at 18 DIV by immunostaining for NgR1 (red) and PSD95 (green). A representative dendrite is shown, revealing punctate NgR1 expression that is specifically lost in neurons from *NgR1*$^{-/-}$mice. Scale bar is 2.5 μm. Further validation is shown in Figure S1A.

(D) NgR1 is broadly expressed in dendrites. Wild-type hippocampal neurons were analyzed by immunostaining (18 DIV) for NgR1 (red) and PSD95 (green). NgR1 (red puncta in i and iii) is expressed broadly along developing dendrites and axons but is largely excluded from overlapping with the excitatory synaptic marker, PSD95 (green puncta in i and ii). Note that apparent NgR1 staining in the soma is likely nonspecific, since this signal is also present in neurons from *NgR1*$^{-/-}$ embryos. Scale bar is 10 μm. NgR1 cell-surface staining is shown in Figure S1C.

(E) NgR1 is dendritic, but is excluded from synapses. Hippocampal neurons were transfected with GFP (9 DIV) and then subsequently analyzed (18 DIV) by costaining for

NgR1 (red) and the indicated markers (blue). Representative dendrites illustrate that NgR1 rarely colocalizes with synaptic markers, including PSD95 (i), GluR2 (ii), SV2 (iii), or GAD67 (iv), though it frequently overlaps with broadly expressed proteins such as filamentous actin (Phalloidin) (v). Scale bar is 1 μm. Quantification of NgR1 overlap with synaptic proteins is presented in Figure S1B.

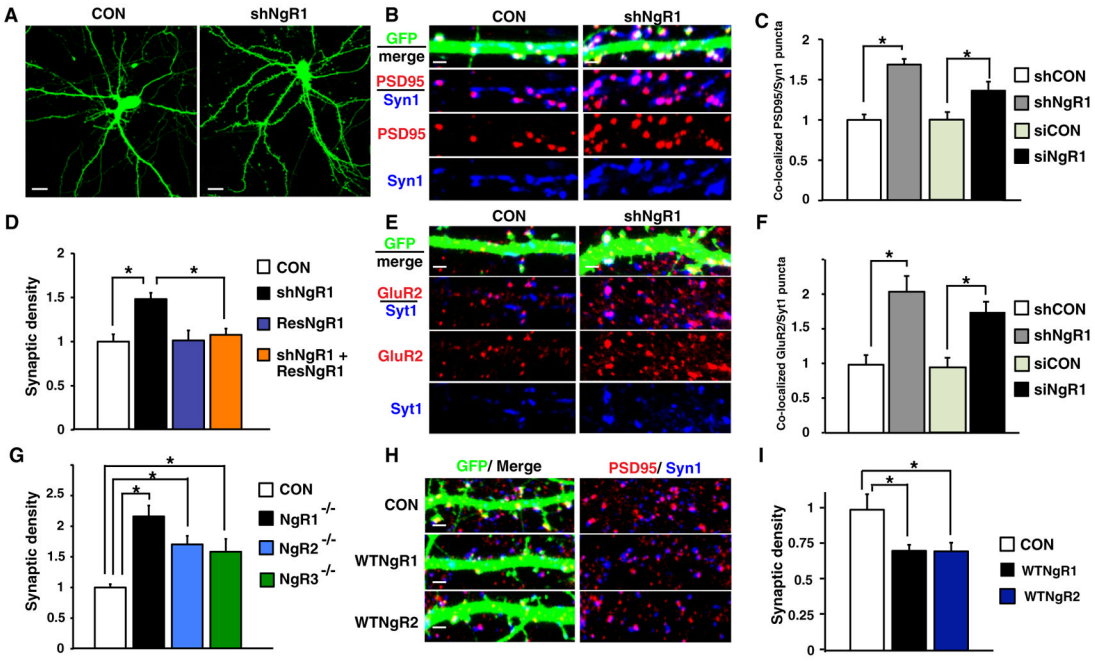

Figure 2. The NgR Family Restricts Synapse Formation in Cultured Neurons

(A–C) Knockdown of NgR1 increases the density of PSD95/Syn1 puncta in cultured hippocampal neurons. Cultured hippocampal neurons were cotransfected with GFP and either shCON (white bar), shNgR1 (gray bar), siCON (green bar), or siNgR1 (black bar) and subsequently immunostained with antibodies against the excitatory postsynaptic marker PSD95 (red) and the presynaptic marker Syn1 (blue). (A) Representative examples of control or shNgR1-transfected neurons. Scale bars represent 15 μm. (B) Representative dendrites from control or shNgR1-transfected neurons. Scale bars represent 2 μm. (C) Quantification of the density of colocalized PSD95 and Syn1 puncta along dendrites of transfected neurons. Data are normalized to respective controls. * indicates $p < 0.05$, one-way ANOVA with pairwise comparison by Bonferroni post hoc test. Data are mean ± SEM from three to five experiments; total numbers of neurons analyzed (n) range from 28 to 54 cells per condition. Note that shNgR1 and siNgR1 were tested in heterologous cells and neurons, where they were found to selectively and efficiently knock down NgR1 protein (see Figure S2).

(D) RNAi-resistant NgR1 rescues the effect of shNgR1 on the density of PSD95/Syn1 puncta. Cultured hippocampal neurons were transfected with GFP and either shCON (white bar), shNgR1 (black bar), shCON and ResNgR1 (blue bar), or shNgR1 and ResNgR1 (orange bar). Neurons were immunostained with antibodies against PSD95 and Syn1, and the normalized density of apposed PSD95/Syn1 puncta along the dendrites of transfected neurons was quantified. * indicates $p < 0.05$, one-way ANOVA with pairwise comparison by Bonferroni post hoc test. Data are mean ± SEM from three experiments; total numbers of neurons analyzed (n) range from 27 to 31cells per condition.

(E and F) A distinct set of synaptic markers (GluR2/Syt1) also reveals increased synapse density upon knockdown of NgR1. Cultured hippocampal neurons were transfected with GFP and either shCON (white bar), shNgR1 (gray bar), siCON (green bar), or siNgR1 (black bar), and subsequently immunostained with antibodies against the postsynaptic marker GluR2 (red) and the presynaptic marker Syt1 (blue). (E) Representative dendrites. Scale bars represent 2 μm. (F) Quantification of the density of colocalized GluR2 and Syt1 puncta along dendrites of transfected neurons. Data are normalized to respective controls. * indicates $p < 0.05$, one-way ANOVA with pairwise comparison by Bonferroni post hoc test.

Data are mean ± SEM from three experiments; total numbers of neurons analyzed (n) range from 28 to 34 cells per condition. Note that knockdown of NgR1 was also found to increase synapse intensity and size in vitro (see Figure S2).

(G) Hippocampal neurons from mice lacking any member of the NgR family (*NgR1*, *NgR2*, or *NgR3*) show elevated synapse density. Cultured hippocampal neurons from littermates of the indicated genotype were transfected with GFP and immunostained antibodies against PSD95 and Syn1 to determine the normalized synapse density. Embryos that were heterozygous for *NgR1*, *NgR2*, and *NgR3* were used as a control (CON; white bar). Neuronal cultures from $NgR1^{-/-}$ (black bar), $NgR2^{-/-}$(blue bar), and $NgR3^{-/-}$ (green bar) mutant embryos were heterozygous for the other respective NgR family members. * indicates $p < 0.05$, one-way ANOVA with pairwise comparison by Bonferroni post hoc test. Data are mean ± SEM from three experiments; total numbers of neurons analyzed (n) range from 45 to 60 cells per condition. Note that acute knockdown of NgR1, NgR2, or NgR3 also resulted in an increase in synapse density (see Figure S2I). Western blotting and quantitative RT-PCR were used to confirm that NgR mutant mice were protein or mRNA nulls (see Figure S5).

(H and I) Overexpression of WTNgR1 or WTNgR2 reduces synapse density. Cultured hippocampal neurons were transfected with GFP alone (CON; white bar) or GFP and either WTNgR1 (black bar) or WTNgR2 (blue bar). Neurons were subsequently immunostained with antibodies against PSD95 (red) and Syn1 (blue). (H) Representative dendrites. Scale bars represent 2 μm. (I) Quantification of the normalized density of colocalized PSD95 and Syn1 puncta along dendrites of transfected neurons. * indicates $p < 0.05$, one-way ANOVA with pairwise comparison by Bonferroni post hoc test. Data are mean ± SEM from three experiments; total numbers of neurons analyzed (n) range from 21 to 49 cells per condition.

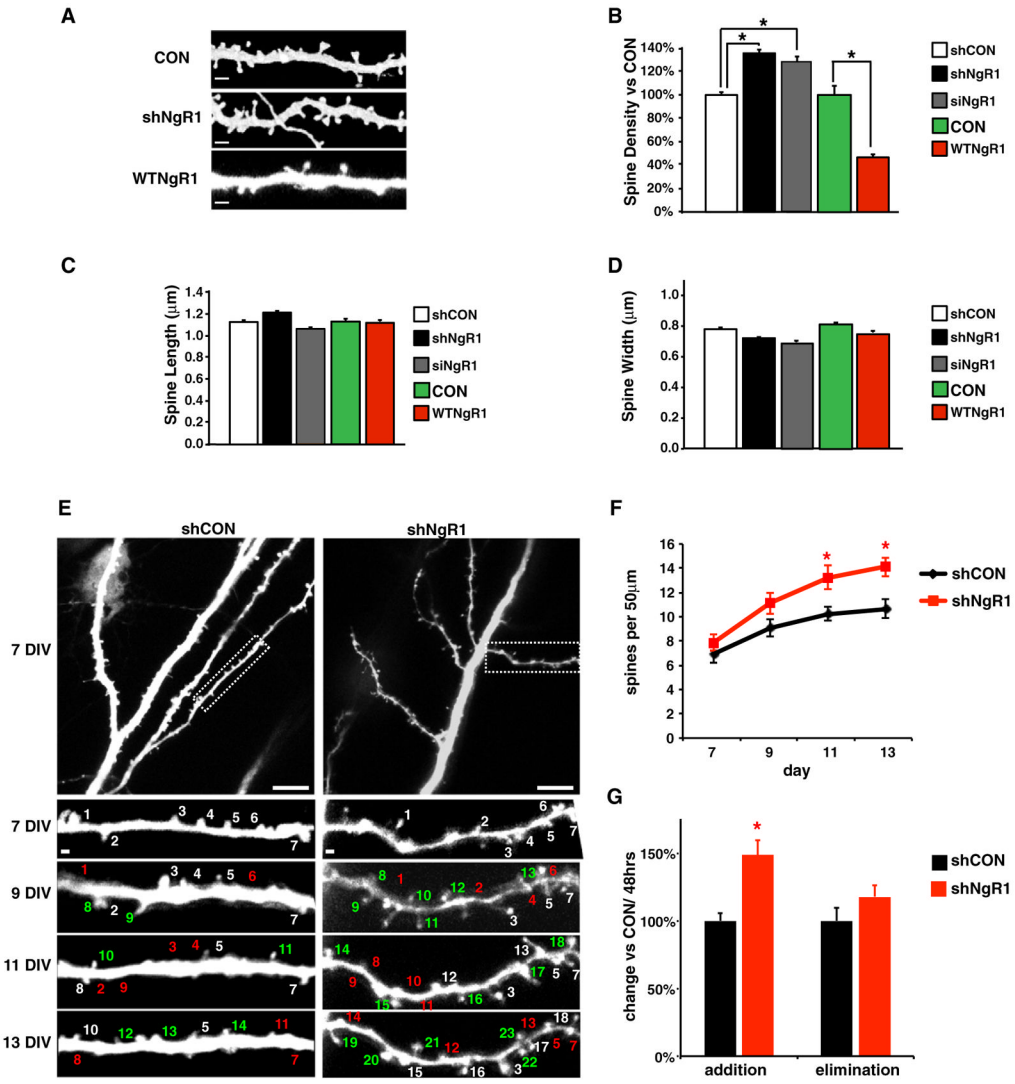

Figure 3. NgR1 Restricts Spine Formation in a Hippocampal Circuit

(A–D) Effects of NgR expression on dendritic spine morphology. Organotypic hippocampal slices were biolistically transfected with GFP alone (CON; green bar) or GFP along with either a control shRNA construct (shCON, white bars), shNgR1 (black bars), siNgR1 (gray bars), or WTNgR1 (red bars), as indicated, and fixed. (A) Representative images of proximal secondary apical dendrites from GFP-labeled CA1 pyramidal neurons from CON, shNgR1, and WTNgR1 are shown. Scale bar is 1 μm. Secondary apical dendrites were analyzed following biolistic introduction of GFP together with the indicated constructs, and the average dendritic spine density (B), spine length (C) and spine width (D) were determined. Spine density is normalized to respective controls; spine length and width are averages. * indicates $p < 0.01$, one-way ANOVA with pairwise comparison by Bonferroni post hoc test. Data are means, with error bars representing ±SEM from three experiments; total numbers of neurons analyzed (n) range from 20 to 30 cells per condition.

(E) Extended live imaging of spine density changes over time. Organotypic hippocampal slices were biolistically transfected with GFP along with either a control shRNA construct (shCON) or an shRNA construct targeting NgR1 (shNgR1). Representative images of proximal secondary apical dendrites from GFP-labeled CA1 pyramidal neurons that were

repeatedly imaged are shown. Top panels show the entire proximal dendritic region of representative neurons at 7 DIV, while a higher magnification image of the boxed regions (white dotted rectangles) is shown below following spine development over 7 days in vitro (7–13 DIV). White numbers mark persistent spines (older than 48 hr), green numbers mark newly formed spines (<48 hr old) and red numbers mark eliminated spines (lost within the last 48 hr). Scale bars in top images indicate 10 μm, and those in the bottom images mark 1 μm.

(F) Quantification of spine density over time. The average spine density of dendritic regions repeatedly imaged following the introduction of shCON (black line) or shNgR1 (red line) is quantified at four time points (7, 9, 11, and 13 DIV). * indicates $p < 0.01$ with a Student's t test. Data are means, with error bars representing ±SEM from three experiments; total number of neurons analyzed (n) was 26 per condition.

(G) Quantification of spine addition and elimination. The average number of spines added or eliminated over all four time points was quantified on a per micron basis following biolistic introduction of shCON (black) or shNgR1 (red). Data are presented as percent change relative to control. * indicates $p < 0.01$ with a Student's t test. Data are means, with error bars representing ±SEM from three experiments. Quantification of spine addition and elimination for each time point is illustrated in Figure S3.

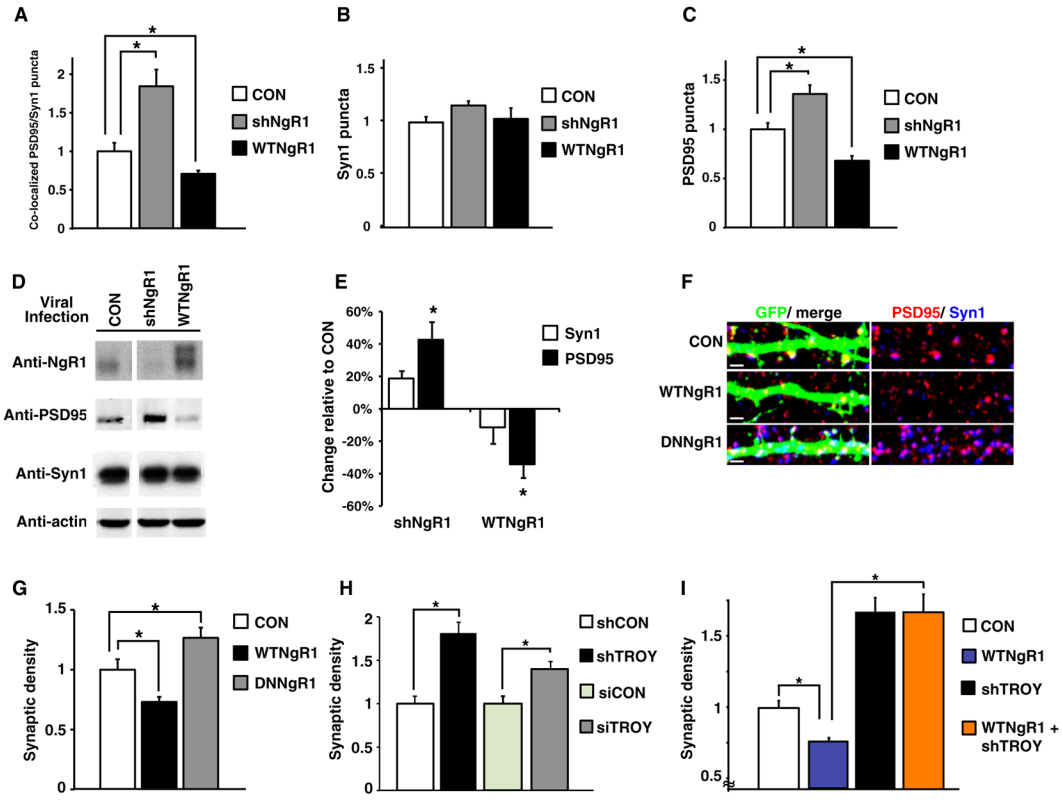

Figure 4. NgR1 Functions Postsynaptically through the Coreceptor TROY to Restrict Synapse Formation

(A–C) Effect of NgR1 on the density of PSD95/Syn1 puncta is due to changes in the postsynaptic protein PSD95. Cultured hippocampal neurons were transfected with GFP alone (CON; white bar) or GFP and either shNgR1 (gray bar) or WTNgR1 (black bar), and subsequently immunolabeled with antibodies against PSD95 and Syn1. (A) Synapse density was quantified by assessing the number of colocalized PSD95/Syn1 puncta along the dendrites of transfected neurons. These data were subsequently deconvolved to determine the density of Syn1 (B) or PSD95 (C) puncta along the dendrites. Similar results were observed upon de-convolution of the Syt1/GluR2 puncta (data not shown). * indicates $p < 0.01$, one-way ANOVA with pairwise comparison by Bonferroni post hoc test. Data are means, with error bars representing ±SEM from three experiments; total numbers of neurons analyzed (n) range from 32 to 49 cells per condition.

(D and E) Modulation of NgR1 expression throughout neuronal cultures affects total levels of PSD95. Cultured hippocampal neurons (5 DIV) were infected with a control lentivirus (CON), an shNgR1 lentivirus, or a WTNgR1 lentivirus. Neurons were lysed at 14 DIV and analyzed by immunoblotting for NgR1, PSD95, Syn1 or actin (used as a loading control). (D) Representative immunoblots. (E) Quantification of protein levels. Integrated intensities were measured by infrared fluorescence detection of immunoblots. Syn1 (white bar) and PSD95 (black bar) protein levels were normalized to actin and expressed as change relative to CON. * indicates $p < 0.01$, one-way ANOVA with pairwise comparison by Bonferroni post hoc test. Data are means, with error bars representing ±SEM from three to six experiments. Note that knockdown of NgR1 also resulted in an increase in the total level of a second postsynaptic protein, GluR2 (see Figure S4).

(F and G) Overexpression of a mutant form of NgR1 (DNNgR1) causes a significant increase in synapse density. Cultured hippocampal neurons were transfected with GFP alone (CON; white bar), or cotransfected with GFP and either WTNgR1 (black bar) or DNNgR1

(gray bar). Samples were immunolabeled for PSD95 and Syn1. (F) Representative dendrites. Scale bar is 1 μm. (G) Quantification of normalized synapse density. * indicates $p < 0.05$, one-way ANOVA with pairwise comparison by Bonferroni post hoc test. Data are means, with error bars representing ±SEM from three experiments; total numbers of neurons analyzed (n) range from 32 to 49 cells per condition.
(H) Knockdown of the NgR1 coreceptor TROY causes a significant increase in synapse density. Cultured hippocampal neurons were transfected with GFP and control RNAis shCON (white bar) or siCON (green bar), or GFP and RNAis targeting TROY, shTROY (black bar) or siTROY (gray bar), as indicated. Five days later, cells were fixed, immunolabeled for PSD95 and Syn1, and quantified to determine the normalized synapse density. * indicates $p < 0.01$, one-way ANOVA with pairwise comparison by Bonferroni post hoc test. Data are means, with error bars representing ±SEM from three experiments; total numbers of neurons analyzed (n) range from 24 to 51 cells per condition.
(I) Inhibition of synapse formation by NgR1 requires TROY. Cultured hippocampal neurons were transfected with GFP alone (CON; white bar), or cotransfected with GFP and WTNgR1 (blue bar), shTROY (black bar), or both (orange bar). Neurons were immunolabeled with antibodies against PSD95 and Syn1 to determine the normalized synapse density. * indicates $p < 0.05$, one-way ANOVA with pairwise comparison by Bonferroni post hoc test. Data are means, with error bars representing ±SEM from three experiments; total numbers of neurons analyzed (n) range from 25 to 67 cells per condition. Note that TROY is highly expressed in cultured hippocampal neurons (data not shown) and that knockdown of TROY significantly reduces its mRNA levels (see Figure S4).

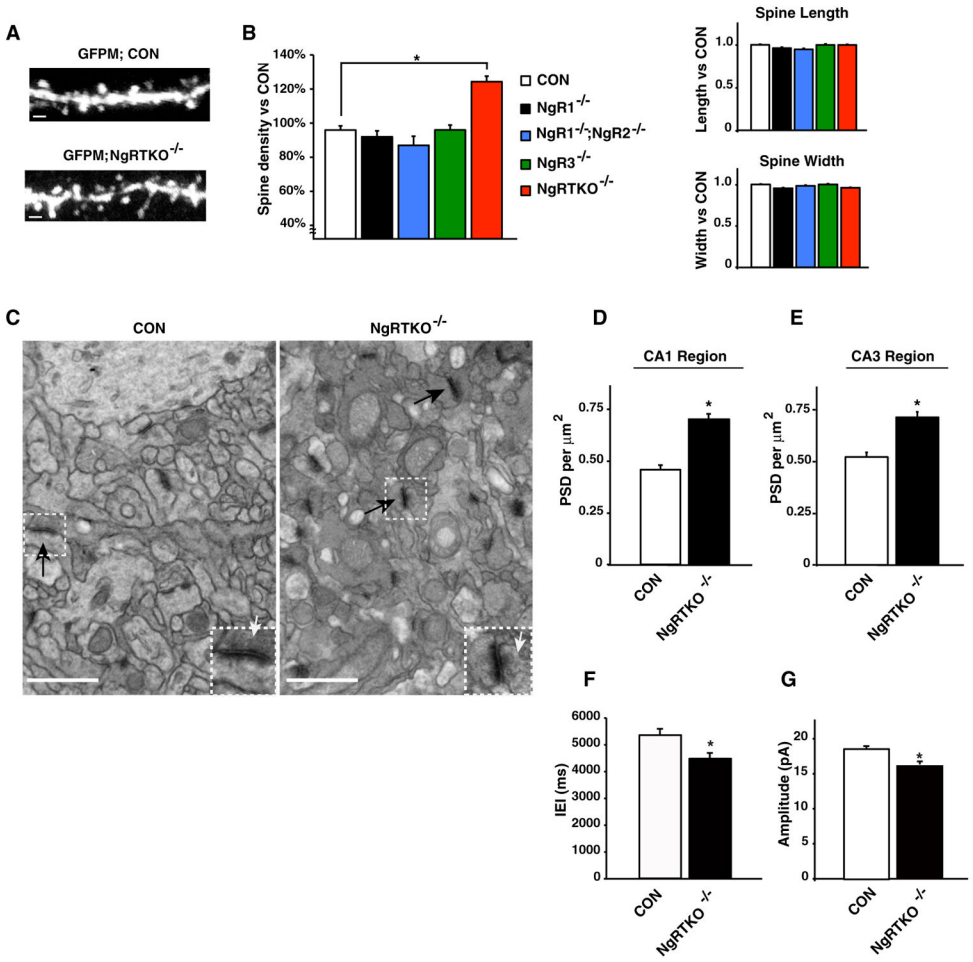

Figure 5. The NgR Family Restricts Synapse Formation in Vivo

(A and B) Mice lacking all three *NgR* family members have elevated spine density. Neurons were labeled genetically by breeding the GFPM allele into triple NgR knockout or control mice. Triple NgR knockout mice (*NgRTKO*$^{-/-}$ [red bar]) and triple heterozygous littermates (CON; white bar) were perfused at P18, sectioned by vibratome and immunolabeled with an anti-GFP antibody. (A) Representative images from proximal secondary apical dendrites. Scale bar is 1 μm. (B) Quantification of spine features. Dendritic spine density, spine length, and spine width from secondary apical dendrites of neurons expressing GFP were determined. Spine density values are expressed as percentage of the control value. Spine length and spine width values for the various genotypes are normalized to the mean value of the triple heterozygotes. Data are mean ±SEM from three independent experiments; total numbers of neurons analyzed (n) range from 30 to 60 cells per condition. * indicates $p < 0.01$, one-way ANOVA with pairwise comparison by Tukey's post hoc test.

(C–E) Ultrastructural analysis reveals that triple *NgR* knockouts have an abnormally high density of synaptic sites. (C) Representative transmission electron micrographs. Hippocampi of either triple heterozygous (CON) or triple knockout (*NgRTKO*$^{-/-}$) P18 littermates were prepared for electron microscopy and apical CA1 regions were analyzed. Black arrows mark examples of asymmetric excitatory postsynaptic densities (PSDs). White dashed boxes mark example PSDs magnified in lower righthand corner, with white arrows highlighting presynaptic vesicles. Scale bar represents 1 μm. (D and E) Quantification of asymmetric PSDs. Asymmetric PSDs from either the CA1 (D) or CA3 (E) regions of the hippocampus

were quantified, analyzing 5 × 5 μm regions. Data are mean ± SEM from two littermate pairs, analyzing 30 regions per condition. * indicates $p < 0.01$, one-way ANOVA with pairwise comparison by Bonferroni post hoc test.

(F and G) Acute slice recordings from triple *NgR* knockouts reveal an increase in the frequency but decrease in the amplitude of mEPSCs. Mini-excitatory postsynaptic currents (mEPSCs) were recorded from acute hippocampal slice preparations obtained from P15 triple heterozygous (CON) or triple knockout (*NgRTKO*$^{-/-}$) animals. Mean interevent intervals (IEI) or amplitudes are represented ± SEM from 10–14 animals. * indicates $p < 0.05$ using a KS test from analysis of cumulative probability plots of mEPSCs IEIs and amplitudes (Figure S5).

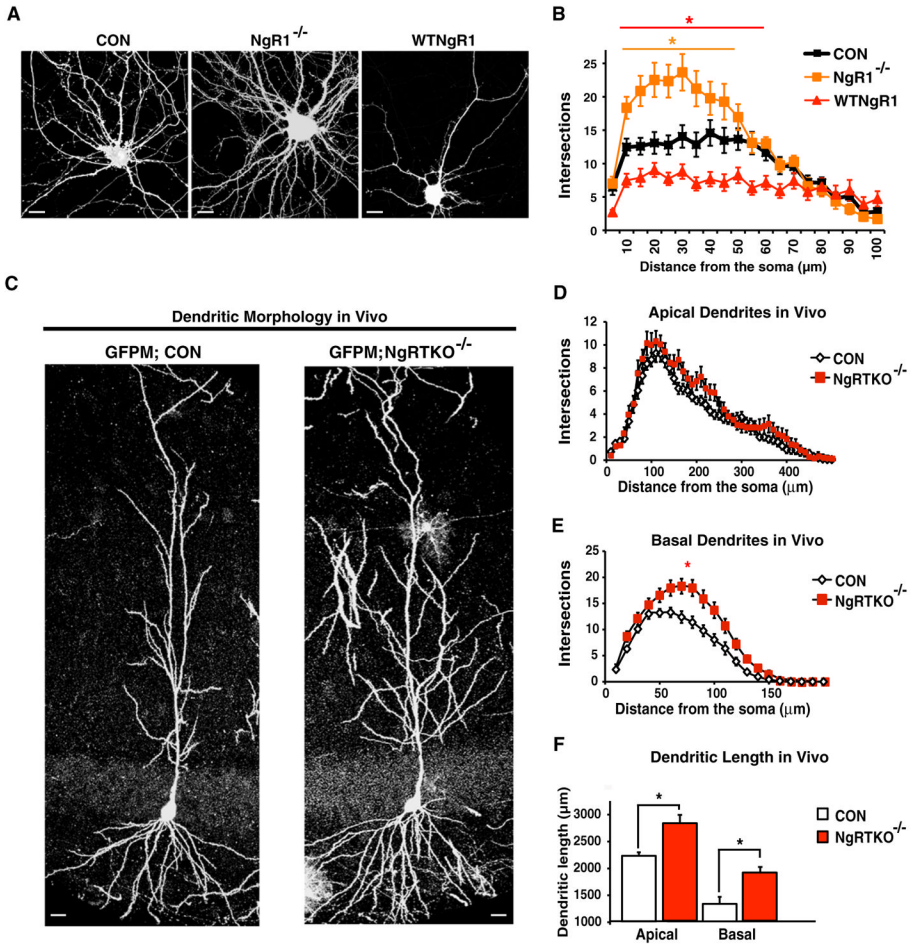

Figure 6. The NgR Family Restricts Dendritic Growth In Vitro and In Vivo

(A and B) NgR1 inhibits the dendritic complexity of hippocampal neurons in vitro. GFP was expressed by transfection of cultured hippocampal neurons from wild-type mice (CON; black bar), embryos lacking *NgR1* (*NgR1*$^{-/-}$; orange bar), or neurons in which WTNgR1 was cotransfected along with GFP (red bar). Subsequently, neurons were fixed and analyzed by confocal microscopy. (A) Representative neurons. Scale bar is 15 μm. (B) Quantification of dendritic complexity by Sholl analysis. Note that knockdown of NgR1 also increased dendritic complexity and length in organotypic slice culture (see Figure S6). Data are mean ± SEM from three experiments; total numbers of neurons analyzed (n) are 23 cells per genotype. * indicates $p < 0.05$, repeated-measures two-way ANOVA with pairwise comparison by Bonferroni post hoc.

(C–F) The length and complexity of dendrites is significantly increased in *NgR* triple knockout mice in vivo. Neurons were genetically labeled by breeding the GFPM allele (Feng et al., 2000) into the background of mice lacking NgR family members. Triple NgR knockout mice (*NgRTKO*$^{-/-}$; red bar) and triple heterozygous littermates (CON; white bar) were perfused at P18, sectioned by vibratome, and labeled with an anti-GFP antibody. (C) Representative neurons from the CA1 region of the hippocampus. Scale bar is 10 μm. (D–F) Quantification of dendritic complexity. Sholl analysis of apical (D) and basal (E) dendrites was performed, and total dendritic length (F) was measured. Data are mean ± SEM from three experiments; total numbers of neurons analyzed (n) range from 20 to 22 cells per genotype. * indicates $p < 0.05$, repeated-measures two-way ANOVA with pairwise comparison by Bonferroni post hoc.

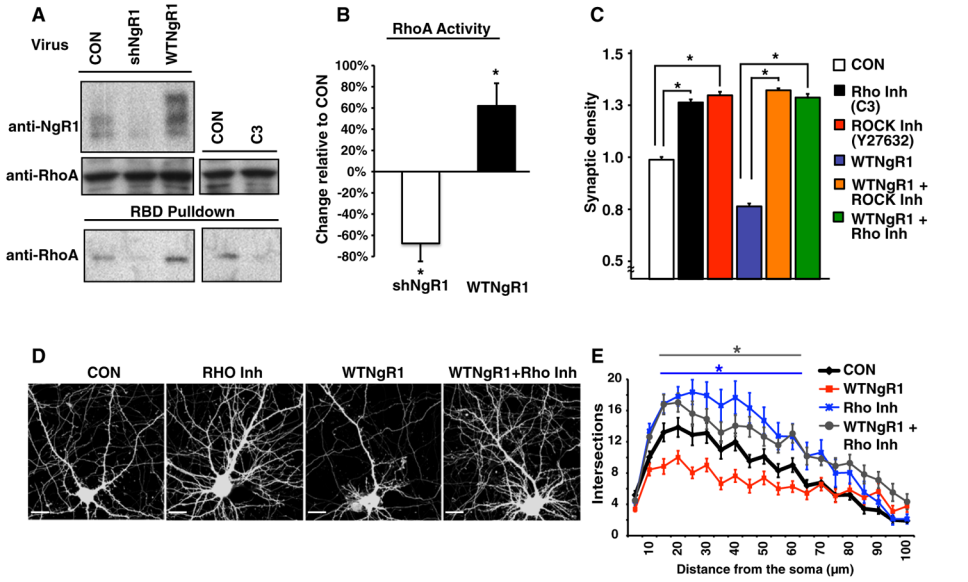

Figure 7. NgR1 Restricts Synaptic and Dendritic Growth through RhoA

(A) NgR1 regulates RhoA activity in hippocampal neurons. Cultured hippocampal neurons were infected with lentivirus expressing a control shRNA (CON), shNgR1, or WTNgR1. Alternatively, hippocampal cultures were treated with the Rho inhibitor C3 (200 ng/ml) or vehicle (CON) for 12 hr. Active Rho was then isolated by performing rhoteckin-binding domain (RBD) pull-downs and visualized by western blotting with antibodies to RhoA (bottom). Total protein levels were also assessed by immunoblot, using antibodies against NgR1 (top) and RhoA (middle).

(B) Quantification of active RhoA. Integrated intensities were measured by densitometry measurements of immunoblots in ImageJ (see Methods). Protein levels were normalized to actin and expressed as change relative to CON. * indicates $p < 0.01–0.05$, one-way ANOVA with pairwise comparison by Bonferroni post hoc test. Data are means, with error bars representing ±SEM from five independent experiments.

(C) Inhibition of synapse formation by NgR1 is reversed by blocking ROCK or Rho activity. Cultured hippocampal neurons were transfected with GFP alone (CON; white bar) or cotransfected with GFP and WTNgR1 (purple bar). Subsequently, transfected neurons were either mock-treated (white and purple bars) or treated with the Rho inhibitor C3 (200 ng/ml, black and green bars) or the ROCK inhibitor Y27632 (1 μM; red and orange bars) for 12 hr prior to immunolabeling with antibodies against PSD95 and Syn1 to determine normalized synapse density. Data are mean ± SEM from three experiments; total numbers of neurons analyzed (n) range from 50 to 70 cells per condition. * indicates $p < 0.05$, repeated-measures two-way ANOVA with pairwise comparison by Bonferroni post hoc.

(D and E) Inhibition of dendritic complexity by NgR1 is reversed by blocking Rho activity. Cultured hippocampal neurons were transfected with GFP alone (black bar) or cotransfected with GFP and WTNgR1 (red bar). Subsequently, neurons were mock-treated or treated with the Rho inhibitor C3 (200 ng/ml, blue and gray bars) for 12 hr, fixed and subjected to Sholl analysis. (D) Representative neurons. Scale bar is 15 μm. (E) Quantification of dendritic complexity. Data are mean ± SEM from three experiments; 30 neurons were analyzed per condition. * indicates $p < 0.05$, repeated-measures two-way ANOVA with pairwise comparison by Bonferroni post hoc. Similar results were observed using the ROCK inhibitor (see Figure S7).

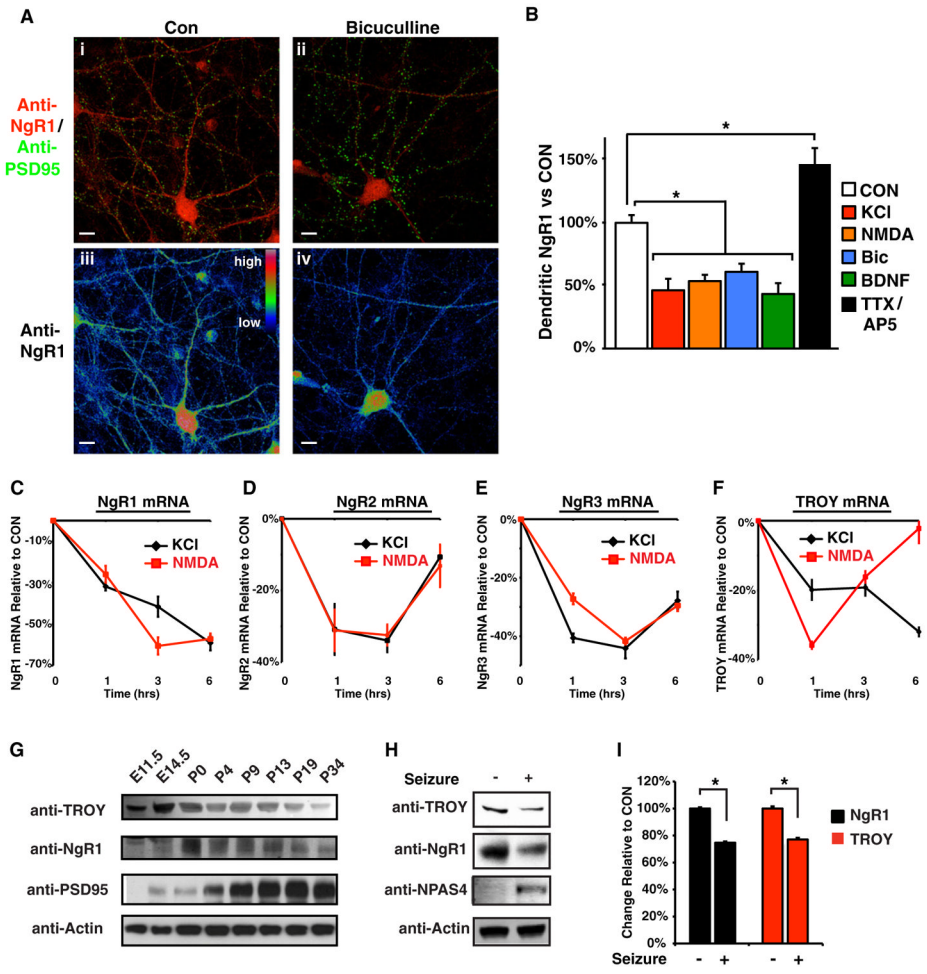

Figure 8. The NgR1 Family and Coreceptor TROY Are Downregulated by Neuronal Activity

(A and B) Expression of NgR1 protein on dendrites is downregulated by increased neuronal activity. (A) Cultured hippocampal neurons were treated with vehicle (CON) or bicuculline (5 μM, 12 hr). Subsequently, cells were fixed and immunolabeled with antibodies against NgR1 and PSD95. Representative images are shown at top (i and ii). At bottom (iii and iv), anti-NgR1 signal has been converted into a heat map (using Rainbow RGB setting in Image J software). Scale bar is 10 μm. (B) Cultured hippocampal neurons were transfected with GFP, treated with compounds for 12 hr and then immunolabeled with antibodies against NgR1. Treatments were vehicle (CON; white bar), KCl (55 mM, red bar), NMDA (30 μM, orange bar), bicuculline (5 μM, blue bar), BDNF (50 nM, green bar), or a combination of tetrodotoxin (TTX, 1 μM) and APV (100 μM, black bar). Data are expressed as percentage change in the number of NgR1 puncta expressed on the dendrites of GFP-transfected neurons relative to mock treatment (CON). * indicates $p < 0.05$, one-way ANOVA with pairwise comparison by Bonferroni post hoc test. Data are mean ± SEM from three experiments; total numbers of neurons analyzed (n) range from 25 to 50 cells per condition. Similar results were observed examining NgR1 protein on the cell surface (see Figure S8A). (C–F) Neuronal activity causes a downregulation in the mRNA for NgR1, NgR2, NgR3 and TROY. Cultures of hippocampal neurons were either mock-treated (CON) or treated with KCl (55 mM, black bar) or NMDA (30 μM, red bar). RNA was collected at the indicated times, and quantitative RT-PCR was performed for NgR1 (C), NgR2 (D), NgR3 (E), and TROY (F). Message levels were normalized to actin and expressed as percent difference

relative to control. Data represent mean ± SEM from four to five experiments. Changes in the mRNA expression of NgR1 and NgR3 were significantly different from control at all time points. NgR2 mRNA was significantly different from control at the 1 hr and 3 hr time points. TROY mRNA was significantly different from control in all but the NMDA 6 hr time point. * indicates $p < 0.01$, repeated-measures ANOVA with pairwise comparisons Bonferroni post hoc test.

(G) TROY protein levels are developmentally downregulated. Protein lysates were prepared from the hippocampi of mice from different developmental ages (E11.5 to P34) and subjected to immunoblot analysis with antibodies directed against TROY, NgR1, PSD95, or actin.

(H) TROY and NgR1 protein levels are downregulated by kainate-induced seizure. Protein lysates were prepared from the hippocampi of two control and two kainite-seized mice. Lysates were subjected to immnoblot analysis with antibodies directed against TROY, NgR1, NPAS4, and actin.

(I) Quantification of TROY and NgR1 protein levels following kainate-induced seizure. Integrated intensities of TROY and NgR1 were measured by infrared fluorescence detection. Data represent mean ± SEM from two independent experiments and are expressed as change relative to control. * indicates a $p < 0.05$ with a Student's t test. Similar results were observed when examining NgR1 and TROY protein levels following mouse exposure to an enriched environment (see Figures S8C and S8D).